SULTAN MOULAY SLIMANE UNIVERSITY
Faculty of Sciences and Technics,
Béni Mellal

Discipline: Mathematics
Ph.D. Specialty: Mathematics

DOCTORAL THESIS

Modeling and Analysis of Anisotropic Nonlinear Diffusion Equations Applied to Digital Images

Author:
Mr. Anas TIARIMTI ALAOUI

Supervisor:
Prof. Mostafa JOURHMANE

A thesis submitted in fulfillment of the requirements
for the degree of Doctor of Mathematics

in the

Information Processing and Decision Support Laboratory
Department of Mathematics

January 8^{th}, 2022

UNIVERSITÉ SULTAN MOULAY SLIMANE
Faculté des Sciences et Techniques
Béni Mellal

Centre des Etudes Doctorales: Sciences et Techniques

Formations Doctorales: Mathématiques et Physique Appliquées

THÈSE DE DOCTORAT

Modélisation et Analyse des Équations de Diffusion Non Linéaires Anisotropes Appliquées aux Images Numériques

Présentée par

Mr. Anas TIARIMTI ALAOUI

Soutenue le Samedi 08 Janvier 2022 devant la commission d'examen :

Président du jury:	Monsieur Said MELLIANI	Professeur, FST-USMS-Béni Mellal
Rapporteurs:	Monsieur Belaid BOUIKHALENE	Professeur, FP-USMS-Béni Mellal
	Monsieur Ahmed MACHMOUM	Professeur, FS-UIZ-Agadir
	Monsieur Mohamed CHABI	Professeur, FST-USMS-Béni Mellal
Examinateur:	Monsieur Khalid HILAL	Professeur, FST-USMS-Béni Mellal
Directeur de thèse:	Monsieur Mostafa JOURHMANE	Professeur, FST-USMS-Béni Mellal

N° d'ordre : 395/21

Publications and Conferences

Published articles:

- A. Tiarimti Alaoui, M. Jourhmane, "Existence and Uniqueness of Weak Solutions for Novel Anisotropic Nonlinear Diffusion Equations Related to Image Analysis", Journal of Mathematics, vol. 2021, Article ID 5553126, 18 pages, 2021.

- A. Tiarimti Alaoui, M. Jourhmane, "Existence and Uniqueness of Weak Solutions for a New Class of Convex Optimization Problems Related to Image Analysis", Journal of Mathematics, vol. 2021, Article ID 6691795, 15 pages, 2021.

Submitted articles:

- A. Tiarimti Alaoui, M. Jourhmane,"Edge-Preserving Smoothing of Perona-Malik Nonlinear Diffusion in Two-Dimensional Space", Manuscript submitted for publication, 2020.

International Conferences:

- A. Tiarimti Alaoui, M. Jourhmane,"Image denoising using efficient diffusion coefficient and suitable adaptive threshold", Fourth International Conference on Business Intelligence (CBI 2018) 25-27 April 2018 Faculty of Sciences and Technology, Beni Mellal, Morocco.

SULTAN MOULAY SLIMANE UNIVERSITY

Abstract

Faculty of Sciences and Technics,
Béni Mellal
Department of Mathematics

Doctor of Mathematics

Modeling and Analysis of Anisotropic Nonlinear Diffusion Equations Applied to Digital Images

by Mr. Anas TIARIMTI ALAOUI

For decades, digital images have been considered a crucial instrument in any artificial vision system. In the meantime, Mathematicians played an essential role in developing theories related to a broad range of applications such as image restoration and edge detection.

In this context, the present thesis first gives an overview of remarkable research studies of various diffusion equation-based models in image processing and analysis. Mainly, a behavioral analysis of the Perona and Malik model is presented and discussed. Then, a new nonlinear diffusion model is constructed as a parabolic evolution equation, based on the assumption that the diffusion needs to be anisotropic, nonlinear, and consistent with the digital image structure.

Next, to conduct a theoretical analysis of the proposed model, we adopt a possible strategy combining the iterative method with the monotonicity method. On the one hand, we apply the implicit iterative method to approximate the evolution problem by elliptic problems. Then, we use a variational approach to prove, step by step, the existence of weak solutions for each elliptic problem in an appropriate functional framework involving the Orlicz spaces. On the other hand, we construct an approximate solution for the evolution problem using the above weak solutions. After that, we show that a unique weak solution for the evolution problem can be extracted using an energy estimate, bounded and uniform integrability in L^1, and the monotonicity method.

Finally, we consider a consistent and stable scheme to numerically implement our nonlinear diffusion model employing explicit and central finite difference schemes.

Keywords: Edge Detection; Convex Optimization Problem; Anisotropic Nonlinear Diffusion; Image Restoration; Partial Differential Equations; Variational Method; Orlicz Space; Weak solutions.

UNIVERSITÉ SULTAN MOULAY SLIMANE

Résumé

Faculté des Sciences et Techniques
Béni Mellal
Departement de Mathématiques

Docteur en Mathématiques

Modélisation et Analyse des Équations de Diffusion Non Linéaires Anisotropes Appliquées aux Images Numériques

by Mr. Anas TIARIMTI ALAOUI

Depuis des décennies, les images numériques sont considérées comme un instrument crucial dans tout système de vision artificielle. Pendant ce temps-là, les mathématiciens ont joué un rôle essentiel dans le développement de théories liées à une grande variété d'applications telles que la restauration d'images et la détection des bords.

Dans ce contexte, la présente thèse donne tout d'abord un aperçu des études de recherche remarquables de divers modèles basés sur l'équation de diffusion dans le traitement et l'analyse des images. Principalement, une analyse comportementale du modèle de Perona et Malik est présentée et discutée. Ensuite, un nouveau modèle de diffusion non linéaire est construit comme une équation d'évolution parabolique, basée sur l'hypothèse que la diffusion doit être anisotrope, non linéaire et cohérente avec la structure de l'image numérique.

Ensuite, pour effectuer une analyse théorique du modèle proposé, nous adoptons une stratégie possible combinant la méthode itérative et la méthode de monotonicité. D'une part, nous appliquons la méthode itérative implicite pour approximer le problème d'évolution par des problèmes elliptiques. Puis, nous utilisons une approche variationnelle pour prouver, étape par étape, l'existence de solutions faibles pour chaque problème elliptique dans un cadre fonctionnel approprié impliquant les espaces d'Orlicz. D'autre part, nous construisons une solution approximative pour le problème d'évolution en utilisant les solutions faibles ci-dessus. Par la suite, nous montrons qu'une unique solution faible pour le problème d'évolution peut être extraite en utilisant une estimation de l'énergie, l'intégrabilité bornée et uniforme dans L^1, et la méthode de monotonicité.

Enfin, nous considérons un schéma cohérent et stable pour implémenter numériquement notre modèle de diffusion non linéaire en utilisant des schémas de différences finies explicites et centraux.

Mots Clés: Détection des Contours; Problème d'Optimization Convexe; Diffusion Non linéaire Anisotrope; Restauration d'Images; Équations aux Dérivée Partilles; Méthode variationnelle; Espace de Orlicz; Solutions Faibles.

Acknowledgements

First of all, I would like to express my most profound gratitude to Almighty Allah; the most gracious and merciful who bestowed on me the strength and courage to take up the ever-widening education and higher research field.

I would also like to express my sincere gratitude to my advisor Prof. Mostafa Jourhmane for the continuous support of my Ph.D. study and research, for his patience, motivation, enthusiasm, and immense knowledge. His guidance helped me in all the time of research and writing of this thesis.

I would also like to thank:

- Prof. Ahmed Zeghal; the former Dean of the Faculty of Sciences and Technics, Sultan Moulay Sliman University, for accepting me and giving me the chance to pursue my doctoral studies.
- Prof. Said Melliani; the current Dean of the Faculty of Sciences and Technics, Sultan Moulay Sliman University, for allowing me to defend my Ph.D. thesis before a committee of experts.
- Prof. Mohamed Fakir; the head of the Information Processing and Decision Making Laboratory, for providing the possibility to carry out this work at his laboratory.

I have been supported and inspired by many people, and it is a pleasure to take this opportunity to express my gratitude to them. Therefore, I would like to thank:

- All the Department of Mathematics group members for providing a friendly and pleasant working environment.
- All the friends, scholars, and Laboratory staff for their cooperation and encouragement throughout this work.

My most profound appreciation also goes to my thesis committee for generously giving their time and offering their valuable comments toward improving this work.

I would also like to express my gratitude to my parents for their unconditional trust, timely encouragement, and endless patience.

Finally, I thank my wife with love for understanding me best as a Ph.D. She has been my best friend and great companion, loved, supported, encouraged, entertained, and helped me get through this agonizing period in the most positive way.

Anas Tiarimti Alaoui

Contents

List of Figures

List of Tables

Chapter 1

Introduction

In our modern society, digital images are ubiquitous in our environment, and their existence in our daily activities substantially influences and impacts different sciences, engineering disciplines, and technologies. They are incorporated in every observation and investigation system to help analyze, understand and interpret objects in various settings and at different scales. At tiny scales, images, for instance, can be produced by electron microscopes scanning the surface using a beam of electrons. Figure 1.1 (a) shows the scanning electron microscope image of SARS-CoV-2[1] (round gold objects) emerging from the surface of cells cultured in the lab. On a regular scale, images can be found everywhere, for example, telephones, televisions, remote monitoring, scanners, medical imaging (cf. Figure 1.1 (b)). However, on vast scales, one can use telescopes or space probes to view images. In particular, humanity can discover distant areas such as the earth's surface or Mars[2] (cf. Figure 1.1 (c)).

(a) (b) (c)

FIGURE 1.1: Digital images at different scales

The human vision system forms and perceives the visual information from the retina (the eye), passing by the optic nerve to the brain (the central nervous system). It has an extraordinary capacity to adapt the light's brightness and possesses highly complex processors to identify, recognize and classify various images collections. In this context, artificial vision attempts to emulate human vision by modeling different image processing tasks, including learning, making decisions, and taking actions based on input image data.

[1] https://www.flickr.com/photos/niaid/49557785797/in/album-72157712914621487/
[2] https://photojournal.jpl.nasa.gov/catalog/PIA24546

Besides, computer vision systems have improved alongside machine calculation power during the last several years. Moreover, the need to develop artificial vision systems for all sorts of imaging areas, from satellite and X-ray imaging to modern computer-aided CT, MRI, and PET imaging in medical sciences, has recently gained tremendous importance. These reasons motivated several researchers, engineers, and mathematicians to develop models and algorithms in image processing and analysis for more efficient, accurate, and stable artificial vision systems.

In computer vision systems, one can distinguish between two independent levels [42]:

- *Low-level vision* mainly refers to image processing and analysis, which is related to all sorts of operations or transformations made onto images or sequences of images to improve their quality, restore their original content, interpolate their missing parts, optimize their transmission, identify regions occupied by objects without telling what they are. Image processing and analysis are becoming increasingly essential in today's sciences and technology, with many image processing applications such as contrast enhancement, denoising, deblurring, inpainting, interpolation, and segmentation.

- The *high-level vision* that refers to image interpretation is of great importance for artificial vision systems. Its central goal is to recognize features and identify real-world contexts, such as face recognition for video surveillance and terrain reading for automatic piloting.

For an artificial vision system to reflect the human vision system ideally, a combination of image processing and analysis and image interpretation is necessary and required for different tasks, including depth perception, motion estimation, and object recognition. In this context, the present study will focus only on the lower-level vision activities that involve mathematical models based on partial differential equations (PDEs).

For automatic image processing, one can focus on specific features and structures of interest, such as edges forming the boundary between two different structures or objects. To this end, one needs good models for the structures to be detected or processed automatically. Furthermore, what is the best way to define an edge? For example, does a sudden change of brightness adequately describe an edge? Overall, what are the proper ways to model, describe and analyze images mathematically? The choice of the model then is the most fundamental step in image processing and analysis.

Let us now talk about what images are and how they can be represented as mathematical objects. An image is a function u that maps every point in a Lipschitz domain Ω to some color space F:

$$u : \Omega \to F. \tag{1.1}$$

We can distinguish between discrete and continuous image domains:

- discrete 2-dimentional images, for example $\Omega = \{1, ..., M\} \times \{1, ..., N\}$.

- continuous 2-dimentional images, for example $\Omega = (0, a) \times (0, b) \subset \mathbb{R}^2$.

Different color spaces for F:

- Black-and-white images (also binary images): $F = \{0, 1\}$.
- Grayscale images with discrete color space with k-bit depth: $F = \{0, ..., 2^k - 1\}$.
- Images with continuous gray values: $F = [0, 1]$ or $F = \mathbb{R}$.
- Images with continuous colors: $F = [0, 1]^3$ or $F = \mathbb{R}^3$.

The following abstract formulation can represent many problems in image processing and analysis:

$$(input)\, u \longmapsto (output)\, T(u), \tag{1.2}$$

where T is an image processor or transformation representing a nonlinear operator and $T(u)$ denotes a critical image or observed features of interest. In this dissertation, we will investigate the following three critical aspects of image processing and analysis.

- Modeling: What are the suitable mathematical models for u and T?
- Model Analysis: Does $T(u)$ exist, and if so, is it unique?
- Computation and Simulation: How can the models be efficiently computed or simulated? Which numerical regularization techniques should be introduced to ensure stability and convergence?

As we will see in this study, the image u can be modeled as an element in a functional space (the Orlicz spaces [3]), and the image processor can be realized by a PDE.

This view governs the structure and organization of this research:

The next chapter (Chapter 2) summarizes the most relevant research on diffusion equations applied in image processing and analysis, exhibits and interprets the proposed anisotropic nonlinear diffusion model. It also suggests a possible strategy to investigate the existence and uniqueness of solutions for the proposed problem.

Chapter 3 investigates a quasilinear second-order elliptic problem by establishing its equivalence to a variational optimization of an energy functional. In this chapter, the existence and uniqueness of weak solutions for this boundary-value problem are proven in an appropriate functional space using a variational approach and the monotonicity of a nonlinear operator.

Chapter 4 establishes the existence and uniqueness of weak solutions for an initial-boundary value problem of an anisotropic nonlinear diffusion partial differential equation utilizing implicit iterative and monotonicity methods.

In Chapter 5, a stable and consistent numerical approximation scheme will be considered to implement the proposed anisotropic nonlinear diffusion model.

Finally, Chapter 6 terminates this dissertation with a general conclusion and some perspectives.

Chapter 2

Image Processing and Analysis Based on Diffusion Equation Methods

2.1 Introduction

During the last four decades, diffusion equations have been and are still of great importance in image processing and analysis. Methods based on these equations provided a better interpretation of several classical methods unified under a mathematical framework. As Weickert [54] has stated, diffusion equations represent the natural framework for scale-space analysis. Since the eighties, image restoration and edge detection problems have motivated researchers to develop new theories and models that preserve meaningful features such as edges of objects detected in the image and eliminate irrelevant information such as noises in the other regions.

This chapter provides the most relevant contributions in image modeling and representation using the diffusion equation. First, we remind the physical background of the diffusion equation in Section 2.2. Then Section 2.3 exposes the related works concerning diffusion equations filtering in image processing and analysis displayed in their chronological order of appearance. This section also gives results [48] of the smoothing-enhancing properties at edge locations of the Perona and Malik (PM) Model in two dimensions. After that, Section 2.4 presents a new anisotropic nonlinear diffusion equation [49, 50], where we discuss its properties. Finally, we conclude this chapter in Section 2.4 with a strategy to solve the proposed equation.

2.2 Diffusion as a Physical Process

The physical interpretation of the diffusion process lies in the equilibration of the concentration differences. In other words, this process aims at minimizing concentration variations of a substance without creating or destroying the mass. In this context, two fundamental equations describe this phenomenon:

- *Fick*'s law states that concentration variations ∇u produce a substance flux $\mathbf{j}$ in the direction of the negative concentration gradient:

$$\mathbf{j} = -\mathbf{D} \cdot \nabla u, \tag{2.1}$$

  where $\mathbf{D}$ is a positive definite symmetric matrix termed the *diffusion tensor*, which describes the speed of the diffusion process.

- The continuity equation expresses that diffusion only transports mass without destroying it or creating a new one:

$$\partial_t u = -\nabla \cdot \mathbf{j}, \tag{2.2}$$

  with t indicating the time.

Now, by inserting *Fick's* law into the continuity equation, we can realize the *diffusion equation*

$$\partial_t u = \nabla \cdot (\mathbf{D} \cdot \nabla u). \tag{2.3}$$

This equation has been used extensively to model many physical transport processes (The heat equation is used to model the heat transfer phenomena, for example). In the context of image processing and analysis, the concentration is identified with the intensity or grey value (the pixel value in a digital image) at a particular location.

For the general setting of the diffusion equation and depending on the choice of the diffusivity $\mathbf{D}$, one can find the standard terminology adopted in the literature (see [10]) to define a whole family of diffusion processes:

- The diffusion equation is called *linear*, *isotropic*, and *homogeneous* when $\mathbf{D} \in \mathbb{R}$. Then, the diffusion is the same in all spatial directions and every location.
- If the diffusivity is space-dependent $(\mathbf{D} = \mathbf{D}(x))$, then the process is called an *inhomogeneous* diffusion.
- If the diffusivity depends on u $(\mathbf{D} = \mathbf{D}(u))$, then the process is called a *nonlinear* diffusion.
- If the diffusivity $\mathbf{D}$ is matrix-valued (not unit matrix), the process is called *anisotropic* diffusion. Then, the equation has different diffusivity in different directions of space.

Next, we will exhibit the relevant contributions that relate diffusion equations to image restoration and edge detection.

2.3 Diffusion Models

At the lowest levels in a visual system's information processing chain, diffusion-based methods are one of the approaches used for processing and analyzing image data. Different diffusion models have

been proposed and investigated, and which can be formally written in the following general form:

$$\begin{cases} \partial_t u\left(x;t\right) = F\left(x, u\left(x;t\right), \nabla u\left(x;t\right), \nabla^2 u\left(x;t\right)\right) & \text{in } \Omega \times (0,T] \\ u\left(x;0\right) = u_0\left(x\right) & \text{in } \Omega, \end{cases} \tag{2.4}$$

where F is a second-order differential operator and $\Omega \subset \mathbb{R}^2$ is a Lipschitz domain.

With this evolutionary process, we can construct a family of functions (i.e., images) $u\left(x;t\right)_{t>0}$ that represent successive versions of the initial image $u_0\left(x\right)$. Accordingly, over time t, $u\left(x;t\right)$ can be regarded as a simplification of the original image $u_0\left(x\right)$. So, we can relate the simplified structures at large scales t with those that correspond to meaningful details in images at small scales.

According to the choice of the operator F, one can obtain a whole of impressive models that have been investigated extensively in image processing and analysis during at least the last four decades, as we will see in the following subsections.

2.3.1 Isotropic Linear Diffusion

The classical approaches in edge detection problems presume that the meaningful pieces of information included in an image are identified and delimited by boundaries. These boundaries are determined wherever there are essential variations in the intensity value of the image. In this regard, we can identify the boundaries of significant objects in the image by thresholding the gradient magnitude of the image intensity values. However, with the presence of noises or oscillations in the image, we can expect some points to have important gradient magnitude values without practical significance in detecting the actual boundaries of objects. Hence, the need for filtering the image before extracting the edges is of crucial importance.

In 1983, Witkin [61] introduced a continuous approach as a new multi-scale representation for filtering one-dimensional signals, namely the *scale-space* formulation. Back then, he observed that no new structure is created in a scale-space representation while the scale parameter increases. He formerly considered this property as a fundamental characteristic of the scale-space formulation. That is, the number of zero-crossings in the derivatives of any order decreased monotonically with scale. Later in 1984, Koenderink [33] generalized this scale-space theory to two-dimensional signals and introduced the notion of *causality*, which means that no new level surfaces have to be created with the increasing scale parameter.

For continuous two-dimensional images, the scale-space representation is formally built as follows: Given an image $u_0 : \Omega \subset \mathbb{R}^2 \to \mathbb{R}$, the scale-space representation $u : \Omega \times \mathbb{R}_+ \to \mathbb{R}$ is defined such that the representation at zero scales is equal to the original image

$$u\left(x;0\right) = u_0\left(x\right) \quad \text{for all } x \in \Omega, \tag{2.5}$$

and the representations at coarser scales are given by the convolution of the given image u_0 with *Gaussian* kernels K of increasing width $\sigma = \sqrt{2t}$.

$$u(x;t) = K(x;t) * u_0(x) \quad \text{for all } x \in \Omega \text{ and for all } t \in \mathbb{R}_+, \tag{2.6}$$

where $K : \Omega \times \mathbb{R}_+^* \to \mathbb{R}$ is the Gaussian kernel

$$K(x;t) = \frac{1}{4\pi t} e^{-\frac{\|x\|^2}{4t}}. \tag{2.7}$$

Besides, Koenderink [33] also pointed out that the scale-space representation is explicitly related to and must fulfill the *heat equation* on an infinitely extended image domain

$$\frac{\partial u}{\partial u}(x;t) = \nabla \cdot [\nabla u(x;t)] = \Delta u(x;t). \tag{2.8}$$

Nevertheless, using this linear diffusion reveals some drawbacks:

- At a small scale t, the noise is constantly interrupting the detection of object boundaries.
- At a large scale t, the noise is smoothed, and the essential features such as edges are blurred, making them more challenging to identify. Not to mention that linear diffusion filtering dislocates edges while the scale parameter is increasing, which means that features detected at high levels do not give suitable locations and have to be traced back to the original image, as Witkin [61] proposed as a practical solution.

Another problem arises since the set of points where the gradient magnitude is more significant than a threshold parameter constitutes regions (i.e., thick edges) and not curves (i.e., thin edges). So, to circumvent this drawback, another condition must be added to the thresholding of the gradient magnitude, namely the *maximum gradient* condition, that the set of edge points must satisfy:

- In one dimension, the extraction of the maximum gradient points is obtained by seeking points $(x;t)$ verifying:

$$u_x(x;t) \neq 0,\ u_{xx}(x;t) = 0, \text{ and } u_x u_{xxx}(x;t) < 0. \tag{2.9}$$

- The maximum gradient condition can be fulfilled in two dimensions using the Marr-Hildreth edge detection method [39]:

$$\|\nabla u(x;t)\| \neq 0, \text{ and } \Delta u(x;t) = 0. \tag{2.10}$$

  We can also use the Haralick-Canny edge detection method [26, 11] that defines the edges as "the set of points for which the gradient magnitude assumes a maximum in the gradient

direction." Then, by introducing a local orthonormal coordinate system (η, ξ), such that in each point, the ξ-direction is parallel to the maximal change of the intensity (the gradient direction of u), and the other is perpendicular to it. So we can define an edge, at any scale t, as the points on the zero-crossing curves of the second-derivative of u in the ξ-direction $\left(u_{\xi\xi}\right)$ for which the third-derivative $u_{\xi\xi\xi}$ is strictly negative, which leads to the following differential geometric definition of an edge:

$$u_{\xi\xi} = \frac{u_{x_1}^2 u_{x_1x_1} + 2u_{x_1}u_{x_2}u_{x_1x_2} + u_{x_2}^2 u_{x_2x_2}}{u_{x_1}^2 + u_{x_2}^2} = 0, \tag{2.11}$$

$$u_{\xi\xi\xi} = \frac{u_{x_1}^3 u_{x_1x_1x_1} + 3u_{x_1}^2 u_{x_2}u_{x_1x_1x_2} + 3u_{x_1}u_{x_2}^2 u_{x_1x_2x_2} + u_{x_2}^3 u_{x_2x_2x_2}}{\left(\sqrt{u_{x_1}^2 + u_{x_2}^2}\right)^3} < 0. \tag{2.12}$$

Additionally, it should be noted, as Clark stated in his paper [15] that the points satisfying (2.11) and (2.12) are the authentic edges, and the points satisfying (2.11) with $u_{\xi\xi\xi} > 0$ are the phantom edges, while the latter ones are not the edges at all.

Therefore, we can summarize the image filtering process in the following three combined steps:

1. First, we need to smooth the image u to remove noises and other fluctuations by using linear isotropic diffusion (or convolution of u_0 with a gaussian kernel).

2. Next, we extract the maximum gradient points using the Marr-Hildreth method or the Haralick-Canny method.

3. Finally, we apply the thresholding condition of the gradient magnitude on these maximum gradient points.

Unfortunately, using the Haralick-Canny or Marr-Hildreth edge detector reveals some inconvenience in blurring the critical structure and dislocating effects in their positions (cf. Figure 2.1).

As we will see in the following subsection, another model has been developed by Perona and Malik [40] to avoid the shortcomings of linear isotropic diffusion.

2.3.2 Isotropic Nonlinear Diffusion

As observed in the last subsection, applying the isotropic linear diffusion filtering to noisy images blurs the essential features and cannot preserve edge locations while the scale increases. For this reason, Perona and Malik (PM) devised in their seminal paper [40] a new concept for the scale-space representation, and they made the diffusion locally adaptive to the structure of the image by

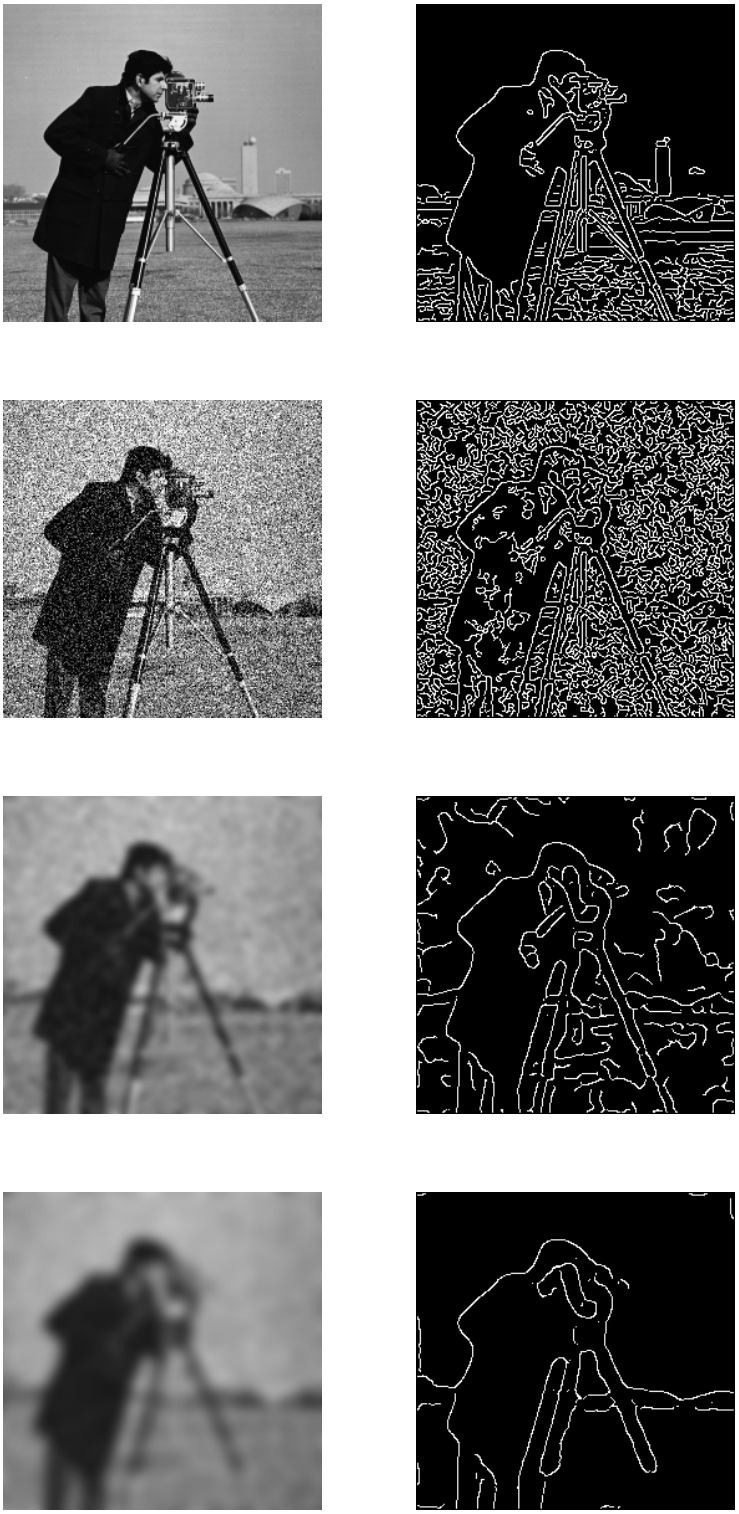

FIGURE 2.1: Cameraman test image (256 x 256): First column on the left (Up to down): Original image; Corrupted image by zero-mean white Gaussian noise with $\sigma^2 = 0.05$; Restored image by convolution with Gaussian smoothing kernel with standard deviation $\sigma^2 = 10$ and $\sigma^2 = 30$. Second column on the right: the corresponding edges using the Canny filter.

introducing a diffusion function g in the equation (2.8), as shown in the following:

$$\begin{aligned}\frac{\partial u}{\partial t} &= \nabla \cdot \left[g\left(\|\nabla u\|^2 \right) \nabla u \right] \\ &= 2g'\left(\|\nabla u\|^2 \right) \left(\nabla u \cdot \mathbf{H}_u \nabla u \right) + g\left(\|\nabla u\|^2 \right) \Delta u,\end{aligned} \tag{2.13}$$

where $\mathbf{H}_u$ is the Hessian matrix of u. Perona and Malik chose such a process to preserve meaningful features such as edges while reducing irrelevant information such as noise in homogeneous areas. To this end, they set the diffusion function g as a function satisfying :

$$\begin{cases} g(0) = 1, \ \lim\limits_{s \to +\infty} g(s) = 0 \\ g'(s) \leq 0, \ g(s) > 0 \quad \text{for all } s \geq 0. \end{cases} \tag{2.14}$$

Several scientific works develop new adaptive diffusion processes for edge detection or image denoising by considering an appropriate diffusion function g [12, 60, 63, 13, 5, 52, 2, 6, 38, 43, 37]. From PM [40] perspective, we can define the *Nonlinear Scale Space*

$$u : \Omega \times (0, T] \to \mathbb{R} \tag{2.15}$$

as the family of derived images constructed by the PM nonlinear diffusion (2.13).

Next, we will examine and perform behavioral analysis on the PM equation (2.13) by investigating the relationship between the *smoothing-enhancing* properties, Koenderinck's causality requirement, and the diffusion function g at specific points such as local extrema or authentic edges [15].

Non-Enhancement of Local Extrema

One of the essential properties of scale-space, as mentioned earlier, is that there are fewer details at higher levels than at lower levels of scales [33]. To illustrate this requirement, the critical points, as defined below, are considered as part of the image structure.

Definition 2.3.1. (*Local Extrema*) At a certain scale level t.

- A point $(x;t) \in \Omega \times (0,T)$ is said to be a *critical point* for the real function u if $\nabla u(x;t) = \mathbf{0}$.
- At a critical point $(x;t)$, $u(x;t)$ is a *strict local maximum*(*minimum*) if the Hessian matrix of u is *negative* (*positive*) *definite*. In this case, $(x;t)$ is said to be a *local maximum* (*minimum*) *point*.

Thus, for some fixed scale level t, if a point $(x;t)$ is said to be a local maximum (minimum) for the PM scale-space representation u, then u must not increase (decrease) while t increases. In this regard, the following proposition will illustrate this nonenhancement property:

Proposition 2.3.1. *(Non-enhancement of local extrema [48]) While the scale parameter t increases and at a critical point $(x;t)$ where $\nabla u = \mathbf{0}$.*

$$\textit{No new local extrema is generated} \Leftrightarrow \operatorname{sign}(u_t) = \operatorname{sign}(\Delta u) \Leftrightarrow g(0) > 0. \tag{2.16}$$

Proof. At a critical point, we have $\nabla u = \mathbf{0}$. Then, by using the equation (2.13) we obtain

$$u_t = g(0)\,\Delta u. \tag{2.17}$$

Now, let us assume that $(x;t)$ is a local maximum where the Hessian matrix of u is negative definite and possesses negative eigenvalues α_+ and α_- as follows:

$$\alpha_{+/-} = \frac{1}{2}\left(\Delta u \pm \sqrt{\Delta u^2 - 4\det(\mathbf{H}_u)}\right) < 0, \tag{2.18}$$

where $\det(\mathbf{H}_u)$ is the determinant of the Hessian matrix $\mathbf{H}_u$.

Since

$$\alpha_+ + \alpha_- = \Delta u < 0. \tag{2.19}$$

Then, we conclude that:

$$\begin{aligned}\text{No new local maximum is created at } (x;t) &\Longleftrightarrow (u_t < 0) \text{ and } (\alpha_{+/-} < 0)\\ &\overset{(2.19)}{\Longleftrightarrow} (u_t < 0) \text{ and } (\Delta u < 0).\end{aligned}$$

Similarly, one proceeds and obtains:

$$\text{No new local minimum is created at } (x;t) \Longleftrightarrow (u_t > 0)\ \textit{and}\ (\Delta u > 0).$$

Thus, in either case, we have:

$$\begin{aligned}\text{No new local extrema is created at } (x;t) &\Longleftrightarrow \operatorname{sign}(u_t) = \operatorname{sign}(\Delta u)\\ &\overset{(2.17)}{\Longleftrightarrow} g(0) > 0.\end{aligned}$$

Which completes the proof. □

The requirement (2.16) prevents local extrema from being enhanced and thus avoids the creation of some false structures in the scale-space representation.

Smoothing-Enhancing of PM Diffusion

Perona and Malik illustrated by experiment in their paper [40] that their model filter shows remarkable results and outperforms the Marr-Hildreth and Canny filters by demonstrating that the edges are not blurred and remain sharp for a long time. The following reasons can explain this improvement:

(i) The PM diffusion filtering combines the smoothing of the homogeneous area with the edge detection operation in the same process.

(ii) The diffusion function g plays at the same time the role of selecting and thresholding the maximum gradient points.

To explain the first reason (i), we can write, using (2.32), the PM equation as

$$\begin{aligned}\frac{\partial u}{\partial t} &= 2\left\|\nabla u\right\|^2 g'\left(\left\|\nabla u\right\|^2\right) u_{\xi\xi} + g\left(\left\|\nabla u\right\|^2\right)\Delta u \\ &= \left[2\left\|\nabla u\right\|^2 g'\left(\left\|\nabla u\right\|^2\right) + g\left(\left\|\nabla u\right\|^2\right)\right] u_{\xi\xi} + g\left(\left\|\nabla u\right\|^2\right) u_{\eta\eta}.\end{aligned} \tag{2.20}$$

Therefore, in a neighborhood of $\left\|\nabla u\right\|^2 = 0$, the PM equation is equivalent to

$$\frac{\partial u}{\partial t} = g\left(0\right) u_{\xi\xi} + g\left(0\right) u_{\eta\eta} = g\left(0\right)\Delta u. \tag{2.21}$$

Thus, at the points where the image has a weak gradient, u locally satisfies (2.21), which means that the PM model acts as a forward parabolic equation at these points and smooths the homogeneous area. However, since g is a decreasing function, we can generally assume, for some $k > 0$, that

$$\begin{cases} 2\left\|\nabla u\right\|^2 g'\left(\left\|\nabla u\right\|^2\right) + g\left(\left\|\nabla u\right\|^2\right) > 0 & \left\|\nabla u\right\|^2 < k \\ 2\left\|\nabla u\right\|^2 g'\left(\left\|\nabla u\right\|^2\right) + g\left(\left\|\nabla u\right\|^2\right) < 0 & \left\|\nabla u\right\|^2 > k. \end{cases} \tag{2.22}$$

As a consequence, the PM model can be thought of as a forward-backward parabolic equation. In that case, the diffusion at edge points can be stopped or reversed, allowing the regions' boundaries to be preserved or enhanced.

For now, let us suppose that equation (2.13) has a sufficiently smooth solution u to bring an explanation to the second reason (ii). To analyze the PM equation's smoothing-enhancing properties at edge points, we need to examine the temporal variation of the gradient magnitude of u.

Proposition 2.3.2. *The temporal variation of the gradient magnitude of u is defined as follows [48]:*

$$\begin{aligned}\left(\left\|\nabla u\right\|^2\right)_t =& 8g''\left[\nabla u \cdot \boldsymbol{H}_u \nabla u\right]^2 \\ &+ 4g'\left[3\,\mathrm{tr}(\boldsymbol{H}_u)\left(\nabla u \cdot \boldsymbol{H}_u \nabla u\right) - 2\left\|\nabla u\right\|^2 \det\left(\boldsymbol{H}_u\right) + \left(\nabla u \cdot \boldsymbol{A}_u \nabla u\right)\right] \\ &+ 2g\,\mathrm{tr}(\boldsymbol{A}_u),\end{aligned} \tag{2.23}$$

where $g := g\left(\left\|\nabla u\right\|^2\right)$, *and*

$$\boldsymbol{A}_u = \begin{pmatrix} \nabla u \cdot \nabla u_{x_1x_1} & \nabla u \cdot \nabla u_{x_1x_2} \\ \nabla u \cdot \nabla u_{x_1x_2} & \nabla u \cdot \nabla u_{x_2x_2} \end{pmatrix}. \tag{2.24}$$

Proof. We have

$$\nabla g = \nabla g\left(\|\nabla u\|^2\right) = 2g'\mathbf{H}_u\nabla u. \tag{2.25}$$

By using the PM equation (2.13), we get

$$\left(\|\nabla u\|^2\right)_t = 2\nabla u\cdot\nabla u_t = 2\nabla u\cdot\nabla\left[\nabla g\cdot\nabla u + g\Delta u\right]. \tag{2.26}$$

Then, according to (2.25), we obtain

$$\begin{aligned}\left(\|\nabla u\|^2\right)_t =& 2\nabla u\cdot\nabla\left[2g'\left(\nabla u\cdot\mathbf{H}_u\nabla u\right)+g\Delta u\right]\\ =& 2\nabla u\cdot\left[2\left(\nabla u\cdot\mathbf{H}_u\nabla u\right)\nabla g' + 2g'\nabla\left(\nabla u\cdot\mathbf{H}_u\nabla u\right)+\Delta u\nabla g + g\nabla\left(\Delta u\right)\right].\end{aligned} \tag{2.27}$$

And knowing that

$$\begin{aligned}\nabla\left[\nabla u\cdot\mathbf{H}_u\nabla u\right] &= \mathbf{J}^{\top}_{\mathbf{H}_u\nabla u}\nabla u + \mathbf{J}^{\top}_{\nabla u}\mathbf{H}_u\nabla u\\ &= \mathbf{J}^{\top}_{\mathbf{H}_u\nabla u}\nabla u + \mathbf{H}_u^2\nabla u\\ &= 2\mathbf{H}_u^2\nabla u + \mathbf{A}_u\nabla u,\end{aligned} \tag{2.28}$$

where $\mathbf{J}^{\top}_{\mathbf{H}_u\nabla u}$ is the transpose of the Jacobian matrix of $\mathbf{H}_u\nabla u$, we get

$$\begin{aligned}\left(\|\nabla u\|^2\right)_t =& 2\nabla u\cdot\Big[4g''\left(\nabla u\cdot\mathbf{H}_u\nabla u\right)\mathbf{H}_u\nabla u + 2g'\left(2\mathbf{H}_u^2\nabla u+\mathbf{A}_u\nabla u\right)\\ &+ 2g'\Delta u\mathbf{H}_u\nabla u + g\nabla\left(\Delta u\right)\Big]\\ =& 8g''\left[\nabla u\cdot\mathbf{H}_u\nabla u\right]^2\\ &+ 4g'\Big[2\left(\nabla u\cdot\mathbf{H}_u^2\nabla u\right)+\left(\nabla u\cdot\mathbf{A}_u\nabla u\right)+\Delta u\left(\nabla u\cdot\mathbf{H}_u\nabla u\right)\Big]\\ &+ 2g\nabla u\cdot\nabla\left(\Delta u\right).\end{aligned} \tag{2.29}$$

Now, according to ***Cayley–Hamilton theorem*** the matrix $\mathbf{H}_u$ is annihilated by its characteristic polynomial. Which means that

$$\mathbf{H}_u^2 - \mathrm{tr}\left(\mathbf{H}_u\right)\mathbf{H}_u + \det\left(\mathbf{H}_u\right)\mathbf{I} = \mathbf{0}, \tag{2.30}$$

where $\mathbf{u}$ is the identity matrix. Then,

$$\nabla u\cdot\mathbf{H}_u^2\nabla u = \mathrm{tr}\left(\mathbf{H}_u\right)\left(\nabla u\cdot\mathbf{H}_u\nabla u\right) - \|\nabla u\|^2\det\left(\mathbf{H}_u\right). \tag{2.31}$$

Finally, by inserting the equation (2.31) into (2.29), we can obtain (2.23). This finishes completes the proof. □

Now, before describing the smoothing-enhancing properties for PM diffusion, we first represent the two conditions (2.11) and (2.12) in a more simplified manner (as it is shown in [48]):

Proposition 2.3.3. *The conditions* (2.11) *and* (2.12) *are equivalent to:*

$$u_{\xi\xi} = \frac{1}{\|\nabla u\|^2}\left[\nabla u \cdot \boldsymbol{H}_u \nabla u\right] = 0, \tag{2.32}$$

$$u_{\xi\xi\xi} = \frac{1}{\|\nabla u\|^3}\left[\nabla u \cdot \boldsymbol{A}_u \nabla u\right] < 0. \tag{2.33}$$

Proof. We know that

$$u_\xi = \nabla u \cdot \frac{1}{\|\nabla u\|}\nabla u = \|\nabla u\|. \tag{2.34}$$

Since,

$$u_{\xi\xi} = \nabla u_\xi \cdot \frac{1}{\|\nabla u\|}\nabla u = \nabla\left(\|\nabla u\|\right) \cdot \frac{1}{\|\nabla u\|}\nabla u \tag{2.35}$$

and

$$\nabla\left(\|\nabla u\|\right) = \frac{1}{\|\nabla u\|}\mathbf{H}_u \nabla u. \tag{2.36}$$

Then, we obtain the second directional derivative of u in the gradient direction that corresponds to (2.11):

$$u_{\xi\xi} = \frac{1}{\|\nabla u\|^2}\left[\nabla u \cdot \mathbf{H}_u \nabla u\right] = 0. \tag{2.37}$$

On the other hand, we have

$$\begin{aligned} u_{\xi\xi\xi} &= \nabla u_{\xi\xi} \cdot \frac{1}{\|\nabla u\|}\nabla u \\ &= \nabla\left[\frac{1}{\|\nabla u\|^2}\left(\nabla u \cdot \mathbf{H}_u \nabla u\right)\right] \cdot \frac{1}{\|\nabla u\|}\nabla u \\ &= \left[\left(\nabla u \cdot \mathbf{H}_u \nabla u\right)\nabla\left(\frac{1}{\|\nabla u\|^2}\right) + \frac{1}{\|\nabla u\|^2}\nabla\left(\nabla u \cdot \mathbf{H}_u \nabla u\right)\right] \cdot \frac{1}{\|\nabla u\|}\nabla u. \end{aligned} \tag{2.38}$$

Since,

$$\nabla\left(\frac{1}{\|\nabla u\|^2}\right) = \frac{-2}{\|\nabla u\|^4}\mathbf{H}_u \nabla u. \tag{2.39}$$

By using (2.28), we get

$$u_{\xi\xi\xi} = \frac{1}{\|\nabla u\|^3}\left[-2\left(\frac{\nabla u \cdot \mathbf{H}_u \nabla u}{\|\nabla u\|}\right)^2 + 2\left(\nabla u \cdot \mathbf{H}_u^2 \nabla u\right) + \left(\nabla u \cdot \mathbf{A}_u \nabla u\right)\right]. \tag{2.40}$$

Finally, by inserting (2.31) into (2.40), we obtain:

$$u_{\xi\xi\xi} = \frac{1}{\|\nabla u\|^3}\left[-2\left(\frac{\nabla u \cdot \mathbf{H}_u \nabla u}{\|\nabla u\|}\right)^2 + 2\,\mathrm{tr}\left(\mathbf{H}_u\right)\left(\nabla u \cdot \mathbf{H}_u \nabla u\right) - 2\,\|\nabla u\|^2 \det\left(\mathbf{H}_u\right) + \left(\nabla u \cdot \mathbf{A}_u \nabla u\right)\right]. \tag{2.41}$$

Now, by considering the condition (2.32) and the fact that $\mathbf{H}_u$ is a real symmetric matrix, we can derive the following:

$$u_{\xi\xi} = \alpha_+ \cos^2(\varphi) + \alpha_- \sin^2(\varphi) = 0, \tag{2.42}$$

where $\alpha_{+/-}$ are the eigenvalues of $\mathbf{H}_u$ and φ is the angle between $\boldsymbol{v}$ and an eigenvector of α_+. Which leads us to three cases [47]:

1. If $\alpha_+ = \alpha_- = 0$, then we have a *flat* shape, which is a case that has to be excluded.
2. If $\alpha_+ \times \alpha_- < 0$, then we obtain *saddle* shapes, that are not considered as edges; This case is also excluded.
3. If $\begin{cases} \alpha_+ = 0, \varphi \equiv 0 \mod(\pi) \\ \alpha_- = 0, \varphi \equiv \frac{\pi}{2} \mod(\pi) \end{cases}$ then we have *cylindrical* shapes.

Accordingly, the only case that corresponds to edge shapes is the third one, which means that

$$\det\left(\mathbf{H}_u\right) = \alpha_+ \times \alpha_- = 0. \tag{2.43}$$

Thus, by considering this result with that of (2.37), we conclude from equation (2.41) that

$$u_{\xi\xi\xi} = \frac{1}{\|\nabla u\|^3}\left[\nabla u \cdot \mathbf{A}_u \nabla u\right] < 0. \tag{2.44}$$

Which ends the demonstration. □

Since, the matrix $\mathbf{A}_u$ is negative definite (2.33). Then its eigenvalues μ_+ and μ_- satisfy

$$\mu_+ + \mu_- = \mathrm{tr}\left(\mathbf{A}_u\right) < 0, \tag{2.45}$$

where $\mathrm{tr}\left(\mathbf{A}_u\right)$ is the trace of $\mathbf{A}_u$. Moreover, we can express $\mu_{+/-}$ as

$$\mu_{+/-} = \frac{1}{2}\left(\mathrm{tr}\left(\mathbf{A}_u\right) \pm \sqrt{\mathrm{tr}\left(\mathbf{A}_u\right)^2 - 4\left|\mathbf{A}_u\right|}\right) = \frac{\mathrm{tr}\left(\mathbf{A}_u\right)}{2}\beta_{+/-} \tag{2.46}$$

such that

$$\beta_{+/-} = 1 \pm \sqrt{1 - 4\frac{\left|\mathbf{A}_u\right|}{\mathrm{tr}\left(\mathbf{A}_u\right)^2}} \tag{2.47}$$

and

$$\begin{cases} 1 \leq \beta_+ < 2 \\ 0 < \beta_- \leq 1. \end{cases} \tag{2.48}$$

On the other hand, since $\mathbf{A}_u$ is a real symmetric matrix. Then, there exists an orthogonal matrix $\mathbf{O}$ such that

$$\mathbf{A}_u = \frac{1}{2}\operatorname{tr}(\mathbf{A}_u)\,\mathbf{O}\Lambda\mathbf{O}^{-1} = \frac{1}{2}\operatorname{tr}(\mathbf{A}_u)\,\mathbf{O}\Lambda\mathbf{O}^{\top}, \tag{2.49}$$

where Λ is the real diagonal matrix

$$\Lambda = \begin{pmatrix} \beta_- & 0 \\ 0 & \beta_+ \end{pmatrix}, \tag{2.50}$$

and the eigenvectors $\boldsymbol{a}_1$ and $\boldsymbol{a}_2$ are the corresponding columns of $\mathbf{O}$.

Now we provide our main result that considers the relationship between the diffusion function g and the smoothing-enhancing properties of the PM diffusion.

Proposition 2.3.4. *At a maximum gradient point where the two conditions (2.32) and (2.33) are met, we have the following results [48]:*

$$\begin{aligned} \textit{The edge is enhanced by (2.13)} &\Longleftrightarrow \left(\|\nabla u(x;t)\|^2\right)_t > 0 \\ &\Longleftrightarrow \|\nabla u\|^2 g'\left(\|\nabla u\|^2\right) Q(\boldsymbol{w}) + g\left(\|\nabla u\|^2\right) < 0. \end{aligned} \tag{2.51}$$

$$\begin{aligned} \textit{The edge is smoothed by (2.13)} &\Longleftrightarrow \left(\|\nabla u(x;t)\|^2\right)_t < 0 \\ &\Longleftrightarrow \|\nabla u\|^2 g'\left(\|\nabla u\|^2\right) Q(\boldsymbol{w}) + g\left(\|\nabla u\|^2\right) > 0. \end{aligned} \tag{2.52}$$

Where, Q denotes the quadratic form associated to Λ and $\boldsymbol{w} = (\xi\cdot\boldsymbol{a}_1 \quad \xi\cdot\boldsymbol{a}_2)^{\top}$ is a unit vector such that:

$$\beta_- \leq Q(\boldsymbol{w}) \leq \beta_+. \tag{2.53}$$

Proof. Suppose that the conditions (2.32) and (2.33) are satisfied. We have $\det(\mathbf{H}_u) = 0$ and according to proposition 2.3.2, we get:

$$\left(\|\nabla u\|^2\right)_t = 4g'\left(\|\nabla u\|^2\right)(\nabla u\cdot\mathbf{A}_u\nabla u) + 2g\left(\|\nabla u\|^2\right)\operatorname{tr}(\mathbf{A}_u). \tag{2.54}$$

Substituting (2.49) into the equation (2.54), we find:

$$\begin{aligned} \left(\|\nabla u\|^2\right)_t =& 4g'\left(\|\nabla u\|^2\right)\nabla u\cdot\left(\frac{1}{2}\operatorname{tr}(\mathbf{A}_u)\,\mathbf{O}\Lambda\mathbf{O}^{\top}\right)\nabla u + 2g\left(\|\nabla u\|^2\right)\operatorname{tr}(\mathbf{A}_u) \\ =& 2\operatorname{tr}(\mathbf{A}_u)\left[\|\nabla u\|^2 g'\left(\|\nabla u\|^2\right)\left(\xi^{\top}\mathbf{O}\Lambda\mathbf{O}^{\top}\xi\right) + g\left(\|\nabla u\|^2\right)\right]. \end{aligned} \tag{2.55}$$

Then, by putting $\boldsymbol{w} = \mathbf{O}^\top \xi$ and $Q(\boldsymbol{w}) = \boldsymbol{w}^\top \Lambda \boldsymbol{w}$. We obtain:

$$\left(\|\nabla u\|^2\right)_t = 2\,\mathrm{tr}\left(\mathbf{A}_u\right)\left[\|\nabla u\|^2 g'\left(\|\nabla u\|^2\right) Q(\boldsymbol{w}) + g\left(\|\nabla u\|^2\right)\right]. \tag{2.56}$$

As long as $\mathrm{tr}\left(\mathbf{A}_u\right) < 0$ (2.45), we conclude that

$$\mathrm{sign}\left[\left(\|\nabla u\|^2\right)_t\right] = -\,\mathrm{sign}\left[\|\nabla u\|^2 g'\left(\|\nabla u\|^2\right) Q(\boldsymbol{w}) + g\left(\|\nabla u\|^2\right)\right]. \tag{2.57}$$

Since

$$\|\boldsymbol{w}\| = \sqrt{(\xi\cdot\boldsymbol{a}_1)^2 + (\xi\cdot\boldsymbol{a}_2)^2} = \sqrt{\cos^2(\theta) + \cos^2\left(\frac{\pi}{2} - \theta\right)} = 1, \tag{2.58}$$

where θ is the angle between ξ and $\boldsymbol{a}_1$. Then we get

$$Q(\boldsymbol{w}) = \beta_- \cos^2(\theta) + \beta_+ \sin^2(\theta) \tag{2.59}$$

and

$$\beta_- \leq Q(\boldsymbol{w}) \leq \beta_+. \tag{2.60}$$

Which terminates the proof. □

Remark 1. if $g' = 0$ and $g = \kappa \in \mathbb{R}$, then

$$\left(\|\nabla u\|^2\right)_t = 2\kappa\,\mathrm{tr}\left(\mathbf{A}_u\right) \tag{2.61}$$

with $\mathrm{tr}\left(\mathbf{A}_u\right) < 0$. In that case, we realize the *Heat* equation and the edge is smoothed if $\kappa > 0$ and is enhanced if $\kappa < 0$.

Remark 2. For every increasing strictly positive (decreasing strictly negative) real function g, the edges are smoothed (enhanced) during the diffusion process (2.13).

Remark 3. In the one-dimensional case, We consider $u : (x;t) \in \Omega \times \mathbb{R}_+ \to u(x;t) \in \mathbb{R}$ such that $\Omega \subset \mathbb{R}$. Perona and Malik investigated the following diffusion process:

$$\begin{aligned} u_t &= \left[g\left(u_x^2\right) u_x\right]_x \\ &= \left[\phi(u_x)\right]_x. \end{aligned} \tag{2.62}$$

If there exists a sufficiently smooth solution u to the above equation, then we have

$$\begin{aligned} \left(u_x^2\right)_t &= 2u_x (u_x)_t \\ &= 8u_x^4 u_{xx}^2 g''\left(u_x^2\right) + 4u_x^2\left(3u_{xx}^2 + u_x u_{xxx}\right) g'\left(u_x^2\right) + 2u_x u_{xxx} g\left(u_x^2\right). \end{aligned} \tag{2.63}$$

Therefore, at edge location where $u_{xx} = 0$, $u_x u_{xxx} < 0$, we have:

$$\begin{aligned} \text{The edge is enhanced by (2.62)} &\Longleftrightarrow \left(u_x^2\right)_t = 2u_x u_{xxx}\left[2u_x^2 g'\left(u_x^2\right) + g\left(u_x^2\right)\right] > 0 \\ &\Longleftrightarrow 2u_x^2 g'\left(u_x^2\right) + g\left(u_x^2\right) < 0 \\ &\Longleftrightarrow \phi'\left(u_x\right) < 0. \end{aligned} \tag{2.64}$$

$$\begin{aligned} \text{The edge is smoothed by (2.62)} &\Longleftrightarrow \left(u_x^2\right)_t = 2u_x u_{xxx}\left[2u_x^2 g'\left(u_x^2\right) + g\left(u_x^2\right)\right] < 0 \\ &\Longleftrightarrow 2u_x^2 g'\left(u_x^2\right) + g\left(u_x^2\right) > 0 \\ &\Longleftrightarrow \phi'\left(u_x\right) > 0. \end{aligned} \tag{2.65}$$

Where ϕ is the flux function defined as $\phi\left(u_x\right) = g\left(u_x^2\right) u_x$.

Now, we can present an explanation to (ii) of (2.3.2) by setting examples for the diffusion function:

Example 1. If we take for example the diffusion functions, proposed by Perona and Malik,

$$g_1(s) = \exp\left(-\frac{s}{\lambda^2}\right) \tag{2.66}$$

and

$$g_2(s) = \frac{1}{1 + \frac{s}{\lambda^2}}, \tag{2.67}$$

where $\lambda > 0$ is a threshold parameter.

- In one-dimensional case: we have

$$2u_x^2 g_1'\left(u_x^2\right) + g_1\left(u_x^2\right) = \left[1 - 2\left(\frac{u_x}{\lambda}\right)^2\right] \exp\left(-\left(\frac{u_x}{\lambda}\right)^2\right) \tag{2.68}$$

and

$$2u_x^2 g_2'\left(u_x^2\right) + g_2\left(u_x^2\right) = \frac{1 - \left(\frac{u_x}{\lambda}\right)^2}{\left[1 + \left(\frac{u_x}{\lambda}\right)^2\right]^2}. \tag{2.69}$$

Therefore, for some scale t and at a local maximum point x, we conclude that

$$\left|u_x(x;t)\right| > K \Rightarrow \left(u_x^2\right)_t (x;t) > 0, \tag{2.70}$$

$$\left|u_x(x;t)\right| < K \Rightarrow \left(u_x^2\right)_t (x;t) < 0, \tag{2.71}$$

where $K = \frac{\lambda}{\sqrt{2}}$ if we use the first diffusion function g_1 (2.66), and $K = \lambda$ if we take the second diffusion function g_2 (2.67).

- In two-dimensional case: We have the following results:

If we use the first diffusion equation g_1 (2.66), we have

$$\|\nabla u\|^2 g_1'\left(\|\nabla u\|^2\right) Q(\boldsymbol{w}) + g_1\left(\|\nabla u\|^2\right) = \left[1 - \left(\frac{\|\nabla u\|}{\lambda}\right)^2 Q(\boldsymbol{w})\right] \exp\left(-\left(\frac{\|\nabla u\|}{\lambda}\right)^2\right). \tag{2.72}$$

Then, we can deduce for some scale t and at a local maximum point x

$$\|\nabla u(x;t)\| > \frac{\lambda}{\sqrt{Q(\boldsymbol{w})}} \Rightarrow \left(\|\nabla u\|^2\right)_t (x;t) > 0, \tag{2.73}$$

$$\|\nabla u(x;t)\| < \frac{\lambda}{\sqrt{Q(\boldsymbol{w})}} \Rightarrow \left(\|\nabla u\|^2\right)_t (x;t) < 0. \tag{2.74}$$

If we use the second diffusion equation g_2 (2.67), we have

$$\|\nabla u\|^2 g_2'\left(\|\nabla u\|^2\right) Q(\boldsymbol{w}) + g_2\left(\|\nabla u\|^2\right) = \frac{1 + (1 - Q(\boldsymbol{w}))\left(\frac{\|\nabla u\|}{\lambda}\right)^2}{\left[1 + \left(\frac{\|\nabla u\|}{\lambda}\right)^2\right]^2}. \tag{2.75}$$

Then, from (2.47) and (2.59) one can derive

$$\begin{aligned} 1 - Q(\boldsymbol{w}) &= 1 - \left(\beta_- \cos^2(\theta) + \beta_+ \sin^2(\theta)\right) \\ &= (1 - \beta_-)\cos^2(\theta) + (1 - \beta_+)\sin^2(\theta) \\ &= (1 - \beta_-)\left(\cos^2(\theta) - \sin^2(\theta)\right). \end{aligned} \tag{2.76}$$

Therefore,

- $Q(\boldsymbol{w}) = 1 \Leftrightarrow \beta_- = \beta_+ = 1 \quad \text{or} \quad \theta = \frac{\pi}{4} + \frac{k\pi}{2}, k \in \mathbb{Z}$
  $\Leftrightarrow (\nabla u \cdot \nabla u_{x_1x_1} - \nabla u \cdot \nabla u_{x_2x_2})^2 + 4(\nabla u \cdot \nabla u_{x_1x_2})^2 = 0 \quad \text{or} \quad \theta = \frac{\pi}{4} + \frac{k\pi}{2}, k \in \mathbb{Z}$
  $\Leftrightarrow \mathbf{A}_u = (\nabla u \cdot \nabla u_{x_1x_1})\mathbf{I} = (\nabla u \cdot \nabla u_{x_2x_2})\mathbf{I} \quad \text{or} \quad \theta = \frac{\pi}{4} + \frac{k\pi}{2}, k \in \mathbb{Z},$
- $Q(\boldsymbol{w}) > 1 \Leftrightarrow \theta \in \cup_{k\in\mathbb{Z}} \left]\frac{\pi}{4} + k\pi, \frac{3\pi}{4} + k\pi\right[,$
- $Q(\boldsymbol{w}) < 1 \Leftrightarrow \theta \in \cup_{k\in\mathbb{Z}} \left]-\frac{\pi}{4} + k\pi, \frac{\pi}{4} + k\pi\right[.$

Thus, at a particular scale t and a local maximum point x, we conclude that

$$\begin{cases} \|\nabla u\| > \frac{\lambda}{\sqrt{Q(\boldsymbol{w})-1}} \\ \theta \in \cup_{k\in\mathbb{Z}} \left]\frac{\pi}{4} + k\pi, \frac{3\pi}{4} + k\pi\right[\end{cases} \Longrightarrow \left(\|\nabla u\|^2\right)_t (x;t) > 0, \tag{2.77}$$

$$\left.\begin{array}{l} \begin{cases} \|\nabla u\| < \frac{\lambda}{\sqrt{Q(\boldsymbol{w})-1}} \\ \theta \in \cup_{k\in\mathbb{Z}} \left]\frac{\pi}{4}+k\pi, \frac{3\pi}{4}+k\pi\right[\end{cases} \\ \text{or} \\ \mathbf{A}_u = \rho\mathbf{I}, \rho \in \mathbb{R}^*_- \\ \text{or} \\ \theta \in \cup_{k\in\mathbb{Z}} \left[-\frac{\pi}{4}+k\pi, \frac{\pi}{4}+k\pi\right] \end{array}\right\} \Longrightarrow \left(\|\nabla u\|^2\right)_t (x;t) < 0. \tag{2.78}$$

Consequently, on the whole, we can conclude from the above results that the maximum gradients points (edges) verifying conditions that lead to $\left(\|\nabla u\|^2\right)_t (x;t) > 0$ are preserved or enhanced during the diffusion process. On the other hand, however, edges that do not satisfy conditions that lead to $\left(\|\nabla u\|^2\right)_t (x;t) > 0$ are smoothed during the PM diffusion.

Example 2. The second example concerns the Charbonnier diffusion function [13]:

$$g_3(s) = \frac{1}{\sqrt{1+\frac{s}{\lambda^2}}}, \text{ where } \lambda > 0. \tag{2.79}$$

Then, by using this function in the result of proposition 2.3.4, we get:

$$\|\nabla u\|^2 g_3'\left(\|\nabla u\|^2\right) Q(\boldsymbol{w}) + g_3\left(\|\nabla u\|^2\right) = \frac{2+(2-Q(\boldsymbol{w}))\left(\frac{\|\nabla u\|}{\lambda}\right)^2}{2\left(\sqrt{1+\left(\frac{\|\nabla u\|}{\lambda}\right)^2}\right)^3}. \tag{2.80}$$

Then, as long as $Q(\boldsymbol{w}) < 2$, the Charbonnier diffusion process smooths the edges constantly.

As can be seen from these examples, we can first assume that the diffusion function's choice directly impacts the behavior of the PM equation at essential locations like edges. Secondly, we have seen that this behavior also changes with dimension; that is, at the edge locations and in contrast to the one-dimensional case, the diffusion behavior in the two-dimensional case depends not only on the threshold parameter λ but also on a local structure expressed by the matrix $\mathbf{A}_u$.

In conclusion, we can presume from the above analysis that the PM equation generalizes and combines the two classical methods, specifically the edge detection and scale-space theories, in only one approach. Besides, this combination has allowed the PM equation to be one of the leading restoration techniques in image processing and analysis.

Some Theoretical Results around PM Equation

Unfortunately, the PM equation presents some theoretical difficulties due to its forward-backward nature, as we have seen earlier. In this respect, the nonmonotonicity of the flux function

$$f(s) = \frac{s}{1 + \left(\frac{s}{\lambda}\right)^2} \tag{2.81}$$

proposed by Perona and Malik made the existence of solutions hard to prove; for more detailed information, we refer to [54] and the references therein. In this context, several attempts have been suggested to provide a mathematical investigation of the PM equation. Kawohl and Kutev [31] proved in one dimension that the PM equation does not have global weak $\mathcal{C}^2$ solutions for initial data that involve backward diffusion. Kichenassamy [32] provides a new notion of generalized solutions that are piecewise linear and contain jumps. You et al. [63] analyzed the energy functional leading to the PM equation as the steepest descent method and proved that such energy has an infinite number of global minima, which are dense in the image space. So, this makes the process unstable for even weak perturbations of the initial image.

Under some challenging conditions, the existence and uniqueness of weak solutions for the PM model have been investigated in the bounded variation space $BV(\Omega)$ [4]. In some other functional frameworks, Wang and Zhou have thoroughly studied in [52] and proved the existence and uniqueness of weak solutions in the Orlicz space $LlogL(\Omega)$ using a new diffusion function

$$g(s) = \begin{cases} \frac{s+(s+1)\log(s+1)}{s(s+1)} & \text{for all } s > 0 \\ 2 & \text{for } s = 0. \end{cases} \tag{2.82}$$

Perona and Malik Regularized models

In case of the need to keep the desired purpose of the forward-backward PM diffusion, one has to introduce a regularization method to stabilize the PM process and make the problem well-posed. Catté et al. [12] proposed inserting the regularization directly into the PM equation by replacing the image gradient in the diffusion function $g\left(\|\nabla u\|^2\right)$ with a smooth version of it $G_\sigma * \nabla u$, where G_σ is a smoothing kernel defined as in (2.7) with $\sigma = \sqrt{2t}$. Catté et al. suggested the following regularized model:

$$\begin{cases} \frac{\partial u}{\partial t}(x;t) = \nabla \cdot \left[g\left(\|(\nabla G_\sigma * u)(x;t)\|^2 \right) \nabla u(x;t) \right] \\ u(x;0) = u_0(x). \end{cases} \tag{2.83}$$

The existence, uniqueness and regularity of a solution for $\sigma > 0$ have been proven in [12]. After that, various studies and analyses for this model were made by Whitaker and Pizer [60] on the regularization parameter σ. Moreover, a thorough examination of the impact of the threshold parameter of this

model has been accomplished by [35].

Another regularized method for the PM equation proposed to restore images using the energy method. Image restoration is considered a necessary preprocessing step for applications that rely on image quality, such as segmentation and pattern recognition. Hence, many researchers showed great interest in using the variational approach [44, 63, 5, 13, 9, 7, 62, 8, 34, 37], which attempts to seek a solution among the minima of some energy functional, which generally has the form:

$$\min_{u} \left\{ F(u) := \int_{\Omega} \left(\phi\left(|\nabla u|\right) + \frac{\rho}{2}\left(u - u_0\right)^2 \right) d\Omega \right\}, \tag{2.84}$$

where

- $\Omega \subset \mathbb{R}^2$ is an open bounded domain,
- u_0 and u are the observed and the reconstructed images defined as functions of $\Omega \subset \mathbb{R}^2 \longrightarrow \mathbb{R}$ that associate each pixel $x \in \Omega$ to the gray level $u(x)$ or $u_0(x)$,
- $\phi : \mathbb{R}^+ \to \mathbb{R}$ is a nonnegative increasing function with $\phi(0) = 0$,
- $\rho \in \mathbb{R}_+$, is a weighting parameter that enables to adjust the influence of the data term in the regularizing term.

For a moment, let us assume that a particular smooth function u is a minimizer of $F(u)$. Then, using variational calculus, one can prove that this function is a solution to the Euler-Lagrange equation

$$\rho\left(u - u_0\right) = \nabla \cdot \left[\frac{\phi'\left(|\nabla u|\right)}{|\nabla u|} \nabla u \right] \tag{2.85}$$

with homogeneous Neumann boundary conditions. Thus, by denoting

$$g(s) = \frac{\phi'(s)}{s} \quad \text{for all } s > 0, \tag{2.86}$$

one can regard the above elliptic PDE as a fully implicit time discretization of the PM diffusion equation; see [45, 57] for more details.

Many variational approaches have been developed during the last thirty years. The most famous one was the total variation (TV) denoising model suggested by Rudin et al. in their seminal paper [44]. In addition, several improved nonlinear diffusion models for image restoration derived from TV model have been proposed in the last twenty years; for more detailed information, we refer to [4, 7, 62, 8, 34, 37] and the references therein.

Furthermore, Weickert [55, 54] has carried out another regularization method for the PM equation leading to anisotropic nonlinear diffusion, as we will see in the following subsection.

2.3.3 Anisotropic Nonlinear Diffusion

As Weickert [54] pointed out, the isotropic nonlinear equation handles (2.13) an image feature with the same amount of blurring in all its directions. For instance, this process is not capable of successfully eliminating noises at edge locations (cf. Figure 2.2).

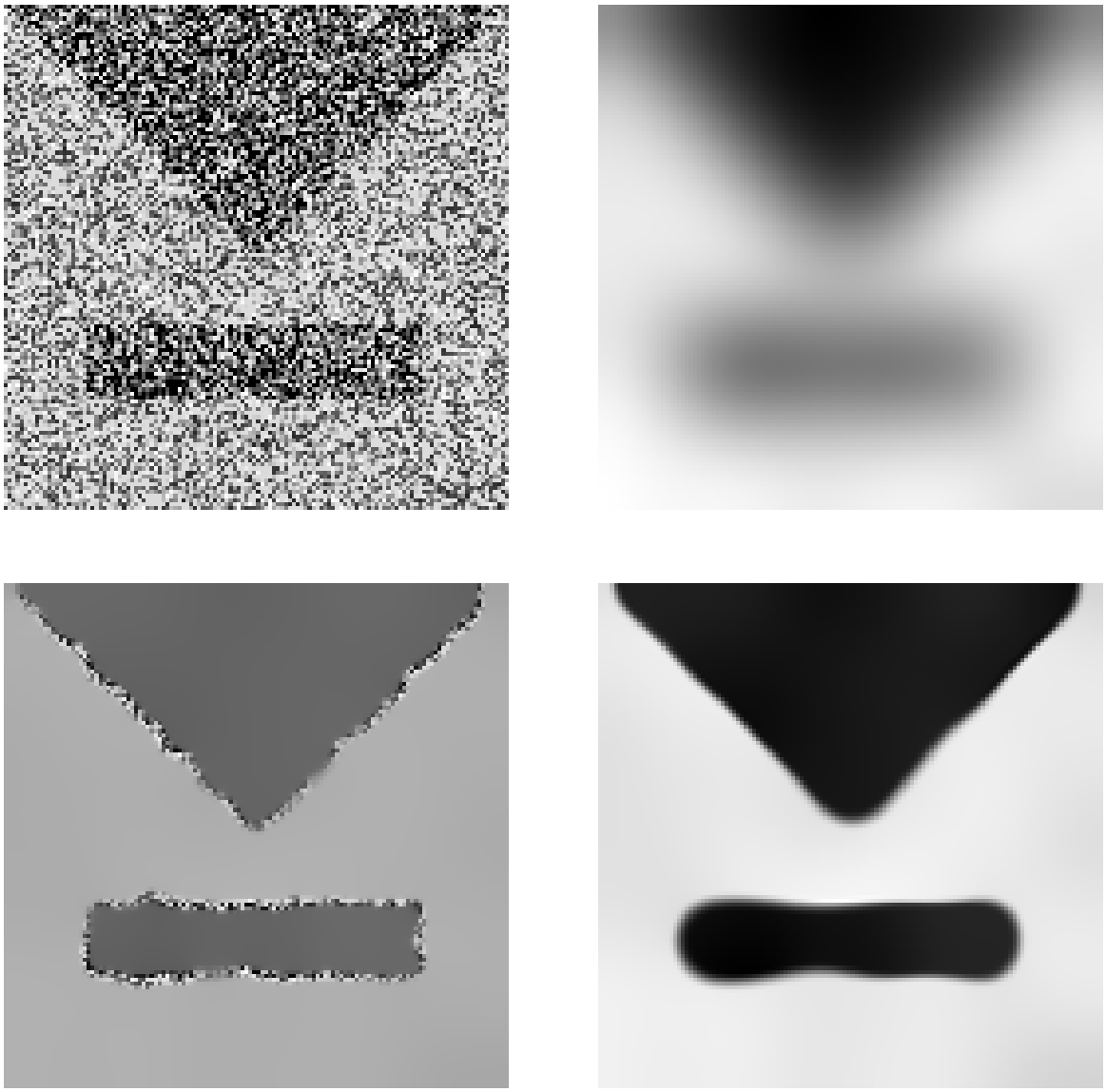

FIGURE 2.2: Image restoration of test image(128 x 128) [54]. TOP LEFT: Test image; TOP RIGHT: Linear diffusion filter, $t = 80$. BOTTOM LEFT: Nonlinear isotropic diffusion filter (Catté et al. model), $\lambda = 3.5$, $\sigma = 3$, $t = 8$. BOTTOM RIGHT: Nonlinear anisotropic diffusion filter, $\lambda = 3.5$, $\sigma = 3$, $t = 8$

To illustrate this observation, we can interpret for a moment the diffusion behavior of the following PM equation at edge locations

$$\frac{\partial u}{\partial t} = \left[2\left\|\nabla u\right\|^2 g'\left(\left\|\nabla u\right\|^2\right) + g\left(\left\|\nabla u\right\|^2\right)\right] u_{\xi\xi} + g\left(\left\|\nabla u\right\|^2\right) u_{\eta\eta}. \tag{2.87}$$

Therefore, to encourage diffusion along with edges rather than across them, we have to suppose that the coefficient of $u_{\xi\xi}$ goes to zero, while the coefficient of $u_{\eta\eta}$ does not disappear, which means that

$$\lim_{s\to\infty} 2sg'(s) + g(s) = 0 \tag{2.88}$$

and

$$\lim_{s\to\infty} g(s) > 0. \tag{2.89}$$

However, condition (2.89) contradicts the hypothesis on which the PM equation is based. Additionally, the above two conditions are not compatible, as it is asserted in [51].

Accordingly, it might be wise to consider the orientation of essential features by using anisotropic diffusion. Weickert introduced this property in his papers [55, 56] by defining at any point (x_1, x_2) in the space Ω, an orientation descriptor $\mathbf{D} = \mathbf{D}\left(J_\rho\left(\nabla u_\sigma\right)\right)$ using the structure tensor, which is convenient to identify features like corners and T-junctions [54]. In this case, the structure tensor is defined by

$$J_\rho\left(\nabla u_\sigma\right) := K_\rho * \left(\nabla u_\sigma \otimes \nabla u_\sigma\right) \quad (\rho \geq 0), \tag{2.90}$$

where u_σ represent the convolution of u with a Gaussian kernel, and K_ρ stands for the Gaussian

$$K_\rho(x) = \frac{1}{2\pi\rho^2} \exp\left(-\frac{|x|^2}{2\rho^2}\right). \tag{2.91}$$

The diffusion tensor $\mathbf{D}$ is obtained using the eigenvectors and eigenvalues of J_ρ as follows:

$$\mathbf{D} := f_+\left(\lambda_+, \lambda_-\right)\theta_+\theta_+^\top + f_-\left(\lambda_+, \lambda_-\right)\theta_-\theta_-^\top, \tag{2.92}$$

where $\lambda_{+/-}$ and $\theta_{+/-}$ are respectively the eigenvalues and eigenvectors of the tensor structure J_ρ and f is the function defined as (see [54]):

$$\begin{cases} f_-\left(\lambda_+, \lambda_-\right) = 1 \\ f_+\left(\lambda_+, \lambda_-\right) = g\left(\lambda_+\right), \end{cases} \tag{2.93}$$

where

$$g(s) := \begin{cases} 1 & (s \leq 0) \\ 1 - \exp\left(\frac{-C_m}{(s/\lambda)}\right) & (s > 0) \end{cases} \tag{2.94}$$

with $C_m = C_4 = 3.31488$, $\lambda > 0$.

Many research studies adopted this approach using different functions f (see, for example, [16, 25] and the reference therein). In the following, a new anisotropic nonlinear diffusion equation is provided and discussed.

2.4 The Proposed Model

This paragraph will discuss the reasons behind the choice of our proposed model. In book chapter [41], Perona et al. mentioned that the remarkable experimental results are performed using a discrete scheme that is consistent with the following anisotropic diffusion

$$\frac{\partial u}{\partial t} = \nabla \cdot \left[\begin{pmatrix} g\left(|u_{x_1}|\right) & 0 \\ 0 & g\left(|u_{x_2}|\right) \end{pmatrix} \begin{pmatrix} u_{x_1} \\ u_{x_2} \end{pmatrix} \right]. \tag{2.95}$$

Moreover, as noted earlier, the type (2.13) model uses the gradient magnitude as a local descriptor operator for the image edge detector. However, digital images present some difficulties in their discrete structure; they are discrete in space and intensity value. Consequently, one may need to adapt to the digital image structure and generalize the equation (2.95) by considering differential operators that respond to vertical, horizontal, and diagonal edges. Therefore, motivated by the above reasoning, we designed a new anisotropic nonlinear diffusion equation with a novel matrix diffusion tensor:

$$\frac{\partial u}{\partial t} - \nabla \cdot \left[\mathbf{D}_{\nabla u} \nabla u\right] = 0, \tag{2.96}$$

where $\mathbf{D}_{\nabla u}$, the diffusion tensor, is a real symmetric matrix of $\mathbb{R}^{2\times 2}$ defined as follows:

$$\mathbf{D}_{\nabla u} = \begin{pmatrix} g\left(|u_{x_1}|\right) + \frac{g\left(|u_{x_{12}}|\right)+g\left(|u_{x_{-12}}|\right)}{2} & \frac{g\left(|u_{x_{12}}|\right)-g\left(|u_{x_{-12}}|\right)}{2} \\ \frac{g\left(|u_{x_{12}}|\right)-g\left(|u_{x_{-12}}|\right)}{2} & g\left(|u_{x_2}|\right) + \frac{g\left(|u_{x_{12}}|\right)+g\left(|u_{x_{-12}}|\right)}{2} \end{pmatrix}, \tag{2.97}$$

$g : \mathbb{R}_+ \to \mathbb{R}$ is a positive function, and

$$\begin{cases} \partial_{x_1} u := u_{x_1} := \nabla u \cdot \mathbf{e}_1 \\ \partial_{x_2} u := u_{x_2} := \nabla u \cdot \mathbf{e}_2 \\ \partial_{x_{12}} u := u_{x_{12}} := \nabla u \cdot \mathbf{e}_{12} := \nabla u \cdot \frac{\mathbf{e}_1+\mathbf{e}_2}{|\mathbf{e}_1+\mathbf{e}_2|} \\ \partial_{x_{-12}} u := u_{x_{-12}} := \nabla u \cdot \mathbf{e}_{-12} := \nabla u \cdot \frac{-\mathbf{e}_1+\mathbf{e}_2}{|-\mathbf{e}_1+\mathbf{e}_2|}, \end{cases}$$

with $(\mathbf{e}_1, \mathbf{e}_2)$ is the canonical basis of $\mathbb{R}^2$. Besides, the matrix $\mathbf{D}_{\nabla u}$ has two eigenvalues $\lambda_{+/-}$ as follows:

$$\begin{aligned} \lambda_{+/-} = \frac{1}{2}\Big(& g\left(|u_{x_1}|\right) + g\left(|u_{x_2}|\right) + g\left(|u_{x_{12}}|\right) + g\left(|u_{x_{-12}}|\right) \\ & \pm \sqrt{\left(g\left(|u_{x_1}|\right) - g\left(|u_{x_2}|\right)\right)^2 + \left(g\left(|u_{x_{12}}|\right) - g\left(|u_{x_{-12}}|\right)\right)^2}\Big). \end{aligned} \tag{2.98}$$

Since $g > 0$ and

$$\begin{aligned}\lambda_- = \frac{1}{2\lambda_+}\Big[&2\left(g\left(|u_{x_1}|\right)g\left(|u_{x_2}|\right)+g\left(|u_{x_{12}}|\right)g\left(\left|u_{x_{-12}}\right|\right)\right)\\&+\left(g\left(|u_{x_1}|\right)+g\left(|u_{x_2}|\right)\right)\left(g\left(|u_{x_{12}}|\right)+g\left(\left|u_{x_{-12}}\right|\right)\right)\Big].\end{aligned} \tag{2.99}$$

Then, we deduce that the matrix $\mathbf{D}_{\nabla u}$ is a real symmetric positive definite matrix.

2.4.1 Description of the Proposed Model

Our model's main objective is to allow strong directional smoothing within the areas where $|u_{x_1}|$, $|u_{x_2}|$, $|u_{x_{12}}|$, or $\left|u_{x_{-12}}\right|$ is small and prevent blurring boundaries, contours, or corners that separate neighboring areas, where one or a combination of these differential operators have substantial value. Some sufficient assumptions have to be made to ensure our nonlinear diffusion meets acceptable behavior along these lines. Therefore, we can assume, as exhibited by Perona-Malik [40], some minimal hypotheses on g:

$$\begin{cases} g : \mathbb{R}_+ \to \mathbb{R} \text{ is } \mathcal{C}^1\text{-function such that } g(s) > 0,\ g'(s) \leq 0 \\ \lim\limits_{s\to 0} g(s) > 0,\ \lim\limits_{s\to\infty} g(s) = 0. \end{cases} \tag{2.100}$$

Besides, due to the decreasing positivity of the function g, it is evident that our model's behavior (2.96) encourages smoothing along edges in the $\mathbf{e}_1$, $\mathbf{e}_2$, $(\mathbf{e}_1+\mathbf{e}_2)$, or $(-\mathbf{e}_1+\mathbf{e}_2)$ directions and ceases across them.

To examine the parabolicity of the proposed model, we may first express the equation (2.96) and present it as:

Proposition 2.4.1. *The equation* (2.96) *is equivalent to:*

$$\begin{aligned}\frac{\partial u}{\partial t} =&\partial_{x_1}\left(g\left(|u_{x_1}|\right)u_{x_1}\right)+\partial_{x_2}\left(g\left(|u_{x_2}|\right)u_{x_2}\right)\\&+\partial_{x_{12}}\left(g\left(|u_{x_{12}}|\right)u_{x_{12}}\right)+\partial_{x_{-12}}\left(g\left(\left|u_{x_{-12}}\right|\right)u_{x_{-12}}\right).\end{aligned} \tag{2.101}$$

Proof. First, it is clear that

$$\partial_{x_1}\left(g\left(|u_{x_1}|\right)u_{x_1}\right)+\partial_{x_2}\left(g\left(|u_{x_2}|\right)u_{x_2}\right)=\nabla\cdot\left[\begin{pmatrix} g\left(|u_{x_1}|\right) & 0\\ 0 & g\left(|u_{x_2}|\right)\end{pmatrix}\begin{pmatrix}u_{x_1}\\ u_{x_2}\end{pmatrix}\right]. \tag{2.102}$$

On the other hand, we have

$$\begin{aligned}
&\partial_{x_{12}}\left(g\left(|u_{x_{12}}|\right)u_{x_{12}}\right)+\partial_{x_{-12}}\left(g\left(\left|u_{x_{-12}}\right|\right)u_{x_{-12}}\right)\\
&=\nabla\left(g\left(|u_{x_{12}}|\right)\nabla u\cdot\frac{e_1+e_2}{|e_1+e_2|}\right)\cdot\frac{e_1+e_2}{|e_1+e_2|}+\nabla\left(g\left(\left|u_{x_{-12}}\right|\right)\nabla u\cdot\frac{-e_1+e_2}{|-e_1+e_2|}\right)\cdot\frac{-e_1+e_2}{|-e_1+e_2|}\\
&=\frac{1}{2}\Big[\partial_{x_1}\left(g\left(|u_{x_{12}}|\right)\left(u_{x_1}+u_{x_2}\right)\right)+\partial_{x_2}\left(g\left(|u_{x_{12}}|\right)\left(u_{x_1}+u_{x_2}\right)\right)\\
&\qquad-\partial_{x_1}\left(g\left(\left|u_{x_{-12}}\right|\right)\left(-u_{x_1}+u_{x_2}\right)\right)+\partial_{x_2}\left(g\left(\left|u_{x_{-12}}\right|\right)\left(-u_{x_1}+u_{x_2}\right)\right)\Big]\\
&=\frac{1}{2}\Big[\partial_{x_1}\left(\left(g\left(|u_{x_{12}}|\right)+g\left(\left|u_{x_{-12}}\right|\right)\right)u_{x_1}\right)+\partial_{x_2}\left(\left(g\left(|u_{x_{12}}|\right)+g\left(\left|u_{x_{-12}}\right|\right)\right)u_{x_2}\right)\\
&\qquad+\partial_{x_2}\left(\left(g\left(|u_{x_{12}}|\right)-g\left(\left|u_{x_{-12}}\right|\right)\right)u_{x_1}\right)+\partial_{x_1}\left(\left(g\left(|u_{x_{12}}|\right)-g\left(\left|u_{x_{-12}}\right|\right)\right)u_{x_2}\right)\Big]\\
&=\frac{1}{2}\nabla\cdot\left[\left(g\left(|u_{x_{12}}|\right)+g\left(\left|u_{x_{-12}}\right|\right)\right)\begin{pmatrix}u_{x_1}\\u_{x_2}\end{pmatrix}+\left(g\left(|u_{x_{12}}|\right)-g\left(\left|u_{x_{-12}}\right|\right)\right)\begin{pmatrix}u_{x_2}\\u_{x_1}\end{pmatrix}\right]\\
&=\frac{1}{2}\nabla\cdot\left[\begin{pmatrix}\left(g\left(|u_{x_{12}}|\right)+g\left(\left|u_{x_{-12}}\right|\right)\right) & \left(g\left(|u_{x_{12}}|\right)-g\left(\left|u_{x_{-12}}\right|\right)\right)\\ \left(g\left(|u_{x_{12}}|\right)-g\left(\left|u_{x_{-12}}\right|\right)\right) & \left(g\left(|u_{x_{12}}|\right)+g\left(\left|u_{x_{-12}}\right|\right)\right)\end{pmatrix}\begin{pmatrix}u_{x_1}\\u_{x_2}\end{pmatrix}\right].
\end{aligned}\tag{2.103}$$

□

Now, let $\phi:\mathbb{R}_+\to\mathbb{R}$ be a function such that $\phi'(s)=sg(s)$.

Proposition 2.4.2. *For a sufficiently smooth function u, it is easy to show that the model (2.101) can be formulated as*

$$\frac{\partial u}{\partial t}=a_{11}u_{x_1x_1}+2a_{12}u_{x_1x_2}+a_{22}u_{x_2x_2},\tag{2.104}$$

where

$$\begin{aligned}
a_{11}&=\left[\phi''\left(|u_{x_1}|\right)+\frac{\phi''\left(|u_{x_{12}}|\right)+\phi''\left(\left|u_{x_{-12}}\right|\right)}{2}\right],\\
a_{12}=a_{21}&=\frac{\phi''\left(|u_{x_{12}}|\right)-\phi''\left(\left|u_{x_{-12}}\right|\right)}{2},\\
a_{22}&=\left[\phi''\left(|u_{x_2}|\right)+\frac{\phi''\left(|u_{x_{12}}|\right)+\phi''\left(\left|u_{x_{-12}}\right|\right)}{2}\right].
\end{aligned}\tag{2.105}$$

Proof. It is easy to make the following algebraic calculations:

$$\partial_{x_i}\left(g\left(|u_{x_i}|\right)u_{x_i}\right)=\phi''\left(|u_{x_i}|\right)u_{x_ix_i},\quad\text{for } i=1,2,\tag{2.106}$$

$$\partial_{x_{12}}\left(g\left(|u_{x_{12}}|\right)u_{x_{12}}\right)=\frac{1}{2}\phi''\left(|u_{x_{12}}|\right)\left(u_{x_1x_1}+2u_{x_1x_2}+u_{x_2x_2}\right),\tag{2.107}$$

and

$$\partial_{x_{-12}}\left(g\left(\left|u_{x_{-12}}\right|\right)u_{x_{-12}}\right)=\frac{1}{2}\phi''\left(\left|u_{x_{-12}}\right|\right)\left(u_{x_1x_1}-2u_{x_1x_2}+u_{x_2x_2}\right). \tag{2.108}$$

□

Therefore, the equation (2.104) is parabolic if and only if $\sum_{i,j=1,2} a_{i,j}\varsigma_i\varsigma_j \geq 0$, for all $\varsigma \in \mathbb{R}^2$. We can express the eigenvalues of the matrix $\left(a_{ij}\right)$ as follows

$$\alpha_{+/-}=\frac{1}{2}\left(a_{11}+a_{22}\pm\sqrt{\left(a_{11}-a_{22}\right)^2+4a_{12}^2}\right). \tag{2.109}$$

Thus, if $\phi'' \geq 0$, then the matrix $\left(a_{ij}\right)$ is symmetric positive semi-definite. Therefore, we conclude that our model (2.96) acts as a *forward parabolic equation*.

Moreover, we may provide another investigation analysis of our model by examining the eigenvalues and the eigenvectors of the matrix $\mathbf{D}_{\nabla u}$. The matrix $\mathbf{D}_{\nabla u}$ has two eigenvalues $\lambda_{+/-}$ with $\theta_{+/-}$ are the corresponding eigenvectors

$$\theta_{+/-}=\frac{\eta_{+/-}}{\left|\eta_{+/-}\right|}, \tag{2.110}$$

where

$$\eta_{+/-}=\begin{pmatrix} g\left(\left|u_{x_1}\right|\right)-g\left(\left|u_{x_2}\right|\right)\pm\sqrt{\left(g\left(\left|u_{x_1}\right|\right)-g\left(\left|u_{x_2}\right|\right)\right)^2+\left(g\left(\left|u_{x_{12}}\right|\right)-g\left(\left|u_{x_{-12}}\right|\right)\right)^2} \\ g\left(\left|u_{x_{12}}\right|\right)-g\left(\left|u_{x_{-12}}\right|\right) \end{pmatrix}, \tag{2.111}$$

provided that $\left|u_{x_{12}}\right| \neq \left|u_{x_{-12}}\right|$. We can then expand the first equation of (2.96) into

$$\frac{\partial u}{\partial t}=\nabla\cdot\left[\lambda_+\theta_+\theta_+^\top\nabla u\right]+\nabla\cdot\left[\lambda_-\theta_-\theta_-^\top\nabla u\right]. \tag{2.112}$$

Accordingly, the diffusion caused by (2.112) is measured by the $\lambda_{+/-}$ values and oriented towards $\theta_{+/-}$. Specifically, it is clear from the expression of $\lambda_{+/-}$ that $\lambda_+ \geq \lambda_- > 0$, which means that the diffusion towards θ_+ is privileged over θ_-. Furthermore, we can deduce the following results:

- In flat areas: we have

  $$\left\{\left|u_{x_1}\right|=\left|u_{x_2}\right| \text{ and } \left|u_{x_{12}}\right|=\left|u_{x_{-12}}\right|\right\} \Longleftrightarrow \left\{\left|u_{x_1}\right|=\left|u_{x_2}\right|=\left|u_{x_{12}}\right|=\left|u_{x_{-12}}\right|=0\right\}.$$

  Which means that, $\lambda_+=\lambda_-=2g\left(0\right)>0$. Then, the diffusion is isotropic, linear, and the smoothing effect is the same in all directions.

- At straight edges $(\lambda_+ > \lambda_- = 0)$:

  For instance, we can assume that $u_{x_1}=u_{x_2}$ and $\left|u_{x_1}\right| >> 0$. Then, we obtain $\left|u_{x_{-12}}\right|=0$ and $\left|u_{x_{12}}\right| >> 0$. Which implies that

$$\begin{cases} \lambda_+ = g(0), & \theta_+ = \left(\frac{1}{\sqrt{2}} \quad -\frac{1}{\sqrt{2}}\right)^\top \\ \lambda_- = 0, & \theta_- = \left(-\frac{1}{\sqrt{2}} \quad -\frac{1}{\sqrt{2}}\right)^\top. \end{cases}$$

Consequently, the diffusion process is anisotropic and oriented along the $(-\mathbf{e}_1 + \mathbf{e}_2)$ direction.

- At corners $(\lambda_+ \geq \lambda_- > 0)$:

  According to the characteristics of the function g, the diffusion is anisotropic and oriented along θ_+ and θ_- directions.

In fact, the difference $(\lambda_+ - \lambda_-)^2 = (g(|u_{x_1}|) - g(|u_{x_2}|))^2 + \left(g(|u_{x_{12}}|) - g\left(\left|u_{x_{-12}}\right|\right)\right)^2$ gives insights into our diffusion model's anisotropic property. In other words, it indicates the isotropic diffusion for the zero value and the anisotropic diffusion for larger values.

2.4.2 New Adaptive Diffusion Function using Hermite Spline

To construct an adaptive diffusion tensor, the function g is approximated numerically by a cubic Hermite splines [46] that interpolate numeric data specified at $0 = k_0 < k_1 < ... < k_m$ with $m \in \mathbb{N}^*$:

$$g(s) = \begin{cases} p_{k_i} P_{1,k_i k_{i+1}}(s) + v_{k_i} P_{2,k_i k_{i+1}}(s) \\ +p_{k_{i+1}} P_{1,k_{i+1} k_i}(s) + v_{k_{i+1}} P_{2,k_{i+1} k_i}(s) & s \in [k_i, k_{i+1}[\text{ and } i \in \{0,1,...,m-1\} \\ p_{k_m} g_{k_m,1}(s) + v_{k_m} g_{k_m,2}(s) & s \in [k_m, \infty[, \end{cases} \tag{2.113}$$

where $p_\cdot$ and $v_\cdot$ are the coefficients used to define the position and the velocity vector at a specific point, k_i are threshold parameters, $\left\{P_{j,cd}\right\}$ is the family of the basis functions composed of polynomials of degree 3 used on the interval $[c,d[$ such that

$$\begin{cases} P_{1,cd}(s) = \frac{(s-d)^2(2s+d-3c)}{(d-c)^3} \\ P_{2,cd}(s) = \frac{(s-d)^2(s-c)}{(d-c)^2}. \end{cases} \tag{2.114}$$

Moreover, we may consider

$$\begin{cases} g_{k_m,1}(s) = \frac{k_m}{\log(k_m)+2} \frac{2s(\log(s)+1) - k_m \log(k_m)}{s^2} \\ g_{k_m,2}(s) = \frac{k_m^2}{\log(k_m)+2} \frac{s(\log(s)+1) - k_m(\log(k_m)+1)}{s^2}. \end{cases} \tag{2.115}$$

Various tools can be used to examine the existence of solutions for nonlinear PDEs, such as variational techniques, compact imbedding theorems,monotonicity method, fixed-point theorems, iterative methods, and truncation techniques; For more detailed information, we refer to [30, 4, 52, 1, 64, 17,

14, 34, 25] and the references therein. The following subsection will discuss the strategy used to prove the existence and uniqueness of weak solutions for the proposed model (2.96).

2.5 Strategies for solving the proposed PDE

To conduct a mathematical analysis of the proposed model, we will adopt the general procedure that investigates nonlinear PDEs through weak convergence methods [18, 17]. So, let us consider that we want to solve PDEs under the following abstract form:

$$\mathbf{P}[u] = 0, \tag{2.116}$$

where $\mathbf{P}[.]$ denotes a nonlinear operator, and u is the unknown. Thus, we first need to carefully choose an appropriate functional space where the problem (2.116) is solvable. Next, an approximation method can be utilized to extract good approximating problems that are solvable. These problems can be written as

$$\mathbf{P}_n[u_n] = 0 \ \ (n = 1, 2, ...), \tag{2.117}$$

where $\mathbf{P}_n[.]$ denotes a nonlinear operator, which is in some way approximates $\mathbf{P}[.]$ for a large enough n, and u_n is a solution. Different approximation methods can be found in the literature; For instance, one can apply the Faedo-Galerkin approximations, regularization techniques, iterative methods, or variational approaches. Finally, we expect the sequence of functions $\{u_n\}_{n=1}^{\infty}$ to converge in a sense to a solution u for the problem (2.116).

Nevertheless, It should be noted that selecting either the functional framework or the approximation method to prove the existence of a solution is crucial. On the one hand, with the infinite-dimensional functional spaces and uniform bounded solutions $\{u_n\}_{n=1}^{\infty}$, we can only confirm the weak convergence of $\{u_n\}_{n=1}^{\infty}$ $\left(\text{ or a subsequence of } \{u_n\}_{n=1}^{\infty}\right)$ to a limit u using the reflexivity property of the functional space, for example.

$$u_n \rightharpoonup u \quad \text{as } n \to \infty. \tag{2.118}$$

On the other hand, the approximation methods mentioned above are not equivalent since they can generally produce different a priori estimates for approximate solutions for the problem (2.117).

Moreover, some difficulties also arise because of the nonlinearity of the operators; If we can build approximate nonlinear operators $\mathbf{P}_n[.]$ that somehow tend to $\mathbf{P}[.]$, it is by no means certain that this leads to justifying passing to limits within the nonlinearity:

$$\mathbf{P}_n[u_n] \to \mathbf{P}[u] \quad \text{as } n \to \infty. \tag{2.119}$$

Therefore, to overcome these difficulties, we introduce the following strategy to conduct a theoretical analysis of the proposed model:

- First of all, we will study, in Chapter 3, the boundary-value problem:

$$\begin{cases} \rho\left(u-u_0\right)-div\left(\mathbf{D}_{\nabla u}\nabla u\right)=0 & \text{in } \Omega \\ \left\langle \mathbf{D}_{\nabla u}\nabla u,\mathbf{n}\right\rangle =0 & \text{on } \partial\Omega. \end{cases} \tag{2.120}$$

We will demonstrate that this elliptic PDE represents the Euler-Lagrange equation associated with the minimization problem of the following energy functional:

$$E\left(u\right)=\int_{\Omega}\left(\left[\phi\left(\left|u_{x_1}\right|\right)+\phi\left(\left|u_{x_2}\right|\right)+\phi\left(\left|u_{x_{12}}\right|\right)+\phi\left(\left|u_{x_{-12}}\right|\right)\right]+\frac{\rho}{2}\left(u-u_0\right)^2\right)dx, \tag{2.121}$$

where $\rho>0$ and $\phi:\mathbb{R}_+\to\mathbb{R}$ is a $\mathcal{C}^2$ function. We will prove that a solution to the Euler-Lagrange equation is equivalent to a minimizer of $E\left(u\right)$. Then, we will establish the existence and uniqueness of weak solutions for problem (2.120) using the variational approach and monotonicity property.

- Secondly, we will examine, in Chapter 4, the proposed initial-boundary value problem:

$$\begin{cases} \frac{\partial u}{\partial t}-\nabla\cdot\left[\mathbf{D}_{\nabla u}\nabla u\right]=0 & \text{in } \Omega\times\left(0,T\right] \\ \left\langle \mathbf{D}_{\nabla u}\nabla u,\mathbf{n}\right\rangle =0 & \text{on } \partial\Omega\times\left(0,T\right] \\ u\left(x;0\right)=u_0\left(x\right) & \text{in } \Omega. \end{cases} \tag{2.122}$$

By adopting the implicit iterative method (discretization in time-variable only), we approximate the nonlinear evolution problem (2.122) through nonlinear elliptic problems. On the one hand, the existence of solutions for these elliptic problems are proven based on Chapter 3. On the other hand, the existence of a unique solution for the proposed model (2.122) is proven using the monotonicity property of the nonlinear operator.

2.6 Conclusion

The following items can summarize this chapter:

1. We have presented the diffusion phenomenon's physical background and have used standard terminology to classify different diffusion equations applied in image processing and analysis.

2. We have mentioned the idea of Perona and Malik in combining two approaches, namely scale-space and edge detection theories, in one model described by a nonlinear isotropic PDE.

3. We have reviewed the anisotropic property established by Weickert concerning the smoothing along edges rather than across them and have shown its importance in reducing noises at edge locations.

4. We have constructed a new nonlinear anisotropic diffusion model in two-dimensional space based on the digital image structure.

5. We have concluded this chapter with a possible strategy to analyze the proposed model.

Chapter 3

Quasilinear Second-Order Elliptic Equation and variational problems

3.1 Introduction

This chapter will investigate the existence and uniqueness of solutions for the following quasilinear second-order elliptic problem:

$$\begin{cases} \rho\,(u-u_0) - div\,(\mathbf{D}_{\nabla u}\nabla u) = 0 & \text{in } \Omega \\ \langle \mathbf{D}_{\nabla u}\nabla u, \mathbf{n}\rangle = 0 & \text{on } \partial\Omega, \end{cases} \tag{3.1}$$

where

- Ω is an open bounded domain of $\mathbb{R}^2$ with Lipschitz boundary $\partial\Omega$,
- $\rho > 0$ is a real positive number,
- u_0 represents a continuous image,
- $\mathbf{D}_{\nabla u}$ is the diffusion tensor defined in (2.97),
- $\langle .,. \rangle$ denotes the Euclidean scalar product in $\mathbb{R}^2$,
- $\mathbf{n}$ is the unit outward normal vector on $\partial\Omega$.

In the next section, we will first present the mathematical framework to establish the theoretical results. Then, we will provide few notations, consider some assumptions, and exhibit preliminary results needed for the analysis. Next, in Section 3.3, we will consider a new convex variational problem and discuss its connection to the above quasilinear second-order elliptic PDE. Finally, we will examine the existence of a unique solution for the above boundary value problem in Section 3.4.

3.2 Notations, Assumptions, and Preliminary Results

First, we assume that u_0 is in $L^2(\Omega)$, and we use the following space $\mathcal{A}$ as a functional framework to discuss solutions of the boundary-value problem (3.1):

$$\mathcal{A} = \left\{ u \in L^2(\Omega) \cap W^{1,1}(\Omega) \;\middle|\; \nabla u \in \left[LlogL^{k_m}(\Omega) \right]^2 \right\}, \tag{3.2}$$

where $LlogL^{k_m}(\Omega)$ is an Orlicz space (see [3]) defined as

$$LlogL^{k_m}(\Omega) := \left\{ u : \Omega \to \mathbb{R} \;\middle|\; \int_{\Omega \cap \{|u| \geq k_m\}} |u| \log(|u|)\, dx < \infty \right\}. \tag{3.3}$$

Next, we supply a few notations and consider some assumptions that will help simplify the theory in this chapter and the next. To this end, we follow the notations set in [17], and let L be a function, called the *Lagrangian*, defined as

$$L : \mathbb{R}^2 \times \mathbb{R} \times \overline{\Omega} \to \mathbb{R}, \tag{3.4}$$

such that

$$L = L(p, z, x) = L(p_1, p_2, z, x_1, x_2) \tag{3.5}$$

for $p \in \mathbb{R}^2$, $z \in \mathbb{R}$, and $x \in \Omega$. Therefore, we denote by p the name of the variable for which we substitute ∇u, z the variable for which we substitute $u(x)$, and we set

$$\begin{cases} D_p L = \left(L_{p_1}, L_{p_2} \right)^\top \\ D_z L = L_z \\ D_x L = \left(L_{x_1}, L_{x_2} \right)^\top. \end{cases} \tag{3.6}$$

After that, we define a $\mathcal{C}^2$ real-valued function ϕ on $[0, \infty)$ by

$$\phi(s) = \int_0^s r g(r)\, dr \quad \text{for all } s \geq 0 \tag{3.7}$$

satisfying the following properties:

$$\begin{cases} \phi(s) > 0,\ \phi'(s) > 0 & \text{for all } s > 0 \\ \phi''(s) \geq 0,\ s\phi''(s) \leq \phi'(s) & \text{for all } s \geq 0 \\ \phi(0) = \phi'(0) = 0,\ \phi''(0) > 0 & \\ 0 < \lim\limits_{s \to \infty} \dfrac{\phi(s)}{s \log(s)} < \infty,\ 0 < \lim\limits_{s \to \infty} \dfrac{\phi'(s)}{\log(s)} < \infty & \\ \lim\limits_{s \to \infty} \dfrac{\phi(s)}{s} = +\infty,\ \lim\limits_{s \to \infty} \dfrac{\phi'(s)}{s} = 0. & \end{cases} \tag{3.8}$$

Therefore, we can deduce from the expression of g (2.113) that

$$\phi(s) = \begin{cases} C_i + \sum_{j=0}^{3} \frac{A_{k_i k_{i+1},j}}{j+2} s^{j+2} & s \in [k_i, k_{i+1}[,\ i \in \{0,1,...,m-1\} \\ C_m + A_{k_m,1} \log(s) + A_{k_m,2} s \log(s) & s \in [k_m, \infty[, \end{cases} \tag{3.9}$$

where, for every $i \in \{0,1,...,m-1\}$, C_i is a constant determined by the continuity of ϕ at k_i. In this case, the values of the coefficients $A_{k_i k_{i+1},j}$ can be determined experimentally provided that ϕ satisfies the above conditions (3.8) on $[0, k_m[$. Besides, we may introduce some sufficient conditions on k_m and $A_{k_m,\cdot}$ that guarantee the properties of ϕ on $[k_m, \infty[$:

$$\begin{cases} k_m \geq 1 \\ A_{k_m,2} > 0 \\ A_{k_m,1} < k_m A_{k_m,2} \\ A_{k_m,1} \geq -\frac{k_m \log(k_m)}{2} A_{k_m,2}. \end{cases} \tag{3.10}$$

Finally, we introduce the following lemma that will be used in this chapter and the next:

Lemma 3.2.1. *(Monotonicity & Convexity)*

Suppose $\phi : \mathbb{R}_+ \to \mathbb{R}_+$ is a C^2 convex function. Then for all $\xi_0, \xi_1 \in \mathbb{R}^2$, we have

$$\left(\boldsymbol{D}_{\xi_1} \xi_1 - \boldsymbol{D}_{\xi_0} \xi_0 \right) \cdot (\xi_1 - \xi_0) \geq 0, \tag{3.11}$$

where $\boldsymbol{D}_{\xi_\cdot}$ is the symmetric positive definite matrix introduced in (2.97). In this case, the vector field $\xi \in \mathbb{R}^2 \longmapsto \boldsymbol{D}_\xi \xi \in \mathbb{R}^2$ is called monotone.

Proof. For each $t \in [0,1]$, we put $\xi_t = (1-t)\xi_0 + t\xi_1$. Then, we have

$$\begin{aligned} \mathbf{D}_{\xi_1} \xi_1 - \mathbf{D}_{\xi_0} \xi_0 = & \int_0^1 d\left[(\xi_t \cdot \mathbf{e}_1) g(|\xi_t \cdot \mathbf{e}_1|) \mathbf{e}_1 \right] \\ & + \int_0^1 d\left[(\xi_t \cdot \mathbf{e}_2) g(|\xi_t \cdot \mathbf{e}_2|) \mathbf{e}_2 \right] \\ & + \int_0^1 d\left[(\xi_t \cdot \mathbf{e}_{12}) g(|\xi_t \cdot \mathbf{e}_{12}|) \mathbf{e}_{12} \right] \\ & + \int_0^1 d\left[(\xi_t \cdot \mathbf{e}_{-12}) g(|\xi_t \cdot \mathbf{e}_{-12}|) \mathbf{e}_{-12} \right]. \end{aligned} \tag{3.12}$$

Since $\phi''(s) = g(s) + sg'(s) \geq 0$, then we conclude

$$\begin{aligned}\mathbf{D}_{\xi_1}\xi_1 - \mathbf{D}_{\xi_0}\xi_0 = &\int_0^1 \left[\phi''\left(|\xi_t \cdot \mathbf{e}_1|\right)\left((\xi_1 - \xi_0)\cdot \mathbf{e}_1\right)\mathbf{e}_1\right] dt \\ &+ \int_0^1 \left[\phi''\left(|\xi_t \cdot \mathbf{e}_2|\right)\left((\xi_1 - \xi_0)\cdot \mathbf{e}_2\right)\mathbf{e}_2\right] dt \\ &+ \int_0^1 \left[\phi''\left(|\xi_t \cdot \mathbf{e}_{12}|\right)\left((\xi_1 - \xi_0)\cdot \mathbf{e}_{12}\right)\mathbf{e}_{12}\right] dt \\ &+ \int_0^1 \left[\phi''\left(|\xi_t \cdot \mathbf{e}_{-12}|\right)\left((\xi_1 - \xi_0)\cdot \mathbf{e}_{-12}\right)\mathbf{e}_{-12}\right] dt\end{aligned} \tag{3.13}$$

and

$$\begin{aligned}\left(\mathbf{D}_{\xi_1}\xi_1 - \mathbf{D}_{\xi_0}\xi_0\right)\cdot(\xi_1 - \xi_0) = &\int_0^1 \left[\phi''\left(|\xi_t \cdot \mathbf{e}_1|\right)\left((\xi_1 - \xi_0)\cdot \mathbf{e}_1\right)^2\right] dt \\ &+ \int_0^1 \left[\phi''\left(|\xi_t \cdot \mathbf{e}_2|\right)\left((\xi_1 - \xi_0)\cdot \mathbf{e}_2\right)^2\right] dt \\ &+ \int_0^1 \left[\phi''\left(|\xi_t \cdot \mathbf{e}_{12}|\right)\left((\xi_1 - \xi_0)\cdot \mathbf{e}_{12}\right)^2\right] dt \\ &+ \int_0^1 \left[\phi''\left(|\xi_t \cdot \mathbf{e}_{-12}|\right)\left((\xi_1 - \xi_0)\cdot \mathbf{e}_{-12}\right)^2\right] dt \geq 0.\end{aligned} \tag{3.14}$$

Which completes the proof. □

3.3 The Variational Problem

The primary purpose of this section is to prove that any solution to the boundary-value problem (3.1) represents a minimizer for an energy functional and vice versa. Hence, by using the four directional derivatives ∂_{x_1}, ∂_{x_2}, $\partial_{x_{12}}$, $\partial_{x_{-12}}$, we propose the following energy minimization problem:

$$\min_{u\in\mathcal{A}} E(u), \tag{3.15}$$

such that

$$\begin{aligned}E(u) &= \int_\Omega \left(\left[\phi\left(|u_{x_1}|\right) + \phi\left(|u_{x_2}|\right) + \phi\left(|u_{x_{12}}|\right) + \phi\left(\left|u_{x_{-12}}\right|\right)\right] + \frac{\rho}{2}\left(u - u_0\right)^2\right) dx \\ &= \int_\Omega L\left(\nabla u, u, x\right) dx.\end{aligned} \tag{3.16}$$

Before showing the connection of this energy minimization problem to the boundary-value problem (3.1), we first need to show some growth conditions on L and its derivatives.

Lemma 3.3.1. *Let u and v be two elements of $\mathcal{A}$, and fix an element $t \in \mathbb{R}$. The Lagrangian L satisfies the following growth conditions:*

$$\begin{aligned} |L(\nabla u + t\nabla v, u + tv, x)| \leq & \sum_{j=1,2} C_{1,j} \left|u_{x_j}\right| \left(\log\left(\left|u_{x_j}\right|\right) + 1\right) \\ & + \sum_{j=1,2} C_{2,j} \left|v_{x_j}\right| \left(\log\left(\left|v_{x_j}\right|\right) + 1\right) \\ & + C_3\left(u^2 + v^2 + u_0^2\right) + C_4, \end{aligned} \tag{3.17}$$

$$\begin{aligned} \left|L_{p_i}(\nabla u + t\nabla v, u + tv, x)\, v_{x_i}\right| \leq & C\left|v_{x_i}\right| + \sum_{j=1,2} C_{1,j} \left|u_{x_j}\right| \log\left(\left|u_{x_j}\right|\right) \\ & + \sum_{j=1,2} C_{2,j} \left|v_{x_j}\right| \log\left(\left|v_{x_j}\right|\right) \qquad \text{for } i = 1,2, \end{aligned} \tag{3.18}$$

$$\left|L_z(\nabla u + t\nabla v, u + tv, x)\, v\right| \leq C\left[u^2 + u_0^2 + v^2\right] \tag{3.19}$$

for some constants C, $C_{1,j}$, $C_{2,j}$, C_3, and C_4 that may depend on t.

Proof. We have

$$|L(\nabla u + t\nabla v, u + tv, x)| \leq 4\phi\left(|\nabla u| + |t|\,|\nabla v|\right) + \frac{\rho}{2}\left(u + tv - u_0\right)^2, \tag{3.20}$$

$$\left|L_{p_i}(\nabla u + t\nabla v, u + tv, x)\, v_{x_i}\right| \leq 3\phi'\left(|\nabla u| + |t|\,|\nabla v|\right)|v_{x_i}| \qquad \text{for } i = 1,2, \tag{3.21}$$

and

$$|L_z(\nabla u + t\nabla v, u + tv, x)\, v| = |\rho\left(u + tv - u_0\right) v| \leq \frac{\rho}{2}\left[\left(u^2 + u_0^2 + 2\left(1 + t\right) v^2\right]\right. . \tag{3.22}$$

Then, we can distinguish between two cases in (3.20) and (3.21):

- $|\nabla u| + |t|\,|\nabla v| < k_m$:

$$|L(\nabla u + t\nabla v, u + tv, x)| \leq 4\phi\left(k_m\right) + \rho\left(2u^2 + 2t^2v^2 + u_0^2\right), \tag{3.23}$$

$$\left|L_{p_i}(\nabla u + t\nabla v, u + tv, x)\, v_{x_i}\right| \leq 3\phi'\left(k_m\right)|v_{x_i}| \qquad \text{for } i = 1,2. \tag{3.24}$$

- $|\nabla u| + |t|\,|\nabla v| \geq k_m$:

  Since

$$\lim_{s\to+\infty} \frac{\phi(s)}{s\log(s)} = \lim_{s\to+\infty} \frac{\phi'(s)}{\log(s)} = A_{k_m,2} > 0, \tag{3.25}$$

  then for fixed $\epsilon_1, \epsilon_2 > 0$, we may find an $l = k_m$ such that for all $s \geq l$

$$\phi(s) \leq M_1 s\log(s), \ \phi'(s) \leq M_2\log(s), \tag{3.26}$$

where $M_1 = \epsilon_1 + A_{k_m,2}$ and $M_2 = \epsilon_2 + A_{k_m,2}$. Thus, using Jensen's inequality (A.9), we can write

$$\begin{aligned}
|L(\nabla u + t\nabla v, u + tv, x)| \leq & 4M_1 (|\nabla u| + |t||\nabla v|) \log (|\nabla u| + |t||\nabla v|) \\
& + \rho \left(2u^2 + 2t^2v^2 + u_0^2\right) \\
\leq & 4M_1 \Bigg[\log (2 + 2|t|) (|\nabla u| + |t||\nabla v|) \\
& + \sum_{i=1,2} (|u_{x_i}| \log (|u_{x_i}|) + |t||v_{x_i}| \log (|v_{x_i}|)) \Bigg] \\
& + \rho \left(2u^2 + 2t^2v^2 + u_0^2\right).
\end{aligned} \tag{3.27}$$

On the other hand, we also have for $i = 1, 2$

$$\begin{aligned}
\left|L_{p_i} (\nabla u + t\nabla v, u + tv, x) v_{x_i}\right| \leq & 3M_2 \log (|\nabla u| + |t||\nabla v|) |v_{x_i}| \\
\leq & 3M_2 \Bigg[\log (2 + 2|t|) |v_{x_i}| \\
& + (|\nabla u| + |t||\nabla v|) \log \left(\frac{|\nabla u| + |t||\nabla v|}{2 + 2|t|} \right) \Bigg] \\
\leq & 3M_2 \Bigg[\log (2 + 2|t|) |v_{x_i}| \\
& + \sum_{j=1,2} \left(\left|u_{x_j}\right| \log \left(\left|u_{x_j}\right| \right) + |t| \left|v_{x_j}\right| \log \left(\left|v_{x_j}\right| \right) \right) \Bigg].
\end{aligned} \tag{3.28}$$

□

Next, we define a weak solution for problem (3.1):

Definition 3.3.1. A function $u \in \mathcal{A}$ is called a weak solution for problem (3.1) if for any $v \in \mathcal{A}$, we have

$$\int_\Omega \rho (u - u_0) v dx + \int_\Omega \mathbf{D}_{\nabla u} \nabla u \cdot \nabla v dx = 0. \tag{3.29}$$

Now, we state the main result for this section:

Theorem 3.3.2. *Assume that $u \in \mathcal{A}$, then*

$$E(u) = \min_{w \in \mathcal{A}} E(w) \Longleftrightarrow u \text{ is a weak solution for problem (3.1).}$$

Proof. First, we suppose that $u \in \mathcal{A}$ such that $E(u) = \min_{w \in \mathcal{A}} E(w)$. Then we have

$$u + tv \in \mathcal{A} \tag{3.30}$$

for any $v \in \mathcal{A}$ and $t \neq 0$ sufficiently small. Thus, according to (3.16)

$$r(t) := E(u + tv) \tag{3.31}$$

is well defined in an interval near zero. Besides, the difference quotient is expressed as

$$\begin{aligned} \frac{r(t) - r(0)}{t} &= \int_\Omega \frac{L(\nabla u + t\nabla v, u + tv, x) - L(\nabla u, u, x)}{t} dx \\ &= \int_\Omega L^t(x)\, dx, \end{aligned} \tag{3.32}$$

where

$$L^t(x) := \frac{L(\nabla u + t\nabla v, u + tv, x) - L(\nabla u, u, x)}{t} \quad \text{for a.e. } x \in \Omega. \tag{3.33}$$

Moreover, it is obvious to see that

$$L^t(x) \longrightarrow L_{p_1}(\nabla u, u, x)\, v_{x_1} + L_{p_2}(\nabla u, u, x)\, v_{x_2} + L_z(\nabla u, u, x)\, v \quad \text{a.e.} \tag{3.34}$$

as $t \to 0$ and

$$\begin{aligned} L^t(x) &= \frac{1}{t}\int_0^t \frac{d}{ds} L(\nabla u + s\nabla v, u + sv, x)\, ds \\ &= \frac{1}{t}\int_0^t \big[L_{p_1}(\nabla u + s\nabla v, u + sv, x)\, v_{x_1} + L_{p_2}(\nabla u + s\nabla v, u + sv, x)\, v_{x_2} \\ &\qquad + L_z(\nabla u + s\nabla v, u + sv, x)\, v\big] ds. \end{aligned} \tag{3.35}$$

As we return to the results showed in lemma 3.3.1, and knowing that $u_0 \in L^2(\Omega)$ and $u, v \in \mathcal{A}$, it is straightforward to deduce for $t \neq 0$ the following

$$\begin{aligned} |L^t(x)| \leq C \Bigg[\sum_{j=1,2} \Big(\Big|u_{x_j}\Big| \Big(\log\Big(\Big|u_{x_j}\Big|\Big) + 1\Big) + \Big|v_{x_j}\Big| \Big(\log\Big(\Big|v_{x_j}\Big|\Big) + 1\Big)\Big) \\ + \left(u^2 + v^2 + u_0^2\right) \Bigg] \in L^1(\Omega). \end{aligned} \tag{3.36}$$

Therefore, according to *Dominated Convergence Theorem*, we can conclude that $r'(0)$ exists and

$$r'(0) = \lim_{t\to 0} \frac{r(t) - r(0)}{t} = \int_\Omega \left[L_{p_1}(\nabla u, u, x)\, v_{x_1} + L_{p_2}(\nabla u, u, x)\, v_{x_2} + L_z(\nabla u, u, x)\, v\right] dx. \tag{3.37}$$

But, since r is minimized at $t = 0$ and E is minimized at u, it follows then

$$\begin{aligned}\int_{\Omega}\Bigg[&\left(\frac{\phi'\left(|u_{x_1}|\right)}{|u_{x_1}|}u_{x_1}+\frac{\phi'\left(|u_{x_{12}}|\right)}{\sqrt{2}\,|u_{x_{12}}|}u_{x_{12}}-\frac{\phi'\left(|u_{x_{-12}}|\right)}{\sqrt{2}\,|u_{x_{-12}}|}u_{x_{-12}}\right)v_{x_1}\\&+\left(\frac{\phi'\left(|u_{x_2}|\right)}{|u_{x_2}|}u_{x_2}+\frac{\phi'\left(|u_{x_{12}}|\right)}{\sqrt{2}\,|u_{x_{12}}|}u_{x_{12}}+\frac{\phi'\left(|u_{x_{-12}}|\right)}{\sqrt{2}\,|u_{x_{-12}}|}u_{x_{-12}}\right)v_{x_2}\\&+\rho\left(u-u_0\right)v\Bigg]dx=0.\end{aligned}\tag{3.38}$$

Which is equivalent to (after some elementary calculations as in the proof of Proposition 2.4.1)

$$\int_{\Omega}\mathbf{D}_{\nabla u}\nabla u\cdot\nabla v dx+\int_{\Omega}\rho\left(u-u_0\right)v dx=0.\tag{3.39}$$

Finally, we conclude that u is a weak solution for the boundary-value problem (3.1).

Conversely, we suppose that $u\in\mathcal{A}$ is a weak solution for the boundary-value problem (3.1). Since the mapping $(\nabla u,u)\longmapsto L\left(\nabla u,u,x\right)$ is convex, then we have

$$\begin{aligned}&L\left(\nabla u,u,x\right)+D_pL\left(\nabla u,u,x\right)\cdot\left(\nabla w\left(x\right)-\nabla u\left(x\right)\right)\\&\qquad+D_zL\left(\nabla u,u,x\right)\left(w\left(x\right)-u\left(x\right)\right)\leq L\left(\nabla w,w,x\right)\quad\text{for any } w\in\mathcal{A}.\end{aligned}\tag{3.40}$$

By integrating over Ω and letting $v=w-u$, we deduce from (3.29) that

$$E\left(u\right)\leq E\left(w\right),\ \text{for all } w\in\mathcal{A},\tag{3.41}$$

which concludes the proof. □

As presented above, we have demonstrated that resolving the boundary-value problem (3.1) is equivalent to seeking a minimizer for the energy functional $E\left(u\right)$.

The following section will discuss the existence and uniqueness of solutions for the problem (3.1) using the variational approach and the monotonicity of a nonlinear operator (3.11).

3.4 Existence and Uniqueness

In this section, we investigate at the outset the existence of weak solutions for the Euler-Lagrange equation (3.1) by minimizing the associated energy functional $E\left(u\right)$ as defined in (3.16). To this end, we will follow three steps described by three lemmas.

First, we need to show the existence of a convergent minimizing sequence in the weak topology:

Lemma 3.4.1. *There exists a minimizing sequence* $\{u_m\}_{m=1}^{\infty}$ *in* $\mathcal{A}$ *such that*

$$\lim_{m\to\infty} E(u_m) = \inf_{u\in\mathcal{A}} E(u) \leq E(u), \text{ for all } u \in \mathcal{A}. \tag{3.42}$$

Furthermore, there exist a subsequence $\left\{u_{m_j}\right\}_{j=1}^{\infty}$ *of* $\{u_m\}_{m=1}^{\infty}$ *and a function* $\widetilde{u} \in L^2(\Omega) \cap W^{1,1}(\Omega)$ *such that*

$$u_{m_j} \rightharpoonup \widetilde{u} \text{ weakly in } L^2(\Omega) \cap W^{1,1}(\Omega). \tag{3.43}$$

Proof. 1. On the one hand, since E is bounded below by zero on $\mathcal{A}$, then it must have a greatest lower bound $\inf_{u\in\mathcal{A}} E(u)$, and therefore there exists a minimizing sequence $\{u_m\}_{m=1}^{\infty}$ in $\mathcal{A}$ such that

$$\lim_{m\to\infty} E(u_m) = \inf_{u\in\mathcal{A}} E(u) \tag{3.44}$$

and

$$E(u_m) < E(0) + 1, \tag{3.45}$$

where $E(0) = \frac{\rho}{2}\int_\Omega u_0^2 dx$. Accordingly, we can get

$$\begin{aligned}\int_\Omega u_m^2 dx &= \int_\Omega (u_m - u_0 + u_0)^2 dx \\ &\leq 2\int_\Omega (u_m - u_0)^2 + 2\int_\Omega u_0^2 dx \\ &\leq \frac{4}{\rho}(E(u_m) + E(0)) \\ &\leq \frac{4}{\rho}(2E(0) + 1).\end{aligned} \tag{3.46}$$

It follows then

$$\sup_m \|u_m\|_{L^2(\Omega)} < \infty. \tag{3.47}$$

2. On the other hand, by fixing any $\alpha > 0$, we may find $\beta = k_m > 0$ such that for all $s \geq k_m$, $\phi(s) \geq \alpha s$. Then, we deduce the following

$$\begin{aligned}\int_\Omega |\partial_{x_i} u_m| dx &= \int_{\Omega\cap\{|\partial_{x_i}u_m|<k_m\}} |\partial_{x_i} u_m| dx + \int_{\Omega\cap\{|\partial_{x_i}u_m|\geq k_m\}} |\partial_{x_i} u_m| dx \\ &\leq k_m |\Omega| + \frac{1}{\alpha}\int_{\Omega\cap\{|\partial_{x_i}u_m|\geq k_m\}} \phi(|\partial_{x_i} u_m|) dx \\ &\leq k_m |\Omega| + \frac{1}{\alpha} E(u_m) \\ &\leq k_m |\Omega| + \frac{1}{\alpha}(E(0) + 1) \quad \text{for } i = 1, 2.\end{aligned} \tag{3.48}$$

It follows then

$$\sup_m \|\partial_{x_i} u_m\|_{L^1(\Omega)} < \infty. \tag{3.49}$$

Moreover, for an $\epsilon > 0$ sufficiently small, we let $\alpha_\epsilon = \frac{E(0)+1}{\epsilon}$ and choose $l \geq k_m \geq 1$ such that for all $s \geq l$, we have $\phi(s) > \alpha_\epsilon s$. Hence

$$\begin{aligned}\int_{\Omega\cap\{|\partial_{x_i}u_m|\geq l\}} |\partial_{x_i}u_m|\,dx &\leq \frac{1}{\alpha_\epsilon}\int_{\Omega\cap\{|\partial_{x_i}u_m|\geq l\}} \phi\left(|\partial_{x_i}u_m|\right)dx \\ &\leq \frac{E(u_m)}{\alpha_\epsilon} \\ &\leq \frac{E(0)+1}{\alpha_\epsilon} \\ &= \epsilon \quad \text{for } i = 1,2,\end{aligned} \tag{3.50}$$

and this is true for all m and arbitrary $\epsilon > 0$. It follows then that

$$\lim_{l\to\infty}\sup_m \int_{\Omega\cap\{|\partial_{x_i}u_m|\geq l\}} |\partial_{x_i}u_m|\,dx = 0 \quad \text{for } i = 1,2. \tag{3.51}$$

We conclude then from (3.47), (3.49), (3.51), the weak compactness in $L^2(\Omega)$, and the *Uniform integrability* and *weak convergence* in L^1 (see appendix A.6), that there exists a subsequence $\left\{u_{m_j}\right\}_{j=1}^{\infty}$ of $\{u_m\}_{m=1}^{\infty}$ and a function $\widetilde{u} \in L^2(\Omega)\cap W^{1,1}(\Omega)$ such that

$$u_{m_j} \rightharpoonup \widetilde{u} \text{ weakly in } L^2(\Omega), \tag{3.52}$$

$$\nabla u_{m_j} \rightharpoonup \nabla\widetilde{u} \text{ weakly in } \left[L^1(\Omega)\right]^2. \tag{3.53}$$

Which ends the proof. □

Next, we will prove that this weak limit $\widetilde{u}$ is indeed in $\mathcal{A}$.

Lemma 3.4.2. *The weak limit $\widetilde{u}$ satisfies $\nabla\widetilde{u} \in \left[LlogL^{k_m}(\Omega)\right]^2$, i.e.,*

$$\widetilde{u} \in \mathcal{A}. \tag{3.54}$$

Proof. Since the function $f(s) := s\log(s)$ for $s \geq 1$ is increasing and convex, so is the function $f(|s|)$ for all $s \geq 1$. Therefore, we can deduce

$$f\left(|\partial_{x_i}\widetilde{u}|\right) \leq f\left(\left|\partial_{x_i}u_{m_j}\right|\right) + f'\left(|\partial_{x_i}\widetilde{u}|\right)\left(\partial_{x_i}\widetilde{u} - \partial_{x_i}u_{m_j}\right) \quad \text{for } i = 1,2. \tag{3.55}$$

For $M > 0$, we denote by $\Omega_M = \Omega \cap \{k_m \leq |\partial_{x_i} \widetilde{u}| \leq M\}$. Then, by integrating the above inequality (3.55) over $\Omega_M \cap \left\{\left|\partial_{x_i} u_{m_j}\right| \geq k_m\right\}$, we obtain

$$\begin{aligned}\int_{\Omega_M} f\left(|\partial_{x_i}\widetilde{u}|\right) dx &\leq \int_{\Omega \cap \left\{\left|\partial_{x_i} u_{m_j}\right| \geq k_m\right\}} f\left(\left|\partial_{x_i} u_{m_j}\right|\right) dx \\ &\quad + \int_{\Omega_M \cap \left\{\left|\partial_{x_i} u_{m_j}\right| \geq k_m\right\}} f'\left(|\partial_{x_i}\widetilde{u}|\right)\left(\partial_{x_i}\widetilde{u} - \partial_{x_i} u_{m_j}\right) dx \\ &\leq \int_{\Omega \cap \left\{\left|\partial_{x_i} u_{m_j}\right| \geq k_m\right\}} f\left(\left|\partial_{x_i} u_{m_j}\right|\right) dx \\ &\quad + \int_{\Omega \cap \left\{\left|\partial_{x_i} u_{m_j}\right| \geq k_m\right\}} f'\left(|\partial_{x_i}\widetilde{u}|\right) \chi_{\left\{k_m \leq |\partial_{x_i}\widetilde{u}| \leq M\right\}}\left(\partial_{x_i}\widetilde{u} - \partial_{x_i} u_{m_j}\right) dx.\end{aligned} \tag{3.56}$$

Since $f'\left(|\partial_{x_i}\widetilde{u}|\right) \chi_{\left\{k_m \leq |\partial_{x_i}\widetilde{u}| \leq M\right\}} \in L^{\infty}(\Omega)$, then by letting $j \to \infty$, we get

$$\int_{\Omega_M} f\left(|\partial_{x_i}\widetilde{u}|\right) dx \leq \liminf_{j\to\infty} \int_{\Omega \cap \left\{\left|\partial_{x_i} u_{m_j}\right| \geq k_m\right\}} f\left(\left|\partial_{x_i} u_{m_j}\right|\right) dx < \infty. \tag{3.57}$$

Then by letting $M \to \infty$, we deduce

$$\int_{\Omega \cap \left\{|\partial_{x_i}\widetilde{u}| \geq k_m\right\}} f\left(|\partial_{x_i}\widetilde{u}|\right) dx < \infty. \tag{3.58}$$

It follows then $\partial_{x_i}\widetilde{u} \in LlogL^{k_m}(\Omega)$, which implies that

$$\widetilde{u} \in \mathcal{A}. \tag{3.59}$$

□

Now that our weak limit $\widetilde{u}$ is in $\mathcal{A}$, it remains then to prove that $\widetilde{u}$ is actually a minimizer, i.e., $E(\widetilde{u}) = \min_{u\in\mathcal{A}} E(u)$. Unfortunately, the functional $E(.)$ is not continuous for weak convergence, and hence we cannot deduce directly from the reasoning above that:

$$E(\widetilde{u}) = \lim_{j\to+\infty} E\left(u_{m_j}\right). \tag{3.60}$$

So, to overcome this difficulty, we only need to prove that $E(.)$ is (*sequentially*) *weakly lower semi-continuous* on $\mathcal{A}$ (see [17] for more details):

$$E(\widetilde{u}) \leq \liminf_{j\to+\infty} E\left(u_{m_j}\right), \tag{3.61}$$

which is the purpose of the following lemma.

Lemma 3.4.3. *$E(.)$ is (sequentially) weakly lower semicontinuous on $\mathcal{A}$, i.e.,*

$$E(\widetilde{u}) \leq \liminf_{j\to+\infty} E\left(u_{m_j}\right). \tag{3.62}$$

Proof. Knowing that $u_0 \in L^2(\Omega)$ and

$$u_{m_j} \rightharpoonup \widetilde{u} \text{ weakly in } L^2(\Omega), \tag{3.63}$$

we have

$$\int_\Omega (\widetilde{u} - u_0)^2 dx \leq \liminf_{j\to\infty} \int_\Omega \left(u_{m_j} - u_0\right)^2 dx. \tag{3.64}$$

Furthermore, by following the same reasoning as set out in the proof of the last lemma, we know that $\phi(s)$ for $s \geq 0$ is increasing and convex function. Then, we can easily deduce that

$$\int_\Omega \phi\left(|\partial_a \widetilde{u}|\right) dx \leq \liminf_{j\to\infty} \int_\Omega \phi\left(\left|\partial_a u_{m_j}\right|\right) dx \tag{3.65}$$

for any $a \in \{x_1, x_2, x_{12}, x_{-12}\}$. Therefore, by combining (3.64) with (3.65) we conclude

$$E(\widetilde{u}) \leq \liminf_{j\to\infty} E\left(u_{m_j}\right) = \inf_{u\in\mathcal{A}} E(u). \tag{3.66}$$

□

Finally, we can state our fundamental existence result theorem:

Theorem 3.4.4. *Assuming that $u_0 \in L^2(\Omega)$, there exists a weak solution in $\mathcal{A}$ for the boundary-value problem (3.1).*

Proof. According to lemma 3.4.1, there exists a minimizing sequence $\{u_m\}_{m=1}^{\infty}$ in $\mathcal{A}$ which has a subsequence that converges weakly to a function $\widetilde{u}$ in $L^2(\Omega) \cap W^{1,1}(\Omega)$. Besides, thanks to the convexity of ϕ, we have demonstrated, in lemma 3.4.3, that

$$E(\widetilde{u}) \leq \liminf_{j\to\infty} E\left(u_{m_j}\right) = \inf_{u\in\mathcal{A}} E(u). \tag{3.67}$$

But since the weak limit function $\widetilde{u}$ happens to be in $\mathcal{A}$ due to lemma 3.4.2. It follows then that $\widetilde{u} \in \mathcal{A}$ is a minimizer of the energy functional $E(u)$, i.e.,

$$E(\widetilde{u}) = \min_{u\in\mathcal{A}} E(u). \tag{3.68}$$

Finally, using the theorem 3.3.2, we conclude that $\widetilde{u}$ is a weak solution to the boundary-value problem (3.1). Which completes the proof. □

Now, we turn our attention to the uniqueness matter:

Theorem 3.4.5. *The weak solution $\widetilde{u}$ is unique.*

Proof. Assuming there is another weak solution $\widehat{u}$ for (3.1). Then, for every $\varphi \in \mathcal{A}$, we have

$$\int_\Omega \rho\,(\widehat{u} - u_0)\,\varphi dx + \int_\Omega \mathbf{D}_{\nabla\widehat{u}} \nabla\widehat{u} \cdot \nabla\varphi dx = 0. \tag{3.69}$$

Which leads to

$$\int_\Omega \rho\,(\widehat{u} - \widetilde{u})\,\varphi dx + \int_\Omega [\mathbf{D}_{\nabla\widehat{u}} \nabla\widehat{u} - \mathbf{D}_{\nabla\widetilde{u}} \nabla\widetilde{u}] \cdot \nabla\varphi dx = 0. \tag{3.70}$$

Then, if we choose $\varphi = \widehat{u} - \widetilde{u} \in \mathcal{A}$, we get

$$\int_\Omega \rho\,(\widehat{u} - \widetilde{u})^2\,dx + \int_\Omega [\mathbf{D}_{\nabla\widehat{u}} \nabla\widehat{u} - \mathbf{D}_{\nabla\widetilde{u}} \nabla\widetilde{u}] \cdot (\nabla\widehat{u} - \nabla\widetilde{u})\,dx = 0. \tag{3.71}$$

Thanks to Lemma 3.2.1, we deduce that

$$\int_\Omega \rho\,(\widehat{u} - \widetilde{u})^2\,dx = 0. \tag{3.72}$$

Therefore, $\widehat{u} = \widetilde{u}$ a.e. in Ω. Thus, the boundary-value problem has a unique solution, which completes the proof. □

3.5 Conclusion

This chapter has first analyzed the quasilinear second-order elliptic problem (3.1) by establishing its equivalence to the convex energy functional minimization problem (3.15). Next, a direct method in the calculus of variations has been adopted to show directly the existence of a minimizer of an energy functional rather than solve the boundary-value problem. Finally, the monotonicity of a nonlinear operator (lemma 3.2.1) has been exploited to demonstrate the uniqueness of solutions to the boundary-value problem.

Chapter 4

Implicit Iterative and Monotone Methods in a Nonlinear Parabolic Problem

4.1 Introduction

This chapter analyzes the existence and uniqueness of weak solutions for the following anisotropic nonlinear parabolic initial-boundary value problem:

$$\begin{cases} \frac{\partial u}{\partial t} - \nabla \cdot \left[\mathbf{D}_{\nabla u} \nabla u\right] = 0 & \text{in } \Omega \times (0,T] \\ \left\langle \mathbf{D}_{\nabla u} \nabla u, \mathbf{n} \right\rangle = 0 & \text{on } \partial\Omega \times (0,T] \\ u(x;0) = u_0(x) & \text{in } \Omega, \end{cases} \tag{4.1}$$

where

- Ω is an open bounded domain of $\mathbb{R}^2$ with Lipschitz boundary $\partial\Omega$,
- $T > 0$ is a real positive number,
- $u_0 \in L^2(\Omega)$ representing a continuous image,
- $\mathbf{D}_{\nabla u}$ is the diffusion tensor defined in (2.97),
- $\langle .,. \rangle$ denotes the Euclidean scalar product in $\mathbb{R}^2$,
- $\mathbf{n}$ is the unit outward normal vector on $\partial\Omega$.

First of all, we define weak solutions for problem (4.1) on $Q_T := \Omega \times (0,T]$ and we denote

$$LlogL^{k_m}(Q_T) := \left\{ u : Q \to \mathbb{R} \;\middle|\; \int_0^T \int_{\Omega \cap \{|u| \geq k_m\}} |u| \log(|u|)\, dxdt < \infty \right\}.$$

Definition 4.1.1. A function $u : \overline{Q}_T \to \mathbb{R}$ is a weak solution for problem (4.1) if the following conditions are satisfied:

(i) $u \in C\left([0,T]; L^2(\Omega)\right) \cap L^1\left(0,T; W^{1,1}(\Omega)\right)$ such that $\nabla u \in \left[LlogL^{k_m}(Q_T)\right]^2$.

(ii) For any $\varphi \in C^1\left(\overline{Q}_T\right)$ with $\varphi(.,T)=0$, we have

$$-\int_\Omega u_0(x)\,\varphi(x,0)\,dx+\int_0^T\int_\Omega\left[-u\varphi_t+\mathbf{D}_{\nabla u}\nabla u\cdot\nabla\varphi\right]dxdt=0. \tag{4.2}$$

Inspired by [52], this chapter will investigate the existence and uniqueness of weak solutions for the problem (4.1) according to the following steps:

- First, we will approximate the nonlinear evolution problem (4.1) by nonlinear elliptic problems using an implicit iterative method (discretization in time-variable only), then we will prove the existence of a unique weak solution for each elliptic problem adopting a variational approach. These solutions will constitute approximate solutions for the problem (4.1).
- Next, we will show the uniqueness of solutions for the initial-boundary value problem (4.1) using the monotonicity of the vector field $\mathbf{D}_{\nabla .}\nabla . : u\in\mathbb{R}^2\to\mathbf{D}_{\nabla u}\nabla u\in\mathbb{R}^2$ (3.11).
- Finally, by passing to the limit in some a priori energy estimates and using again the monotonicity of the above vector field, we will demonstrate the existence of weak solutions for the problem (4.1).

4.2 Approximate Solutions

Our approach aims to construct a solution to the initial-boundary value problem (4.1) as the limit of some approximate solutions. Therefore, to get approximate solutions for the problem (4.1), we discretize the time variable interval $[0,T]$ and denote $\tau=\frac{T}{N}$ with $N\in\mathbb{N}^*$. Then, We gradually define from $n=1,2,...,N$ the following elliptic problems:

$$\begin{cases}\frac{u^n-u^{n-1}}{\tau}-\nabla\cdot\left[\mathbf{D}_{\nabla u^n}\nabla u^n\right]=0 & \text{in }\Omega\\ \left\langle\mathbf{D}_{\nabla u^n}\nabla u^n,\mathbf{n}\right\rangle=0 & \text{on }\partial\Omega.\end{cases} \tag{4.3}$$

Theorem 4.2.1. *For each integer $n=1,2,...,N$, the quasilinear elliptic problem (4.3) has a unique weak solution in $\mathcal{A}$.*

Proof. To solve the equations (4.3) step by step, we only need to prove the existence and uniqueness of weak solutions of the following elliptic problem:

$$\begin{cases}\frac{u^1-u^0}{\tau}-\nabla\cdot\left[\mathbf{D}_{\nabla u^1}\nabla u^1\right]=0 & \text{in }\Omega\\ \left\langle\mathbf{D}_{\nabla u^1}\nabla u^1,\mathbf{n}\right\rangle=0 & \text{on }\partial\Omega,\end{cases} \tag{4.4}$$

where $u^0=u_0$. So, according to the result set out in chapter 3, this problem has a unique solution u_1 in $\mathcal{A}$. Hence, we can show, by induction, that there exists, for every $n\in\{1,2,...,N\}$, a unique weak

solution $u_n \in \mathcal{A}$ such that

$$\begin{cases} \frac{u_n - u_{n-1}}{\tau} - \nabla \cdot \left[\mathbf{D}_{\nabla u_n} \nabla u_n \right] = 0 & \text{in } \Omega \\ \left\langle \mathbf{D}_{\nabla u_n} \nabla u_n, \mathbf{n} \right\rangle = 0 & \text{on } \partial\Omega. \end{cases} \tag{4.5}$$

□

Consequently, for every $\tau = \frac{T}{N}$, the following function u_τ is an approximate solution to the problem (4.1):

$$u_\tau(x,t) = \begin{cases} u_0(x) & t = 0 \\ u_j(x) & t \in ((j-1)\tau, j\tau], \ j \in \{1,2,...,N\}. \end{cases} \tag{4.6}$$

Now, in order to take the limit as $\tau \to 0$, we need to establish some a priori energy estimates for u_τ.

4.3 Energy Estimates

The following theorem introduces some uniform energy estimates for u_τ. These energy estimates will allow us to show the existence of a convergent subsequence of $\{u_\tau\}$ in the weak sense.

Theorem 4.3.1. *For every $\tau > 0$, the approximate solution u_τ satisfies the following energy estimate:*

$$\|u_\tau\|^2_{L^\infty(0,T;L^2(\Omega))} + \|u_\tau\|_{L^1\left(0,T;W^{1,1}(\Omega)\right)} \leq C\left(1 + \|u_0\|^2_{L^2(\Omega)}\right) \tag{4.7}$$

for some positive constant C. Additionally, the sequence $\{u_\tau\}$ satisfies

$$\int_0^T \int_{\Omega \cap \{|\partial_{x_i} u_\tau| \geq k_m\}} |\partial_{x_i} u_\tau| \log\left(|\partial_{x_i} u_\tau|\right) dxdt \leq \frac{3}{2} M \|u_0\|^2_{L^2(\Omega)} \tag{4.8}$$

for some fixed positive constant M.

Proof. If we multiply (4.5) by a test function $\varphi \in C^1\left(\overline{\Omega}\right)$ and integrate by parts, we get the equality

$$\int_\Omega \frac{u_n - u_{n-1}}{\tau} \varphi dx + \int_\Omega \mathbf{D}_{\nabla u_n} \nabla u_n \cdot \nabla \varphi dx = 0. \tag{4.9}$$

Then, by taking $\varphi = u_n$ in (4.9) and using $u_n u_{n-1} \leq \frac{u_n^2 + u_{n-1}^2}{2}$, we get

$$\frac{1}{2}\int_\Omega u_n^2 dx + \tau \int_\Omega \mathbf{D}_{\nabla u_n} \nabla u_n \cdot \nabla u_n dx \leq \frac{1}{2}\int_\Omega u_{n-1}^2 dx. \tag{4.10}$$

For each $t \in (0,T]$, we can find $j \in \{1,...,N\}$ such that $t \in ((j-1)\tau, j\tau]$. Then, by adding all the inequalities (4.10) from $n=1$ to $n=j$, we get

$$\frac{1}{2}\int_\Omega u_j^2 dx + \tau \sum_{n=1}^{j} \int_\Omega \mathbf{D}_{\nabla u_n} \nabla u_n \cdot \nabla u_n dx \leq \frac{1}{2}\int_\Omega u_0^2 dx. \tag{4.11}$$

Then, by the definition of u_τ, we obtain for $t \in ((j-1)\tau, j\tau]$ that

$$\frac{1}{2}\int_\Omega u_\tau^2(x,t)\,dx + \int_0^{j\tau}\int_\Omega \mathbf{D}_{\nabla u_\tau} \nabla u_\tau \cdot \nabla u_\tau dx d\delta \leq \frac{1}{2}\int_\Omega u_0^2 dx. \tag{4.12}$$

Since $\mathbf{D}_{\nabla u_\tau}$ is a symmetric positive definite matrix, then we have

$$\frac{1}{2}\int_\Omega u_\tau^2(x,t)\,dx + \int_0^{t}\int_\Omega \mathbf{D}_{\nabla u_\tau} \nabla u_\tau \cdot \nabla u_\tau dx d\delta \leq \frac{1}{2}\int_\Omega u_0^2 dx \tag{4.13}$$

and

$$\int_\Omega u_\tau^2(x,t)\,dx \leq \int_\Omega u_0^2 dx. \tag{4.14}$$

Therefore, after taking the supremum over $(0,T]$, we deduce that

$$\frac{1}{2}\sup_{0<t\leq T}\int_\Omega u_\tau^2(x,t)\,dx + \int_0^{T}\int_\Omega \mathbf{D}_{\nabla u_\tau} \nabla u_\tau \cdot \nabla u_\tau dx d\delta \leq \frac{1}{2}\int_\Omega u_0^2 dx \tag{4.15}$$

and

$$\sup_{0\leq t\leq T}\int_\Omega u_\tau^2(x,t)\,dx \leq \int_\Omega u_0^2 dx. \tag{4.16}$$

Thus, it follows from (4.15) and (4.16) that

$$\begin{aligned}\sup_{0\leq t\leq T}\int_\Omega u_\tau^2(x,t)\,dx + \int_0^{T}\int_\Omega \mathbf{D}_{\nabla u_\tau} \nabla u_\tau \cdot \nabla u_\tau dx d\delta &\leq \int_\Omega u_0^2 dx + \frac{1}{2}\sup_{0<t\leq T}\int_\Omega u_\tau^2(x,t)\,dx \\ &\quad + \int_0^{T}\int_\Omega \mathbf{D}_{\nabla u_\tau} \nabla u_\tau \cdot \nabla u_\tau dx d\delta \\ &\leq \frac{3}{2}\int_\Omega u_0^2 dx.\end{aligned} \tag{4.17}$$

Furthermore, from the definition of $\mathbf{D}_{\nabla u_\tau}$ (2.97), and recalling that

$$\begin{cases} g(s) = \frac{\phi'(s)}{s} & \text{for all } s \geq 0 \\ 0 \leq \phi(s) \leq s\phi'(s) & \text{for all } s \geq 0, \end{cases} \tag{4.18}$$

we can derive the following

$$\begin{aligned}\mathbf{D}_{\nabla u_\tau}\nabla u_\tau\cdot\nabla u_\tau =& \left|\nabla u_\tau\cdot\mathbf{e}_1\right|\phi'\left(\left|\nabla u_\tau\cdot\mathbf{e}_1\right|\right)+\left|\nabla u_\tau\cdot\mathbf{e}_2\right|\phi'\left(\left|\nabla u_\tau\cdot\mathbf{e}_2\right|\right)\\ &+\left|\nabla u_\tau\cdot\mathbf{e}_{12}\right|\phi'\left(\left|\nabla u_\tau\cdot\mathbf{e}_{12}\right|\right)+\left|\nabla u_\tau\cdot\mathbf{e}_{-12}\right|\phi'\left(\left|\nabla u_\tau\cdot\mathbf{e}_{-12}\right|\right)\\ \geq&\phi\left(\left|\nabla u_\tau\cdot\mathbf{e}_1\right|\right)+\phi\left(\left|\nabla u_\tau\cdot\mathbf{e}_2\right|\right)+\phi\left(\left|\nabla u_\tau\cdot\mathbf{e}_{12}\right|\right)+\phi\left(\left|\nabla u_\tau\cdot\mathbf{e}_{-12}\right|\right).\end{aligned} \tag{4.19}$$

As in (3.48), for a fixed $\alpha>0$, we can find $\beta=k_m>0$ such that for all $s\geq k_m$, $\phi(s)\geq\alpha s$. Then, we have for i=1,2

$$\begin{aligned}\int_0^T\int_\Omega\left|\partial_{x_i}u_\tau\right|dxdt &\leq k_m T\left|\Omega\right|+\frac{1}{\alpha}\int_0^T\int_{\Omega\cap\left\{\left|\partial_{x_i}u_\tau\right|\geq k_m\right\}}\phi\left(\left|\partial_{x_i}u_\tau\right|\right)dxdt\\ &\leq k_m T\left|\Omega\right|+\frac{1}{\alpha}\int_0^T\int_{\Omega\cap\left\{\left|\partial_{x_i}u_\tau\right|\geq k_m\right\}}\mathbf{D}_{\nabla u_\tau}\nabla u_\tau\cdot\nabla u_\tau dxdt\\ &\leq k_m T\left|\Omega\right|+\frac{1}{\alpha}\int_0^T\int_\Omega\mathbf{D}_{\nabla u_\tau}\nabla u_\tau\cdot\nabla u_\tau dxdt.\end{aligned} \tag{4.20}$$

On the other hand, we can write from (4.14)

$$\int_\Omega\left|u_\tau(x,t)\right|dx\leq\frac{1}{2}\left(\left|\Omega\right|+\int_\Omega u_0^2dx\right). \tag{4.21}$$

Therefore, we conclude from (4.17), (4.20) and (4.21) that

$$\left\|u_\tau\right\|^2_{L^\infty(0,T;L^2(\Omega))}+\left\|u_\tau\right\|_{L^1\left(0,T;W^{1,1}(\Omega)\right)}\leq C\left(1+\left\|u_0\right\|^2_{L^2(\Omega)}\right) \tag{4.22}$$

for some positive constant C depending on k_m, T, $|\Omega|$, and α.

Besides, for an $\epsilon>0$, we can choose $\beta=k_m\geq 1$ such that for all $s\geq k_m$, $s\log(s)\leq M\phi(s)$ where $M=\epsilon+\frac{1}{A_{k_m,2}}$ and $A_{k_m,2}$ is the positive constant defined in (3.10). Then we have

$$\begin{aligned}\int_0^T\int_{\Omega\cap\left\{\left|\partial_{x_i}u_\tau\right|\geq k_m\right\}}\left|\partial_{x_i}u_\tau\right|\log\left(\left|\partial_{x_i}u_\tau\right|\right)dxdt &\leq M\int_0^T\int_{\Omega\cap\left\{\left|\partial_{x_i}u_\tau\right|\geq k_m\right\}}\phi\left(\left|\partial_{x_i}u_\tau\right|\right)dxdt\\ &\leq M\int_0^T\int_\Omega\mathbf{D}_{\nabla u_\tau}\nabla u_\tau\cdot\nabla u_\tau dxdt\quad\text{for } i=1,2.\end{aligned} \tag{4.23}$$

Thus, we deduce from (4.17) that

$$\int_0^T\int_{\Omega\cap\left\{\left|\partial_{x_i}u_\tau\right|\geq k_m\right\}}\left|\partial_{x_i}u_\tau\right|\log\left(\left|\partial_{x_i}u_\tau\right|\right)dxdt\leq\frac{3}{2}M\left\|u_0\right\|^2_{L^2(\Omega)}. \tag{4.24}$$

It follows then

$$\nabla u_\tau\in\left[LlogL^{k_m}(Q_T)\right]^2. \tag{4.25}$$

Which completes the proof. □

Now, we intend to use the energy estimate (4.7) to pass to the limit as $\tau \to 0$ and prove the existence of a weak solution for problem (4.1).

4.4 Existence and Uniqueness of weak solutions

The first step is to employ the energy estimate (4.7) to obtain a subsequence of $\{u_\tau\}$ that converges weakly in some functional spaces to a limit u, which we expect it to satisfy (4.2).

Lemma 4.4.1. *There exist a subsequence of $\{u_\tau\}$ (for simplicity, we also denote it by $\{u_\tau\}$), and u in $L^1\left(0,T;W^{1,1}(\Omega)\right)\cap L^\infty\left(0,T;L^2(\Omega)\right)$ such that*

$$u_\tau \rightharpoonup u, \text{ weakly\_* in } L^\infty\left(0,T;L^2(\Omega)\right) \tag{4.26}$$

$$u_\tau \rightharpoonup u, \text{ weakly in } L^1\left(0,T;W^{1,1}(\Omega)\right) \tag{4.27}$$

and

$$\nabla u \in \left[LlogL^{k_m}(Q_T)\right]^2. \tag{4.28}$$

Proof. As in (3.42), we can choose $\alpha_\epsilon = \frac{2}{\epsilon}\|u_0\|_{L^2(\Omega)}$ and $l \geq k_m \geq 1$ such that for all $s \geq l$, we have $\phi(s) > \alpha_\epsilon s$. Thus

$$\begin{aligned}
\int_0^T \int_{\Omega\cap\{|\partial_{x_i}u_\tau|\geq l\}} |\partial_{x_i}u_\tau|\,dxdt &\leq \frac{1}{\alpha_\epsilon}\int_0^T \int_{\Omega\cap\{|\partial_{x_i}u_\tau|\geq l\}} \phi\left(|\partial_{x_i}u_\tau|\right)dxdt \\
&\leq \frac{1}{\alpha_\epsilon}\int_0^T \int_{\Omega\cap\{|\partial_{x_i}u_\tau|\geq k_m\}} \mathbf{D}_{\nabla u_\tau}\nabla u_\tau\cdot\nabla u_\tau dxdt \\
&\leq \frac{2}{\alpha_\epsilon}\int_\Omega u_0^2 dx \\
&= \epsilon \quad \text{for } i=1,2,
\end{aligned} \tag{4.29}$$

and this is true for all τ and arbitrary $\epsilon > 0$. It follows then that

$$\lim_{l\to\infty}\sup_\tau \int_0^T \int_{\Omega\cap\{|\partial_{x_i}u_\tau|\geq l\}} |\partial_{x_i}u_\tau|\,dxdt = 0 \quad \text{for } i=1,2. \tag{4.30}$$

Therefore, from the energy estimates (4.7), and according to the weak compactness in $L^2(\Omega)$, and the *uniform integrability* and *weak convergence* in $L^1(\Omega)$ (see appendix A.6), we can find a subsequence of $\{u_\tau\}$ (for simplicity, we also denote it by u_τ) such that [18]

$$u_\tau \rightharpoonup u, \text{ weakly\_* in } L^\infty\left(0,T;L^2(\Omega)\right) \tag{4.31}$$

$$u_\tau \rightharpoonup u, \text{ weakly in } L^1\left(0,T;W^{1,1}(\Omega)\right), \tag{4.32}$$

where

$$u \in L^1\left(0,T;W^{1,1}(\Omega)\right) \cap L^\infty\left(0,T;L^2(\Omega)\right). \tag{4.33}$$

On the other hand, since

$$\nabla u_\tau \in \left[LlogL^{k_m}(Q_T)\right]^2. \tag{4.34}$$

Then, by following the same argumentation as in lemma 3.4.2, we can easily show that

$$\nabla u \in \left[LlogL^{k_m}(Q_T)\right]^2. \tag{4.35}$$

□

So, it remains to prove that u is just a weak solution for the problem (4.1). The next step is to show that $\xi_\tau := \mathbf{D}_{\nabla u_\tau}\nabla u_\tau$ is bounded in $\left[L^2(Q_T)\right]^2$, so that we can extract a subsequence of ξ_τ that converges weakly in $\left[L^2(Q_T)\right]^2$ to a particular vector-valued function ξ. Then, we will prove that ξ is equal almost everywhere to $\mathbf{D}_{\nabla u}\nabla u$ in Q_T through the monotonicity condition (3.11).

Lemma 4.4.2. *The sequence $\{\xi_\tau\}$ is bounded in $\left[L^2(Q_T)\right]^2$ and thus there exists a subsequence, also denoted by $\{\xi_\tau\}$, and ξ in $\left[L^2(Q_T)\right]^2$ such that*

$$\xi_\tau \rightharpoonup \xi \text{ weakly in } \left[L^2(Q_T)\right]^2. \tag{4.36}$$

Additionally, the vector-valued function ξ satisfies

$$\xi \cdot \nabla u \in L^1(Q_T) \tag{4.37}$$

$$\int_\Omega u_0(x)\,\varphi(x,0)\,dx + \int_0^T\int_\Omega u\varphi_t dxdt = \int_0^T\int_\Omega \xi\cdot\nabla\varphi dxdt \tag{4.38}$$

for each $\varphi \in C^1\left(\overline{Q}_T\right)$ with $\varphi(.,T)=0$, and

$$\xi = \boldsymbol{D}_{\nabla u}\nabla u, \text{ a.e. in } Q_T. \tag{4.39}$$

Proof. 1. From the expression of $\mathbf{D}_{\nabla u_\tau}$, we can derive the following

$$\begin{aligned}
|\xi_\tau| =& \left|\frac{\partial_{x_1}u_\tau}{|\partial_{x_1}u_\tau|}\phi'(|\partial_{x_1}u_\tau|)\,\mathbf{e}_1 + \frac{\partial_{x_2}u_\tau}{|\partial_{x_2}u_\tau|}\phi'(|\partial_{x_2}u_\tau|)\,\mathbf{e}_2\right.\\
&\left. + \frac{\partial_{x_{12}}u_\tau}{|\partial_{x_{12}}u_\tau|}\phi'(|\partial_{x_{12}}u_\tau|)\,\mathbf{e}_{12} + \frac{\partial_{x_{-12}}u_\tau}{|\partial_{x_{-12}}u_\tau|}\phi'\left(|\partial_{x_{-12}}u_\tau|\right)\mathbf{e}_{-12}\right|\\
\leq& \phi'(|\partial_{x_1}u_\tau|) + \phi'(|\partial_{x_2}u_\tau|) + \phi'(|\partial_{x_{12}}u_\tau|) + \phi'\left(|\partial_{x_{-12}}u_\tau|\right)\\
\leq& 4\phi'(|\partial_{x_1}u_\tau| + |\partial_{x_2}u_\tau|).
\end{aligned} \tag{4.40}$$

Given $\epsilon > 0$, we may find $l = k_m$ such that

$$\phi'(s) \leq M \log(s) \quad \text{for all } s \geq k_m, \tag{4.41}$$

where $M = \left(\epsilon + A_{k_m,2}\right)$. Thus, we can distinguish two cases:

- If $|\partial_{x_1} u_\tau| + |\partial_{x_2} u_\tau| < k_m$ then
$$|\xi_\tau|^2 \leq \left(4\phi'(k_m)\right)^2. \tag{4.42}$$
- If $|\partial_{x_1} u_\tau| + |\partial_{x_2} u_\tau| \geq k_m$ then
$$|\xi_\tau| \leq 4M \log\left(|\partial_{x_1} u_\tau| + |\partial_{x_2} u_\tau|\right) \tag{4.43}$$
$$\begin{aligned} |\xi_\tau|^2 &\leq (4M)^2 \left(|\partial_{x_1} u_\tau| + |\partial_{x_2} u_\tau|\right) \log\left(|\partial_{x_1} u_\tau| + |\partial_{x_2} u_\tau|\right) \\ &\leq (4M)^2 \Big[|\partial_{x_1} u_\tau| \log\left(|\partial_{x_1} u_\tau|\right) + |\partial_{x_2} u_\tau| \log\left(|\partial_{x_2} u_\tau|\right) \\ &\qquad + \log(2) \left(|\partial_{x_1} u_\tau| + |\partial_{x_2} u_\tau|\right) \Big]. \end{aligned} \tag{4.44}$$

Then, according to (4.7) and (4.8), $\{\xi_\tau\}$ is bounded in $\left[L^2(Q_T)\right]^2$, which means that we can find a subsequence of $\{\xi_\tau\}$ (denote it also by $\{\xi_\tau\}$) and a function $\xi \in \left[L^2(Q_T)\right]^2$ such that

$$\xi_\tau \rightharpoonup \xi \text{ weakly in } \left[L^2(Q_T)\right]^2. \tag{4.45}$$

2. Next, we demonstrate that $\xi \cdot \nabla u \in L^1(Q_T)$. To this end, we will proceed as above:

For $|\partial_{x_1} u_\tau| + |\partial_{x_2} u_\tau| \geq k_m$, we have

$$\begin{aligned} |\xi_\tau| \exp\left(\frac{|\xi_\tau|}{4M}\right) &\leq 4M \left(|\partial_{x_1} u_\tau| + |\partial_{x_2} u_\tau|\right) \log\left(|\partial_{x_1} u_\tau| + |\partial_{x_2} u_\tau|\right) \\ &\leq 4M \big[\left(|\partial_{x_1} u_\tau| \log\left(|\partial_{x_1} u_\tau|\right) + |\partial_{x_2} u_\tau| \log\left(|\partial_{x_2} u_\tau|\right)\right) \\ &\qquad + \log(2) \left(|\partial_{x_1} u_\tau| + |\partial_{x_2} u_\tau|\right) \big]. \end{aligned} \tag{4.46}$$

Since $s \mapsto s \exp(s)$ $(s \geq 0)$ is increasing and convex, then as in the proof of Lemma 3.4.2, we deduce that

$$\begin{aligned} &\int_0^T \int_{\Omega \cap \left\{|\partial_{x_1} u| + |\partial_{x_2} u| \geq k_m\right\}} |\xi| \exp\left(\frac{|\xi|}{4M}\right) dxdt \leq \\ &\qquad \liminf_{\tau \to 0} \int_0^T \int_{\Omega \cap \left\{|\partial_{x_1} u_\tau| + |\partial_{x_2} u_\tau| \geq k_m\right\}} |\xi_\tau| \exp\left(\frac{|\xi_\tau|}{4M}\right) dxdt < \infty. \end{aligned} \tag{4.47}$$

Then, thanks to (A.5) we get

$$\begin{aligned}\int_0^T\int_\Omega |\xi\cdot\nabla u|\,dxdt &\le \int_0^T\int_\Omega |\xi|\,|\nabla u|\,dxdt\\ &\le \int_0^T\int_\Omega |\xi|\left(|\partial_{x_1}u|+|\partial_{x_2}u|\right)dxdt\\ &\le k_m\int_0^T\int_{\Omega\cap\{|\partial_{x_1}u|+|\partial_{x_2}u|<k_m\}} |\xi|\,dxdt\\ &\quad+\int_0^T\int_{\Omega\cap\{|\partial_{x_1}u|+|\partial_{x_2}u|\ge k_m\}} |\xi|\exp\left(\frac{|\xi|}{4M}\right)dxdt\\ &\quad+4M\left[\int_0^T\int_{\Omega\cap\{|\partial_{x_1}u|\ge k_m\}} |\partial_{x_1}u|\log\left(|\partial_{x_1}u|\right)dxdt\right.\\ &\qquad\left.+\int_0^T\int_{\Omega\cap\{|\partial_{x_2}u|\ge k_m\}} |\partial_{x_2}u|\log\left(|\partial_{x_2}u|\right)dxdt\right]<\infty.\end{aligned} \tag{4.48}$$

It follows then $\xi\cdot\nabla u\in L^1(Q_T)$.

3. For each $\varphi\in C^1\left(\overline{Q}_T\right)$ with $\varphi(.,T)=0$, we take $\varphi(x,nh)$ as a test function in (4.5)

$$\int_\Omega \frac{u_n(x)-u_{n-1}(x)}{\tau}\varphi(x,nh)\,dx+\int_\Omega \mathbf{D}_{\nabla u_n}\nabla u_n\cdot\nabla\varphi(x,nh)\,dx=0\quad\text{for } n\in\{1,2,...,N\}. \tag{4.49}$$

By summing n from 1 to N, we obtain

$$\begin{aligned}-\frac{1}{\tau}\int_\Omega u_0(x)\,\varphi(x,0)\,dx+\sum_{n=0}^{N-1}\int_\Omega u_n(x)\,\frac{\varphi(x,nh)-\varphi(x,(n+1)\tau)}{\tau}dx\\ +\sum_{n=1}^{N}\int_\Omega \mathbf{D}_{\nabla u_n}\nabla u_n\cdot\nabla\varphi(x,nh)\,dx=0.\end{aligned} \tag{4.50}$$

From the definition of u_τ (4.6), we have

$$\begin{aligned}\sum_{n=0}^{N-1}\int_\Omega u_n(x)\,\frac{\varphi(x,nh)-\varphi(x,(n+1)\tau)}{\tau}dx&=-\sum_{n=0}^{N-1}\int_{nh}^{(n+1)\tau}\int_\Omega u_\tau(x,t)\,\frac{\varphi_t(x,t)}{\tau}dxdt\\ &=-\frac{1}{\tau}\int_0^T\int_\Omega u_\tau(x,t)\,\varphi_t(x,t)\,dxdt.\end{aligned} \tag{4.51}$$

Therefore

$$-\int_{\Omega} u_0(x)\,\varphi(x,0)\,dx-\int_0^T\int_{\Omega} u_\tau(x,t)\,\varphi_t(x,t)\,dxdt+\int_0^T\int_{\Omega}\mathbf{D}_{\nabla u_\tau}\nabla u_\tau\cdot\nabla\varphi dxdt \\ +\sum_{n=1}^{N}\int_{(n-1)\tau}^{nh}\int_{\Omega}\mathbf{D}_{\nabla u_n}\nabla u_n\cdot[\nabla\varphi(x,nh)-\nabla\varphi(x,t)]\,dxdt=0. \tag{4.52}$$

Letting τ tends to zero, we get

$$\int_{\Omega} u_0(x)\,\varphi(x,0)\,dx+\int_0^T\int_{\Omega} u\varphi_t dxdt=\int_0^T\int_{\Omega}\xi\cdot\nabla\varphi dxdt. \tag{4.53}$$

4. Now, we will show that $\xi=\mathbf{D}_{\nabla u}\nabla u$ a.e. in Q_T. So, we let $v\in L^1(Q_T)$ with

$$\int_0^T\int_{\Omega\cap\{|\partial_{x_i}v|\geq k_m\}}|\partial_{x_i}v|\log(|\partial_{x_i}v|)\,dxdt<\infty\quad\text{for } i=1,2. \tag{4.54}$$

We sum up the inequalities (4.11)

$$\frac{1}{2}\int_{\Omega}u_\tau^2(T)\,dx+\int_0^T\int_{\Omega}\mathbf{D}_{\nabla u_\tau}\nabla u_\tau\cdot\nabla u_\tau dxdt\leq\frac{1}{2}\int_{\Omega}u_0^2dx. \tag{4.55}$$

Since we have from Lemma 3.2.1 that

$$\int_0^T\int_{\Omega}\left(\mathbf{D}_{\nabla u_\tau}\nabla u_\tau-\mathbf{D}_{\nabla v}\nabla v\right)\cdot(\nabla u_\tau-\nabla v)\,dxdt\geq 0. \tag{4.56}$$

Then, we obtain

$$\frac{1}{2}\int_{\Omega}u_\tau^2(T)\,dx+\int_0^T\int_{\Omega}\mathbf{D}_{\nabla u_\tau}\nabla u_\tau\cdot\nabla v dxdt+\int_0^T\int_{\Omega}\mathbf{D}_{\nabla v}\nabla v\cdot\nabla u_\tau dxdt \\ -\int_0^T\int_{\Omega}\mathbf{D}_{\nabla v}\nabla v\cdot\nabla v dxdt\leq\frac{1}{2}\int_{\Omega}u_0^2dx. \tag{4.57}$$

Letting $\tau\to 0$ and noting that

$$\int_{\Omega}u^2(T)\,dx\leq\liminf_{\tau\to 0}\int_{\Omega}u_\tau^2(T)\,dx, \tag{4.58}$$

we obtain

$$\frac{1}{2}\int_{\Omega}u^2(T)\,dx+\int_0^T\int_{\Omega}\xi\cdot\nabla v dxdt+\int_0^T\int_{\Omega}\mathbf{D}_{\nabla v}\nabla v\cdot\nabla u dxdt \\ -\int_0^T\int_{\Omega}\mathbf{D}_{\nabla v}\nabla v\cdot\nabla v dxdt\leq\frac{1}{2}\int_{\Omega}u_0^2dx. \tag{4.59}$$

By using $\varphi=u$ in (4.53), we get

$$\frac{1}{2}\int_{\Omega}u^2(T)\,dx+\frac{1}{2}\int_{\Omega}u_0^2dx=\int_0^T\int_{\Omega}\xi\cdot\nabla u dxdt. \tag{4.60}$$

Combining (4.59) with (4.60), we have

$$\int_0^T \int_\Omega (\xi - \mathbf{D}_{\nabla v} \nabla v) \cdot (\nabla v - \nabla u)\, dxdt \leq -\int_\Omega u^2(T)\, dx. \tag{4.61}$$

Now, set $v = u + \lambda w$ for any $\lambda > 0$, $w \in W^{1,2}(Q_T)$, we derive from the above inequality

$$\int_0^T \int_\Omega \left(\xi - \mathbf{D}_{\nabla(u+\lambda w)} \nabla (u + \lambda w)\right) \cdot \nabla w dxdt \leq 0. \tag{4.62}$$

By letting $\lambda \to 0$ and using Lebesgue's dominated convergence theorem, we obtain

$$\int_0^T \int_\Omega (\xi - \mathbf{D}_{\nabla u} \nabla u) \cdot \nabla w dxdt \leq 0 \quad \text{for all } w \in W^{1,2}(Q_T). \tag{4.63}$$

Replacing w by $-w$, we deduce

$$\int_0^T \int_\Omega (\xi - \mathbf{D}_{\nabla u} \nabla u) \cdot \nabla w dxdt = 0 \quad \text{for all } w \in W^{1,2}(Q_T). \tag{4.64}$$

It follows then

$$\xi = \mathbf{D}_{\nabla u} \nabla u \quad \text{a.e. in } Q_T. \tag{4.65}$$

Which completes the proof. □

Finally, we state our main theorem:

Theorem 4.4.3. *Assuming that $u_0 \in L^2(\Omega)$, a unique weak solution exists for the initial-boundary value problem (4.1).*

Proof. 1. In the beginning, we establish the uniqueness of solutions for the problem (4.1). For this purpose, we suppose that the problem (4.1) has two weak solutions u and v. Then we obtain the following:

$$\begin{cases} \frac{\partial (u-v)}{\partial t} - \nabla \cdot [\mathbf{D}_{\nabla u} \nabla u - \mathbf{D}_{\nabla v} \nabla v] = 0 & \text{in } Q_T \\ \langle \mathbf{D}_{\nabla u} \nabla u - \mathbf{D}_{\nabla v} \nabla v, \mathbf{n} \rangle = 0 & \text{on } \partial\Omega \times (0, T] \\ (u - v)(x; 0) = 0 & \text{in } \Omega. \end{cases} \tag{4.66}$$

By multiplying the first equation of the above problem by $(u - v)$ and integrating over Ω and $[0, t]$, we get

$$\frac{1}{2} \int_\Omega (u - v)^2(t)\, dx + \int_0^t \int_\Omega [\mathbf{D}_{\nabla u} \nabla u - \mathbf{D}_{\nabla v} \nabla v] \cdot \nabla (u - v)\, dxd\delta = 0 \tag{4.67}$$

for every $t \in (0, T]$. Since the second term of the above equation is nonnegative (thanks to Lemma 3.2.1), it follows then $u = v$ a.e. in Q_T.

2. Now we turn our attention to the question of existence:

According to lemma 4.4.1 there exist a subsequence of $\{u_\tau\}$ and u such that

$$u_\tau \rightharpoonup u, \text{ weakly\_* in } L^\infty\left(0,T;L^2(\Omega)\right) \tag{4.68}$$

$$u_\tau \rightharpoonup u, \text{ weakly in } L^1\left(0,T;W^{1,1}(\Omega)\right) \tag{4.69}$$

and

$$\nabla u \in \left[LlogL^{k_m}(Q_T)\right]^2. \tag{4.70}$$

Besides, we deduce from lemma 4.4.2 that

$$-\int_\Omega u_0(x)\,\varphi(x,0)\,dx + \int_0^T\int_\Omega \left[-u\varphi_t + \mathbf{D}_{\nabla u}\nabla u\cdot\nabla\varphi\right]dxdt = 0 \tag{4.71}$$

for any $\varphi \in C^1\left(\overline{Q}_T\right)$ with $\varphi(.,T) = 0$.

Now, it remains to prove that $u \in C\left([0,T],L^2(\Omega)\right)$. If we choose $\varphi \in C_0^\infty(Q_T)$ in (4.53), we obtain

$$\int_0^T\int_\Omega u\varphi_t dxdt = \int_0^T\int_\Omega \xi\cdot\nabla\varphi dxdt. \tag{4.72}$$

Since $\xi \in \left[L^2(Q_T)\right]^2$, we conclude that $u_t \in L^1\left(0,T;H^{-1}(\Omega)\right)$ where $H^{-1}(\Omega)$ is the dual space of $W_0^{1,2}(\Omega)$. Since

$$u = \int_0^t u_\delta d\delta + u_0 \text{ and } u_0 \in L^2(\Omega) \hookrightarrow H^{-1}(\Omega), \tag{4.73}$$

it follows then that $u \in C\left(0,T;H^{-1}(\Omega)\right)$.

Besides, for every $\tau > 0$, let $v_\tau(x,t) = u(x,t+\tau)$ be the weak solution for the problem (4.1) satisfying $v_\tau(x;0) = u(x,\tau)$.

Then $w_\tau(x,t) = u(x,t+\tau) - u(x,t)$ satisfies

$$\begin{cases} \frac{\partial w_\tau}{\partial t} - \nabla\cdot\left[\mathbf{D}_{\nabla v_\tau}\nabla v_\tau - \mathbf{D}_{\nabla u}\nabla u\right] = 0 & \text{in } \Omega\times(0,T] \\ \left\langle \mathbf{D}_{\nabla v_\tau}\nabla v_\tau - \mathbf{D}_{\nabla u}\nabla u, \mathbf{n}\right\rangle = 0 & \text{on } \partial\Omega\times(0,T] \\ w_\tau(x;0) = u(x,\tau) - u_0(x) & \text{in } \Omega. \end{cases} \tag{4.74}$$

For each $t_0 \in [0,T]$, we may choose w_τ as a test function in the first equation of the problem (4.74) over $[0,t_0]$

$$\frac{1}{2}\int_\Omega w_\tau^2(x,t_0)\,dx + \int_0^{t_0}\int_\Omega \left(\mathbf{D}_{\nabla v_\tau}\nabla v_\tau - \mathbf{D}_{\nabla u}\nabla u\right)\cdot\left(\nabla v_\tau - \nabla u\right)dxdt \le \frac{1}{2}\int_\Omega w_\tau^2(x,0)\,dx. \tag{4.75}$$

Thanks to Lemma 3.2.1, we deduce

$$\int_\Omega |u(x,t_0+\tau) - u(x,t_0)|^2\,dx \le \int_\Omega |u(x,\tau) - u_0(x)|^2\,dx. \tag{4.76}$$

Now, in order to prove that $u \in C\left([0,T], L^2(\Omega)\right)$, we need to prove

$$\limsup_{\tau \to 0^+} \int_\Omega |u(x,\tau) - u_0(x)|^2 \, dx = 0. \tag{4.77}$$

We suppose that (4.77) is not true. Then there exist a positive number η and a sequence $\{h_i\}$ with $h_i \to 0$ as $i \to \infty$ such that

$$\lim_{h_i \to 0^+} \int_\Omega |u(x,h_i) - u_0(x)|^2 \, dx \geq \eta. \tag{4.78}$$

From the estimate (4.13), we have

$$\int_\Omega |u(x,h_i)|^2 \, dx \leq \int_\Omega |u_0(x)|^2 \, dx. \tag{4.79}$$

Then, from (4.78) we get

$$\liminf_{h_i \to 0^+} \left(\int_\Omega |u_0(x)|^2 \, dx - \int_\Omega u_0(x)\, u(x,h_i) \, dx \right) \geq \frac{\eta}{2}. \tag{4.80}$$

From (4.79), we conclude that $\{u(x,h_i)\}$ is a bounded sequence in $L^2(\Omega)$. Then we may find a subsequence (denote it also by $\{u(x,h_i)\}$) such that there exists a function $\tilde{u}_0 \in L^2(\Omega)$ such that

$$u(x,h_i) \rightharpoonup \tilde{u}_0 \text{ weakly in } L^2(\Omega). \tag{4.81}$$

Since $u \in C\left(0,T; H^{-1}(\Omega)\right)$, it follows that

$$u(x,h_i) \rightharpoonup u_0 \text{ weakly in } H^{-1}(\Omega). \tag{4.82}$$

Therefore we must have $\tilde{u}_0 = u_0$ and since $u \in C\left(0,T; H^{-1}(\Omega)\right)$, it follows that

$$u(x,h_i) \rightharpoonup u_0 \text{ weakly in } L^2(\Omega), \tag{4.83}$$

which is contradictory with (4.80).

Therefore, we conclude that (4.77) is true and $u \in C\left([0,T], L^2(\Omega)\right)$. This completes the proof. □

4.5 Conclusion

This chapter principally investigates a new anisotropic nonlinear diffusion partial differential equation related to image processing and analysis. The existence and uniqueness of weak solutions for this problem have been proven in a particular functional space and under sufficient conditions satisfied

by ϕ. First, we have applied an implicit iterative method (discretization in time-variable only) to approximate the nonlinear evolution problem by nonlinear elliptic problems. Next, we have utilized the variational approach to show the existence of weak solutions for each elliptic problem. Finally, we used some energy estimates and the monotonicity of a nonlinear operator to establish the existence and uniqueness of weak solutions for the evolution problem (4.1).

Chapter 5

Numerical Approximation Method and Application

5.1 Introduction

This chapter aims to construct a fully discrete approximation to the problem (4.1) using a consistent and stable numerical method. According to proposition 2.4.1, problem (4.1) is equivalent to

$$\begin{cases} \frac{\partial u}{\partial t} = \partial_{x_1}\left(g\left(|u_{x_1}|\right)u_{x_1}\right) + \partial_{x_2}\left(g\left(|u_{x_2}|\right)u_{x_2}\right) \\ \qquad\qquad +\partial_{x_{12}}\left(g\left(|u_{x_{12}}|\right)u_{x_{12}}\right) + \partial_{x_{-12}}\left(g\left(\left|u_{x_{-12}}\right|\right)u_{x_{-12}}\right) & \text{in } \Omega\times(0,T] \\ \langle \mathbf{D}_{\nabla u}\nabla u, \mathbf{n}\rangle = 0 & \text{on } \partial\Omega\times(0,T] \\ u\left(x;0\right) = u_0\left(x\right) & \text{in } \Omega, \end{cases} \tag{5.1}$$

where

- $\Omega = (0,a)\times(0,b) \subset \mathbb{R}^2$ with Lipschitz boundary $\partial\Omega$,
- $T > 0$ is a real positive number,
- u_0 is the initial data,
- g is the function introduced in section 2.4.2,
- $\mathbf{D}_{\nabla u}$ is the diffusion tensor defined in (2.97),
- $\langle .,. \rangle$ denotes the Euclidean scalar product in $\mathbb{R}^2$,
- $\mathbf{n}$ is the unit outward normal vector on $\partial\Omega$.

In the sequel, we will first introduce an explicit and central finite difference scheme. Next, we will provide a new diffusion function based on cubic Hermite splines defined by specific parameters (see (2.113)) that can be determined using an automatic direct search algorithm. Finally, we will illustrate some experiments on different actual brain Magnetic Resonance Imaging (MRI) scans.

5.2 Explicit and Central Finite Difference Method

This part estimates an approximate solution in particular points $\left(x_i, y_j; t_n\right)$ of the domain $\overline{\Omega} \times [0, T]$. To this end, we denote by

- $t_n = n\delta_t$ the time step where $n \geq 0$ and $0 < \delta_t \leq T$,
- $x_i = i\delta$, $y_j = j\delta$ the mesh points where $0 \leq i \leq$ N+1, $0 \leq j \leq$ M+1, and $0 < \delta \leq \min(a, b)$,
- $u_{i,j}^n$ the finite difference approximation of $u\left(x_i, y_j; t_n\right)$.

Furthermore, we approximate the differential operators ∂_{x_1}, ∂_{x_2}, $\partial_{x_{12}}$, $\partial_{x_{-12}}$, and ∂_t using the following explicit and central finite difference schemes:

$$u_{x_1}\left(x_i, y_j; t_n\right) = \frac{u\left(x_{i+\frac{1}{2}}, y_j; t_n\right) - u\left(x_{i-\frac{1}{2}}, y_j; t_n\right)}{\delta} + \mathcal{O}\left(\delta^2\right) \tag{5.2}$$

$$u_{x_2}\left(x_i, y_j; t_n\right) = \frac{u\left(x_i, y_{j+\frac{1}{2}}; t_n\right) - u\left(x_i, y_{j-\frac{1}{2}}; t_n\right)}{\delta} + \mathcal{O}\left(\delta^2\right) \tag{5.3}$$

$$u_{x_{12}}\left(x_i, y_j; t_n\right) = \frac{u\left(x_{i+\frac{1}{2}}, y_{j+\frac{1}{2}}; t_n\right) - u\left(x_{i-\frac{1}{2}}, y_{j-\frac{1}{2}}; t_n\right)}{\sqrt{2}\delta} + \mathcal{O}\left(\delta^2\right) \tag{5.4}$$

$$u_{x_{-12}}\left(x_i, y_j; t_n\right) = \frac{u\left(x_{i-\frac{1}{2}}, y_{j+\frac{1}{2}}; t_n\right) - u\left(x_{i+\frac{1}{2}}, y_{j-\frac{1}{2}}; t_n\right)}{\sqrt{2}\delta} + \mathcal{O}\left(\delta^2\right) \tag{5.5}$$

$$u_t\left(x_i, y_j; t_n\right) = \frac{u\left(x_i, y_j; t_{n+1}\right) - u\left(x_i, y_j; t_n\right)}{\delta_t} + \mathcal{O}\left(\delta_t\right). \tag{5.6}$$

We assume $\delta = 1$ and denote by

$$\begin{cases} g^n_{N_{i,j}} &= g\left(\left|\Delta_N u^n_{i,j}\right|\right) \\ g^n_{E_{i,j}} &= g\left(\left|\Delta_E u^n_{i,j}\right|\right) \\ g^n_{S_{i,j}} &= g\left(\left|\Delta_S u^n_{i,j}\right|\right) \\ g^n_{W_{i,j}} &= g\left(\left|\Delta_W u^n_{i,j}\right|\right) \\ g^n_{NE_{i,j}} &= g\left(\left|\frac{\Delta_{NE} u^n_{i,j}}{\sqrt{2}}\right|\right) \\ g^n_{SE_{i,j}} &= g\left(\left|\frac{\Delta_{SE} u^n_{i,j}}{\sqrt{2}}\right|\right) \\ g^n_{SW_{i,j}} &= g\left(\left|\frac{\Delta_{SW} u^n_{i,j}}{\sqrt{2}}\right|\right) \\ g^n_{NW_{i,j}} &= g\left(\left|\frac{\Delta_{NW} u^n_{i,j}}{\sqrt{2}}\right|\right) \end{cases} \quad with \quad \begin{cases} \Delta_N u^n_{i,j} &= u^n_{i,j+1} - u^n_{i,j} \\ \Delta_E u^n_{i,j} &= u^n_{i+1,j} - u^n_{i,j} \\ \Delta_S u^n_{i,j} &= u^n_{i,j-1} - u^n_{i,j} \\ \Delta_W u^n_{i,j} &= u^n_{i-1,j} - u^n_{i,j} \\ \Delta_{NE} u^n_{i,j} &= u^n_{i+1,j+1} - u^n_{i,j} \\ \Delta_{SE} u^n_{i,j} &= u^n_{i+1,j-1} - u^n_{i,j} \\ \Delta_{SW} u^n_{i,j} &= u^n_{i-1,j-1} - u^n_{i,j} \\ \Delta_{NW} u^n_{i,j} &= u^n_{i-1,j+1} - u^n_{i,j}, \end{cases} \tag{5.7}$$

where g is the function defined in section 2.4.2. Then, we approximate the problem (5.1) using the above discretization and obtain the following discrete nonlinear diffusion filter:

$$\begin{aligned} u^{n+1}_{i,j} = u^n_{i,j} + \delta_t \Big[& g_N \Delta_N u + g_E \Delta_E u + g_S \Delta_S u + g_W \Delta_W u \\ & + \frac{g_{NE} \Delta_{NE} u + g_{SE} \Delta_{SE} u + g_{SW} \Delta_{SW} u + g_{NW} \Delta_{NW} u}{2} \Big]^n_{i,j}, \end{aligned} \tag{5.8}$$

where $u^0_{i,j}$ is the initial data, $1 \leq i \leq \mathrm{N}$, $1 \leq j \leq \mathrm{M}$, and $n \geq 0$. Furthermore, we use the discrete *Neumann* boundary condition:

$$\begin{cases} u^n_{0,j} = u^n_{1,j}, \quad u^n_{\mathrm{N}+1,j} = u^n_{\mathrm{N},j} & \text{, for } 1 \leq j \leq \mathrm{M} \\ u^n_{i,0} = u^n_{i,1}, \quad u^n_{i,\mathrm{M}+1} = u^n_{i,\mathrm{M}} & \text{, for } 1 \leq i \leq \mathrm{N} \\ u^n_{0,0} = u^n_{1,1}, \quad u^n_{\mathrm{N}+1,0} = u^n_{\mathrm{N},1} & \\ u^n_{0,\mathrm{M}+1} = u^n_{1,\mathrm{M}}, \; u^n_{\mathrm{N}+1,\mathrm{M}+1} = u^n_{\mathrm{N},\mathrm{M}}. & \end{cases} \tag{5.9}$$

The discrete scheme (5.8) can be reformulated and represented as :

$$U^{n+1} = Q\left(U^n\right) U^n \quad \forall n \in \mathbb{N}, \tag{5.10}$$

where $U^n \in \mathbb{R}^{MN}$ is the $M \times N$ column vector of $\left(u^n\right)$ such that

$$U^n = \left(u^n_{1,1}\, u^n_{1,2}\, \ldots\, u^n_{1,M}\, u^n_{2,1}\, \ldots\, u^n_{2,M}\, \ldots\, u^n_{i,1}\, \ldots\, u^n_{i,j}\, \ldots\, u^n_{i,M}\, \ldots\, u^n_{N,1}\, \ldots\, u^n_{N,M}\right)^\top \tag{5.11}$$

and $Q\left(U^n\right)$ is a block tridiagonal matrix defined as

$$Q\left(U^n\right) = \begin{pmatrix} \mathbf{A}_1^n + \mathbf{C}_1^n & \mathbf{B}_1^n & 0 & \cdots & & 0 \\ \mathbf{C}_2^n & \mathbf{A}_2^n & \mathbf{B}_2^n & & & \\ 0 & \ddots & \ddots & \ddots & \ddots & \vdots \\ & & \ddots & \ddots & \ddots & \\ \vdots & & \ddots & \ddots & \ddots & \ddots & 0 \\ & & & & \mathbf{C}_{N-1}^n & \mathbf{A}_{N-1}^n & \mathbf{B}_{N-1}^n \\ 0 & & \cdots & & 0 & \mathbf{C}_N^n & \mathbf{A}_N^n + \mathbf{B}_N^n \end{pmatrix} \tag{5.12}$$

where $\mathbf{A}_i^n$, $\mathbf{B}_i^n$, and $\mathbf{C}_i^n$ are $M \times M$-matrices defined for $i \in \{1, 2, \ldots, N\}$ as

$$\mathbf{A}_i^n = \begin{pmatrix} \left(\beta_{i,1}^n + 2\alpha g_{S_{i,1}}^n\right) & 2\alpha g_{N_{i,1}}^n & 0 & \cdots & & 0 \\ 2\alpha g_{S_{i,2}}^n & \beta_{i,2}^n & 2\alpha g_{N_{i,2}}^n & & & \\ 0 & \ddots & \ddots & \ddots & \ddots & \vdots \\ & & \ddots & \ddots & \ddots & \\ \vdots & & \ddots & \ddots & \ddots & \ddots & 0 \\ & & & & 2\alpha g_{S_{i,M-1}}^n & \beta_{i,M-1}^n & 2\alpha g_{N_{i,M-1}}^n \\ 0 & & \cdots & & 0 & 2\alpha g_{S_{i,M}}^n & \left(\beta_{i,M}^n + 2\alpha g_{N_{i,M}}^n\right) \end{pmatrix}, \tag{5.13}$$

$$\mathbf{B}_i^n = \alpha \begin{pmatrix} \left(2g_{E_{i,1}}^n + g_{SE_{i,1}}^n\right) & g_{NE_{i,1}}^n & 0 & \cdots & & 0 \\ g_{SE_{i,2}}^n & 2g_{E_{i,2}}^n & g_{NE_{i,2}}^n & & & \\ 0 & \ddots & \ddots & \ddots & \ddots & \vdots \\ & & \ddots & \ddots & \ddots & \\ \vdots & & \ddots & \ddots & \ddots & \ddots & 0 \\ & & & & g_{SE_{i,M-1}}^n & 2g_{E_{i,M-1}}^n & g_{NE_{i,M-1}}^n \\ 0 & & \cdots & & 0 & g_{SE_{i,M}}^n & \left(2g_{E_{i,M}}^n + g_{NE_{i,M}}^n\right) \end{pmatrix}, \tag{5.14}$$

$$\mathbf{C}_i^n = \alpha \begin{pmatrix} \left(2g_{W_{i,1}}^n + g_{SW_{i,1}}^n\right) & g_{NW_{i,1}}^n & 0 & \cdots & & 0 \\ g_{SW_{i,2}}^n & 2g_{W_{i,2}}^n & g_{NW_{i,2}}^n & & & \\ 0 & \ddots & \ddots & \ddots & \ddots & \vdots \\ & & \ddots & \ddots & \ddots & \\ \vdots & & \ddots & \ddots & \ddots & \ddots & 0 \\ & & & & g_{SW_{i,M-1}}^n & 2g_{W_{i,M-1}}^n & g_{NW_{i,M-1}}^n \\ 0 & & \cdots & & 0 & g_{SW_{i,M}}^n & \left(2g_{W_{i,M}}^n + g_{NW_{i,M}}^n\right) \end{pmatrix} \tag{5.15}$$

with $\alpha = \frac{\delta_t}{2}$ and $\beta^n_{i,j} = 1 - \delta_t \left(g_N + g_S + g_E + g_W + \frac{g_{NE}+g_{SE}+g_{SW}+g_{NW}}{2} \right)^n_{i,j}$.

According to [54], filter (5.10) yields a unique sequence $(U^n)_{n\in\mathbb{N}}$ on every initial image U^0. Indeed, due to the continuity of the function g, U^n depends continuously on U^0 for every finite n. Besides, filter (5.8) satisfies the following maximum-minimum principle under a specific condition, which describes a stability property for the discrete scheme(5.8).

Theorem 5.2.1. *(Discrete extremum principle)*

For an iteration step δ_t satisfying

$$0 < \delta_t < \frac{1}{6 \max\limits_{s\in\mathbb{R}_+} g(s)}, \tag{5.16}$$

the scheme (5.8) satisfies:

$$\min_{i,j} u^0_{i,j} \le u^n_{i,j} \le \max_{i,j} u^0_{i,j} \tag{5.17}$$

for all $1 \le i \le N$, $1 \le j \le M$ and $n \in \mathbb{N}$.

Proof. For all $1 \le i \le \mathrm{N}$, $1 \le j \le \mathrm{M}$, and $n \in \mathbb{N}$, we have:

$$\begin{aligned} u^{n+1}_{i,j} =& \delta_t \left(g^n_{N_{i,j}} u^n_{i,j+1} + g^n_{E_{i,j}} u^n_{i+1,j} + g^n_{S_{i,j}} u^n_{i,j-1} + g^n_{W_{i,j}} u^n_{i-1,j} \right) \\ &+ \frac{\delta_t}{2} \left(g^n_{NE_{i,j}} u^n_{i+1,j+1} + g^n_{SE_{i,j}} u^n_{i+1,j-1} + g^n_{SW_{i,j}} u^n_{i-1,j-1} + g^n_{NW_{i,j}} u^n_{i-1,j+1} \right) \\ &+ \left[1 - \delta_t \left(g^n_{N_{i,j}} + g^n_{E_{i,j}} + g^n_{S_{i,j}} + g^n_{W_{i,j}} + \frac{g^n_{NE_{i,j}} + g^n_{SE_{i,j}} + g^n_{SW_{i,j}} + g^n_{NW_{i,j}}}{2} \right) \right] u^n_{i,j}. \end{aligned} \tag{5.18}$$

Since $0 < \delta_t < \frac{1}{6 \max\limits_{s\in\mathbb{R}_+} g(s)}$ and $g > 0$, the following inequality holds:

$$1 - \delta_t \left(g^n_{N_{i,j}} + g^n_{E_{i,j}} + g^n_{S_{i,j}} + g^n_{W_{i,j}} + \frac{g^n_{NE_{i,j}} + g^n_{SE_{i,j}} + g^n_{SW_{i,j}} + g^n_{NW_{i,j}}}{2} \right) > 0. \tag{5.19}$$

It follows then

$$\begin{aligned} u^{n+1}_{i,j} <& \delta_t \left(g^n_{N_{i,j}} + g^n_{E_{i,j}} + g^n_{S_{i,j}} + g^n_{W_{i,j}} \right) \max_{i,j} u^n_{i,j} + \frac{\delta_t}{2} \left(g^n_{NE_{i,j}} + g^n_{SE_{i,j}} + g^n_{SW_{i,j}} + g^n_{NW_{i,j}} \right) \max_{i,j} u^n_{i,j} \\ &+ \left[1 - \delta_t \left(g^n_{N_{i,j}} + g^n_{E_{i,j}} + g^n_{S_{i,j}} + g^n_{W_{i,j}} + \frac{g^n_{NE_{i,j}} + g^n_{SE_{i,j}} + g^n_{SW_{i,j}} + g^n_{NW_{i,j}}}{2} \right) \right] \max_{i,j} u^n_{i,j} \\ =& \max_{i,j} u^n_{i,j}. \end{aligned} \tag{5.20}$$

Similarly, we have

$$\begin{aligned} u_{i,j}^{n+1} >& \delta_t \left(g_{N_{i,j}}^n + g_{E_{i,j}}^n + g_{S_{i,j}}^n + g_{W_{i,j}}^n \right) \min_{i,j} u_{i,j}^n + \frac{\delta_t}{2} \left(g_{NE_{i,j}}^n + g_{SE_{i,j}}^n + g_{SW_{i,j}}^n + g_{NW_{i,j}}^n \right) \min_{i,j} u_{i,j}^n \\ &+ \left[1 - \delta_t \left(g_{N_{i,j}}^n + g_{E_{i,j}}^n + g_{S_{i,j}}^n + g_{W_{i,j}}^n + \frac{g_{NE_{i,j}}^n + g_{SE_{i,j}}^n + g_{SW_{i,j}}^n + g_{NW_{i,j}}^n}{2} \right) \right] \min_{i,j} u_{i,j}^n \\ &= \min_{i,j} u_{i,j}^n. \end{aligned} \tag{5.21}$$

Consequently, the result (5.17) is true for $n = 1$ because

$$\min_{i,j} u_{i,j}^0 < u_{i,j}^1 < \max_{i,j} u_{i,j}^0. \tag{5.22}$$

Therefore, by induction, it is easy to prove the result (5.17). Which completes the proof. □

5.3 Experimental Procedures and Results

5.3.1 Experimental Procedures

This subsection is devoted to comparing our model (5.8),(5.9), as an image denoising algorithm, with the ones proposed by Perona and Malik (PM) [40], Charbonnier et al. (C) [13], Wang and Zhou (W-Z) [52] and Maiseli (M) [37]. All the experiments are conducted under Windows 10 and Matlab 2018*b*, running on a laptop with an Intel® Core™ i7-10510U (8 MB cache, 4 Core, up to 4.9 GHz), 16 GB memory (LPDDR3, Dual-channel, 2133 MHz), and 512 GB storage (PCIe, SSD, 3×4). The experiments were done on three actual MRI scans (Figure 5.1) affected by different σ^2-values of zero-mean white Gaussian noise and restored using our filter (5.8) with the boundary-initial conditions (5.9), provided that the proposed diffusion function g (see (2.113)) satisfies the assumptions ((2.100), (3.5), (3.8)).

We also used the discrete diffusion filter suggested by Perona and Malik [40] with the following diffusion functions:

- Perona and Malik diffusion function [40]:

$$g(s) = \frac{1}{1 + \left(\frac{s}{k}\right)^2}, \; k > 0. \tag{5.23}$$

- Charbonnier et al. diffusion function [13]:

$$g(s) = \frac{1}{\sqrt{1 + \left(\frac{s}{k}\right)^2}}, \; k > 0. \tag{5.24}$$

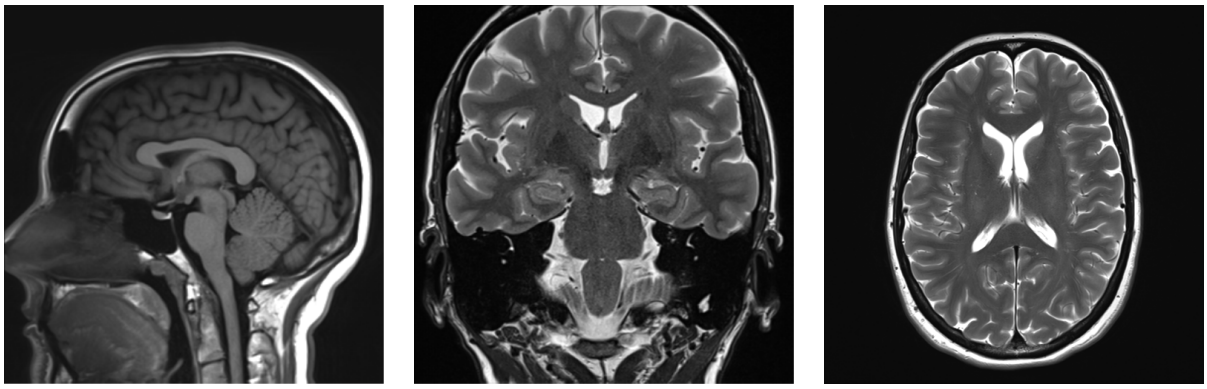

FIGURE 5.1: Brain MRI scans (512 x 512): (a) Patient30: Sagittal T1 of a 30 years old female patient [20]. (b) Patient50: Coronal T2 of a 50 years old female patient [21]. (c) Patient55: Axial T2 of a 55 years old patient [22].

- Wang and Zhou diffusion function [52]:

$$g(s) = \frac{1}{s+1} + \frac{\log(s+1)}{s} \quad s \geq 0. \tag{5.25}$$

- Maiseli diffusion function [37]:

$$g(s) = \begin{cases} \frac{1}{1+\left(\frac{s}{k_1}\right)^2} & s < k_1 \\ \frac{1}{\sqrt{1+\left(\frac{s}{k_2}\right)^2}} & s \geq k_1, \end{cases} \tag{5.26}$$

  where k_1 and k_2 are positive constants.

Besides, in order to evaluate the quality of the restored images from the above different image denoising methods, we used two image quality metrics:

- Peak Signal-to-Noise Ratio ($PSNR$) [23]:

$$PSNR = 10\log_{10}\left(\frac{255^2 MN}{\|u-I\|_2^2}\right), \tag{5.27}$$

  where I is the original or the uncorrupted image, and u is the distorted or the restored image. $PSNR$ is one of the oldest image quality metrics evaluating an image's signal strength relative to noise, which is always positive. We evaluate the $PSNR$ metric by using the Matlab 2018b built-in function "psnr." However, due to its limitations and its failure in some circumstances as an adequate image quality model [53], we used another metric that significantly correlates with human visual perception.

- Structural SIMilarity Index ($SSIM$) [65]:

$$SSIM = \frac{(2\mu_u\mu_I + c_1)(2\sigma_{uI} + c_2)}{(\mu_u^2 + \mu_I^2 + c_1)(\sigma_u^2 + \sigma_I^2 + c_2)}, \tag{5.28}$$

  where c_1 and c_2 are tuning parameters. μ_u, σ_u^2, and σ_{uI} stand for the mean, variance, and covariance, respectively. It is a method for measuring the similarity between a degraded image and a perfect one, and it is bounded between zero and one. For a good similarity between the original and the restored images, we need higher values of $SSIM$-index. We evaluate the $SSIM$ metric by using the Matlab 2018b built-in function "ssim."

In the following, to quantify the quality of the restored images, we use IQM to denote one of the two quality metrics: $PSNR$ or $SSIM$. The iterations are stopped when the IQM value reaches the maximum.

The image denoising process using the proposed model (5.8) can be implemented as shown in Algorithm 1, denoted by the function $MaxIQM()$: First, we consider I as one of the three original brain MRI scans (Figure 5.1) and generate in it a Gaussian white noise with zero-mean and σ^2-value, using the Matlab 2018b built-in function "imnoise." Next, the initial value u^0 is set to be the noisy image in the while-loop. After that, a while-loop is executed, where our filter is used to build a new image with a new IQM value in each iteration. Finally, when the stopping criterion is confirmed, we obtain the restored image with the corresponding iteration.

On the other hand, as introduced in section 2.4.2, the diffusion function g is constructed using cubic Hermite splines, determined by specific parameters $\{k_0, k_1, p_0, p_1, v_0, v_1\}$ $(m = 1)$. Hence, how can we select the most appropriate parameters that indicate our model's best possible adaptive diffusion function?

The following optimization problem can give a possible answer to this question:

$$\begin{cases} \max\limits_{\mathbf{z}} \ IQM(\mathbf{z}) \\ \text{subject to } \mathbf{z} \in \mathbf{S}, \end{cases} \tag{5.29}$$

where $IQM : \mathbb{R}^6 \to \mathbb{R}_+$ such that $\mathbf{z} = (\delta_t, k_1, p_0, p_1, v_0, v_1)$.

$\mathbf{S} \subset \mathbb{R}^m$ is a feasible decision space defined by box constraints, and $\mathbf{z} \in \mathbf{S}$ is the decision vector. Then, a solution $\mathbf{z}_1 \in \mathbf{S}$ is better than another solution, $\mathbf{z}_2 \in \mathbf{S}$ if and only if $IQM(\mathbf{z}_1) > IQM(\mathbf{z}_2)$. Unfortunately, we do not have an explicit expression that relates the decision vector $\mathbf{z}$ to IQM. Thus we seek the best possible solution $\mathbf{z}$ that maximizes locally our objective IQM using a Direct-Search

input : I.

output : u, $iter$, $\texttt{IQM}$.

Initialize: I;

$u^0 \leftarrow \texttt{imnoise}\left(I, "gaussian", 0, \sigma^2\right)$;

$\texttt{IQM}_0 \leftarrow \texttt{PSNR}\left(I, u^0\right)$ $\left(\text{or } \texttt{SSIM}\left(I, u^0\right)\right)$;

$u \leftarrow u^0$;

$iter \leftarrow 0$;

$\texttt{IQM} \leftarrow \texttt{IQM}_0$;

$n \leftarrow 0$;

while *true* **do**

$\Delta_{N} u^n \leftarrow [\texttt{zeros}\,(1, M)\ ;\ (u^n\,(1 : N-1, :) - u^n\,(2 : N, :))]$;

$\Delta_{S} u^n \leftarrow [(-\Delta_{N} u^n\,(2 : N, :))\ ;\ \texttt{zeros}(1, M)]$;

$\Delta_{E} u^n \leftarrow [(u^n\,(:, 2 : M) - u^n\,(:, 1 : M-1))\ \texttt{zeros}\,(N, 1)]$;

$\Delta_{W} u^n \leftarrow [\texttt{zeros}\,(N, 1)\ \ (-\Delta_{E} u^n\,(:, 1 : M-1))]$;

$\Delta_{NE} u^n \leftarrow [\Delta_{E} u^n\,(1, 1 : M-1)\ 0\ ;\ (u^n\,(1 : N-1, 2 : M) - u^n\,(2 : N, 1 : M-1))\ \Delta_{N} u^n\,(2 : N, M)]$;

$\Delta_{SW} u^n \leftarrow -\,[\Delta_{N} u^n\,(2 : N, 1)\ \Delta_{NE} u^n\,(2 : N, 1 : M-1)\ ;\ 0\ \Delta_{E} u^n\,(N, 1 : M-1)]$;

$\Delta_{SE} u^n \leftarrow [(u^n\,(2 : N, 2 : M) - u^n\,(1 : N-1, 1 : M-1))\ \Delta_{S} u^n\,(1 : N-1, M)\ ;\ \Delta_{E} u^n\,(N, 1 : M-1)\ 0]$;

$\Delta_{NW} u^n \leftarrow -\,[0\ \Delta_{E} u^n\,(1, 1 : M-1)\ ;\ \Delta_{S} u^n\,(1 : N-1, 1)\ \Delta_{SE} u^n\,(1 : N-1, 1 : M-1)]$;

$g_{\alpha}^n \leftarrow g_{\alpha}^n\,(|\Delta_{\alpha} u^n|)\,,\ \alpha \in \Lambda_1 = \{N, E, S, W\}$;

$g_{\beta}^n \leftarrow g_{\beta}^n \left(\frac{\left|\Delta_{\beta} u^n\right|}{\sqrt{2}}\right),\ \beta \in \Lambda_2 = \{NE, SE, SW, NW\}$;

$u^{n+1} \leftarrow u^n + \delta_t \left[\sum_{\alpha \in \Lambda_1} g_{\alpha}^n \Delta_{\alpha} u^n + \sum_{\beta \in \Lambda_2} \frac{g_{\beta}^n \Delta_{\beta} u^n}{2}\right]$;

$\texttt{IQM}_{n+1} \leftarrow \texttt{PSNR}\left(I, u^{n+1}\right)$ $\left(\text{or } \texttt{SSIM}\left(I, u^{n+1}\right)\right)$;

if $(\texttt{IQM}_{n+1} > \texttt{IQM})$ **then**

$\texttt{IQM} \leftarrow \texttt{IQM}_{n+1}$;

$iter \leftarrow n + 1$;

$u \leftarrow u^{n+1}$;

else

`Break`;

end

$n \leftarrow n + 1$;

end

Algorithm 1: Proposed image denoising algorithm.

Algorithm 5.2 that solves the following problem:

$$\begin{cases} \max\limits_{\mathbf{z}} IQM(\mathbf{z}) \\ \quad \text{subject to } g(s) > 0 \quad s \geq 0 \\ \qquad\qquad g'(s) \leq 0 \quad s \geq 0 \\ \qquad\qquad g(s) + sg'(s) \geq 0 \quad s \geq 0 \\ \qquad\qquad 0 < \delta_t < \dfrac{1}{6g(0)}. \end{cases} \tag{5.30}$$

In brief, while respecting the requirements of the above optimization problem, our algorithm 5.2 modifies the parameters of $\mathbf{z}$, so the IQM value increases. This process recurs consecutively until the IQM value reaches a local maximum. Each parameter is a decimal number that comprises digits and precision. Moreover, as depicted in the flowchart of Figure 5.2, the instructions of the algorithm are described as follows:

1. The process begins by initializing the decision vector $\mathbf{z}(i)$, their precision p_r, and a test image I.

2. Next, $\{u, iter, IQM\}$ are computed using $MaxIQM()$ (defined by algorithm 1).

3. Finally, a nested loop (While-For) is used to determine the local optimal decision vector $\mathbf{z}_{op}$, $iter_{op}$, IQM_{op}, and u_{op}(the restored image). At each iteration, $FindingOptimum()$ changes the parameter $\mathbf{z}(i)$ under the constraints of 5.30, and accepts the new parameter value in case of a better IQM.

5.3.2 Experimental Results

Several tests have been performed using Algorithm 5.2 on the images in Figure 5.1 to obtain the best possible parameters, as shown in Tables 5.3, 5.4, 5.5, and 5.6.

Tables 5.1 and 5.2 show quantitative results on actual images, corrupted with various white Gaussian noises, filtered by different filters. From Table 5.1, it is clear that the $PSNR$ value of the restored images via the proposed method has, in most cases, higher values with slight differences over the Maiseli and Wang-Zhou methods. However, as shown in Table 5.2, when it comes to the $SSIM$-index, the proposed method reveals impressive results against the Wang-Zhou and Maiseli methods.

From a visual comparison, Figures 5.3, 5.4, and 5.5 show that the denoising process using $SSIM$-index removes noises more efficiently and preserves basic image features better than using $PSNR$. Additionally, the images obtained using $PSNR$ are more affected by blocky artifacts than those achieved by $SSIM$-index. Finally, it can be seen from images related to $SSIM$-index in Figures 5.3, 5.4, and 5.5 that the Wang and Zhou method, Maiseli method, and the proposed method remove noise more effectively and generate sharper edges than those of Charbonnier et al. and Perona and Malik. In addition, these three schemes remain flat areas smoother and cleaner with less noticeable artifacts.

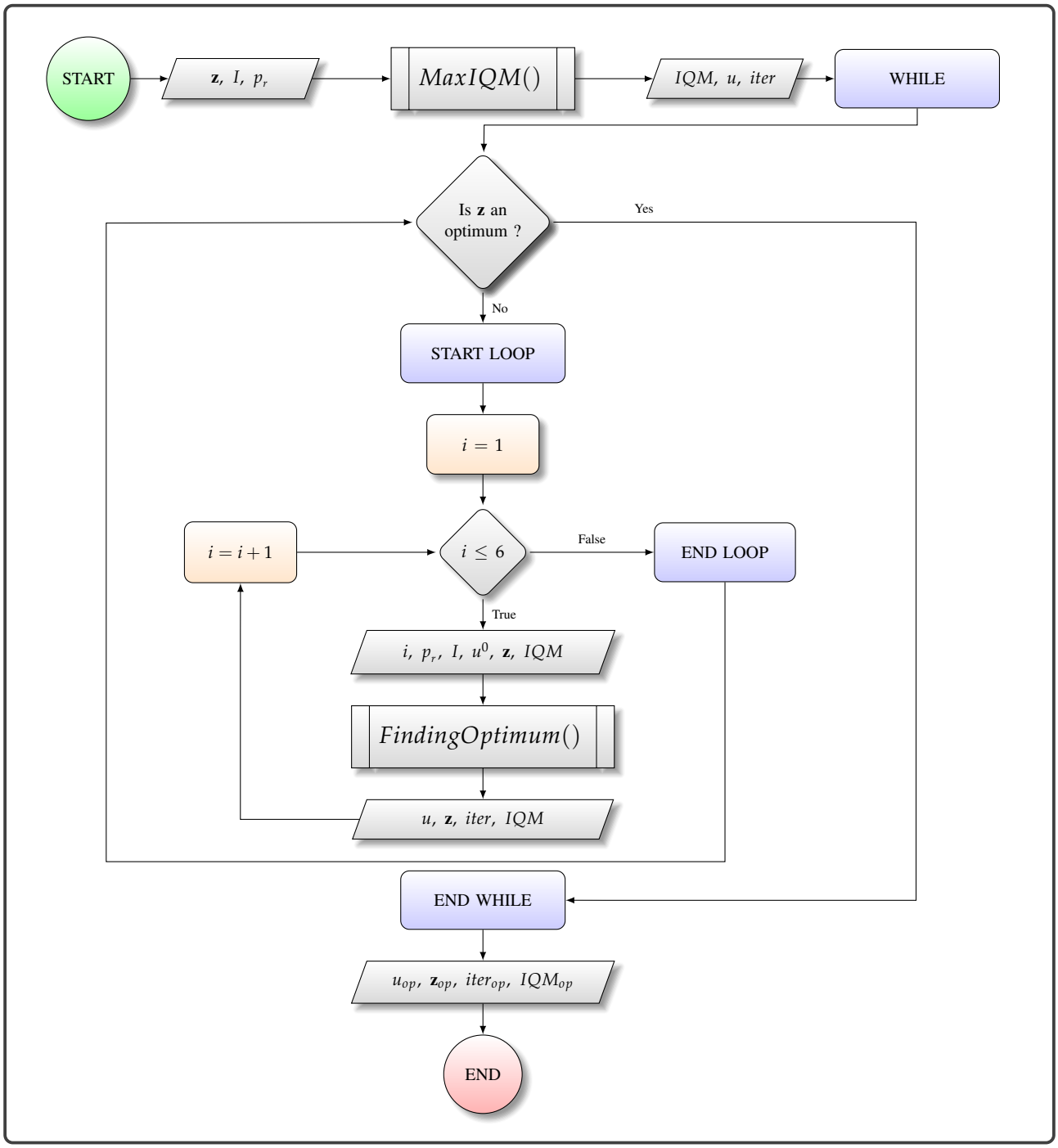

FIGURE 5.2: Optimal image denoising algorithm

TABLE 5.1: $PSNR$ values of the images in Figure 5.1 affected by different σ^2-values of zero-mean white Gaussian noise and restored from different methods with their corresponding iteration number.

		Noisy	Perona-Malik [40]		Charbonnier et al. [13]		Wang-Zhou [52]		Maiseli [37]		Proposed	
	σ^2	$PSNR$	$PSNR$	$Iter$	$PSNR$	$Iter$	$PSNR$	$Iter$	$PSNR$	$Iter$	$PSNR$	$Iter$
Patient30	0.005	23.4349	33.2195	19	33.0492	8	34.0154	15	33.9567	8	**34.0486**	9
	0.010	20.6756	31.0058	22	30.9157	12	31.7695	20	31.7113	11	**31.7889**	13
	0.015	19.1190	29.9431	70	29.6214	14	30.3924	24	30.3565	17	**30.4188**	24
Patient50	0.005	23.6170	31.1280	2	31.0768	3	31.4137	12	**31.4998**	3	31.4370	5
	0.010	20.7956	29.0150	3	28.9615	5	29.3396	16	**29.3553**	5	29.3499	6
	0.015	19.1148	27.6709	4	27.6651	4	28.0386	30	27.9866	18	**28.0518**	29
Patient55	0.005	24.0017	30.9334	14	30.6366	6	31.8453	12	**31.8617**	8	31.7777	15
	0.010	21.2623	29.0902	57	28.4924	9	**29.4402**	16	29.4208	14	29.4188	22
	0.015	19.5904	27.9457	80	27.0896	11	**27.9935**	36	27.9027	18	27.9465	39

TABLE 5.2: $SSIM$ values of the images in Figure 5.1 affected by different σ^2-values of zero-mean white Gaussian noise and restored from different methods with their corresponding iteration number.

		Noisy	Perona-Malik [40]		Charbonnier et al. [13]		Wang-Zhou [52]		Maiseli [37]		Proposed	
	σ^2	$SSIM$	$SSIM$	$Iter$	$SSIM$	$Iter$	$SSIM$	$Iter$	$SSIM$	$Iter$	$SSIM$	$Iter$
Patient30	0.005	0.3425	0.9237	21	0.9219	13	0.9367	19	0.9339	16	**0.9384**	14
	0.010	0.2425	0.8976	28	0.8958	17	0.9144	26	0.9100	22	**0.9167**	20
	0.015	0.1962	0.8778	28	0.8766	21	0.8972	31	0.8923	26	**0.9001**	24
Patient50	0.005	0.4405	0.8601	8	0.8594	9	0.8763	14	0.8757	12	**0.8767**	12
	0.010	0.3287	0.8148	54	0.8046	14	0.8263	21	0.8275	21	**0.8276**	21
	0.015	0.2696	0.7871	88	0.7658	15	0.7900	25	0.7912	26	**0.7918**	25
Patient55	0.005	0.3858	0.8994	20	0.8943	14	0.9230	17	0.9209	20	**0.9268**	21
	0.010	0.2903	0.8543	23	0.8500	18	0.8842	26	0.8838	30	**0.8893**	29
	0.015	0.2404	0.8400	100	0.8142	21	0.8512	30	0.8513	30	**0.8570**	37

TABLE 5.3: The best possible parameters for the proposed diffusion function used to calculate $PSNR$.

		Proposed					
	σ^2	δ_t	k_1	p_0	p_{k_1}	v_0	v_{k_1}
Patient30	0.005	0.14731	4.37351	1.13131	0.86851	-0.00001	-0.15601
	0.010	0.15631	2.68581	1.06001	0.87661	-0.00021	-0.15701
	0.015	0.14721	2.68711	0.84211	0.67931	-0.00101	-0.15601
Patient50	0.005	0.18831	3.87641	0.88501	0.70731	-0.00001	-0.00061
	0.010	0.24821	4.91501	0.66801	0.58141	-0.00001	-0.02571
	0.015	0.14721	1.70631	0.74111	0.57931	-0.00001	-0.14821
Patient55	0.005	0.14731	3.67421	1.03131	0.57671	-0.00021	-0.15591
	0.010	0.14731	3.58521	0.86541	0.56361	-0.00001	-0.15601
	0.015	0.10151	3.64241	0.83071	0.56871	-0.00001	-0.15601

TABLE 5.4: The best possible parameters for the proposed diffusion function used to calculate $SSIM$.

		Proposed					
	σ^2	δ_t	k_1	p_0	p_{k_1}	v_0	v_{k_1}
Patient30	0.005	0.14731	3.58591	1.12901	0.77571	-0.00101	-0.15501
	0.010	0.14651	3.48321	1.13121	0.77841	-0.00001	-0.17611
	0.015	0.14721	3.45081	1.13201	0.76951	-0.00011	-0.17471
Patient50	0.005	0.14711	2.68461	1.04221	0.77941	-0.00021	-0.15631
	0.010	0.14721	2.60841	1.03391	0.66971	-0.00011	-0.15601
	0.015	0.14831	2.68631	1.05321	0.66851	-0.00101	-0.15601
Patient55	0.005	0.14731	3.58611	1.13111	0.56851	-0.00001	-0.15601
	0.010	0.14731	3.57621	1.13111	1.13111	-0.00011	-0.15601
	0.015	0.13931	3.58751	1.13111	0.56861	-0.00001	-0.15521

TABLE 5.5: The best possible parameters for different diffusion functions used to calculate $PSNR$.

		Perona-Malik		Charbonnier el al.		Wang-Zhou	Maiseli		
	σ^2	δ_t	K	δ_t	K	δ_t	δ_t	K_1	K_2
Patient30	0.005	0.24961	84.47201	0.24631	70.57291	0.24001	0.24011	0.28231	8.38981
	0.010	0.24951	104.36341	0.23211	70.29221	0.24111	0.24041	0.28231	8.18761
	0.015	0.14551	94.47301	0.24051	70.58301	0.23311	0.23831	0.28231	6.19131
Patient50	0.005	0.24991	553.83011	0.24201	202.58391	0.23311	0.24901	30.01511	21.99781
	0.010	0.24991	524.54311	0.24021	159.68481	0.23321	0.23541	27.42691	18.31031
	0.015	0.24991	473.95011	0.24451	279.60871	0.16111	0.14441	0.28231	8.51031
Patient55	0.005	0.24951	94.47301	0.24951	71.39501	0.23311	0.24741	0.28231	6.00191
	0.010	0.24971	64.68911	0.24011	70.67491	0.24341	0.14951	0.28231	8.39261
	0.015	0.14911	88.44791	0.24111	70.59201	0.13731	0.14641	0.28231	8.31861

TABLE 5.6: The best possible parameters for different diffusion functions used to calculate $SSIM$.

		Perona-Malik		Charbonnier el al.		Wang-Zhou	Maiseli		
	σ^2	δ_t	K	δ_t	K	δ_t	δ_t	K_1	K_2
Patient30	0.005	0.24971	94.47991	0.24211	69.58341	0.24411	0.22541	0.28231	5.08241
	0.010	0.24921	103.47301	0.24411	71.59401	0.24141	0.23711	0.28231	4.85231
	0.015	0.24961	124.66331	0.24141	70.58391	0.24411	0.23561	0.28231	4.97171
Patient50	0.005	0.24321	184.59611	0.24211	81.39391	0.24861	0.22961	0.28231	5.29161
	0.010	0.24111	70.59391	0.24111	69.69521	0.23321	0.24941	0.28231	3.68091
	0.015	0.24711	70.49311	0.24211	79.57381	0.23331	0.23751	0.28231	3.91881
Patient55	0.005	0.24771	93.47311	0.24021	55.70261	0.24111	0.22341	0.28231	3.40061
	0.010	0.24971	112.47421	0.23281	60.59351	0.21991	0.24831	0.28231	2.95851
	0.015	0.24961	67.48391	0.24201	60.57301	0.23211	0.22811	0.28231	3.98981

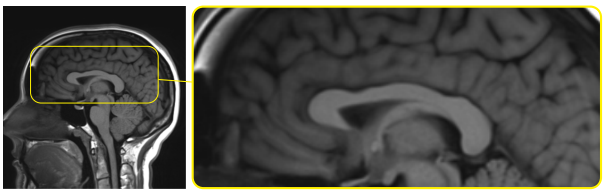

(a) Original

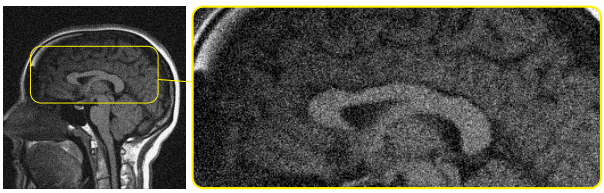

(b) Noisy

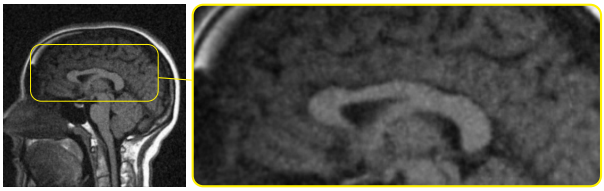

(c) PM-Restored-PSNR

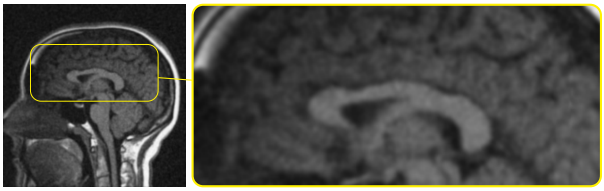

(d) PM-Restored-SSIM

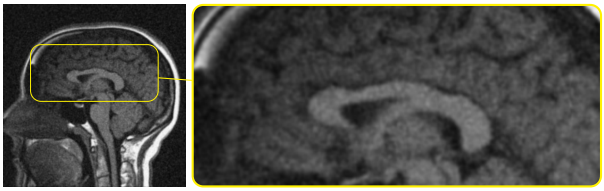

(e) C-Restored-PSNR

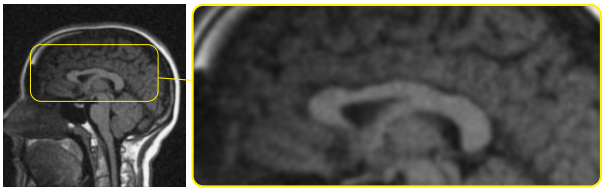

(f) C-Restored-SSIM

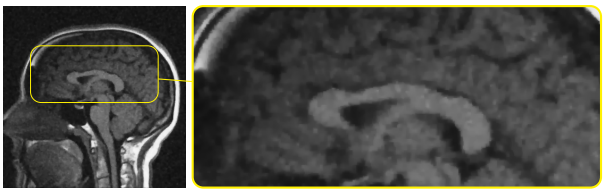

(g) WZ-Restored-PSNR

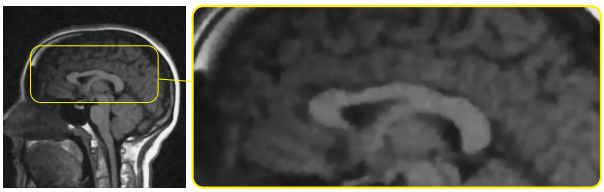

(h) WZ-Restored-SSIM

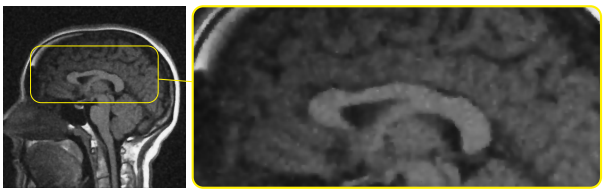

(i) M-Restored-PSNR

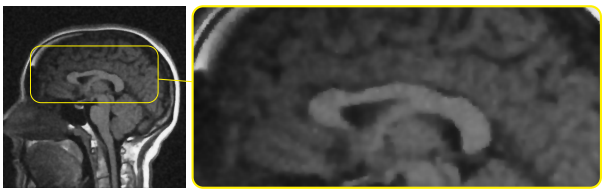

(j) M-Restored-SSIM

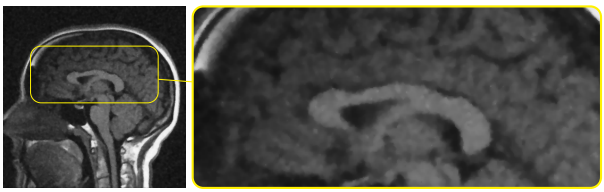

(k) P-Restored-PSNR

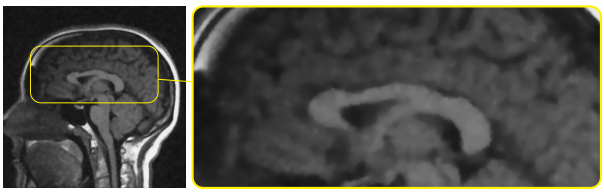

(l) P-Restored-SSIM

FIGURE 5.3: Visual comparison on actual MRI scan of Patient30 corrupted by zero-mean white Gaussian noise with $\sigma^2 = 0.015$ and restored from various methods.

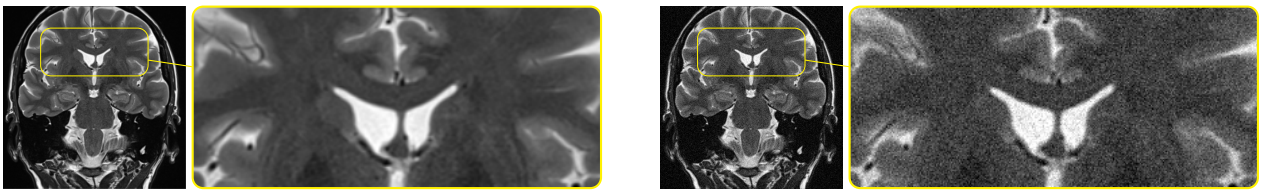

(a) Original

(b) Noisy

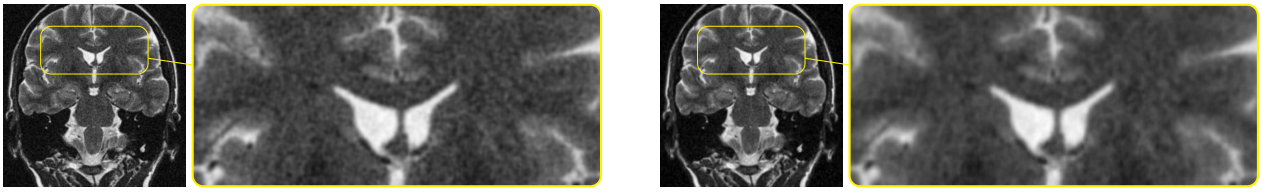

(c) PM-Restored-PSNR

(d) PM-Restored-SSIM

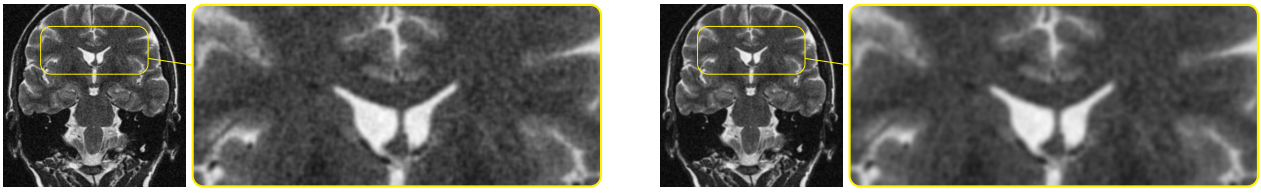

(e) C-Restored-PSNR

(f) C-Restored-SSIM

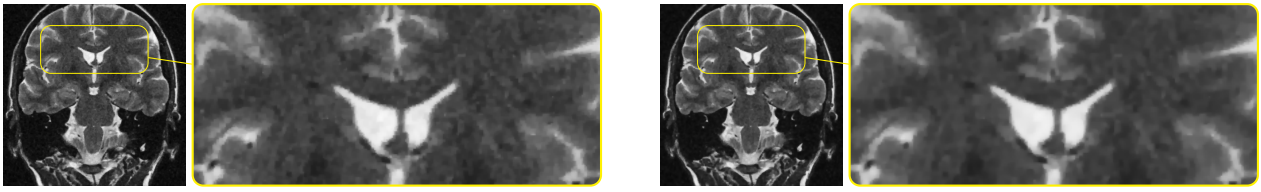

(g) WZ-Restored-PSNR

(h) WZ-Restored-SSIM

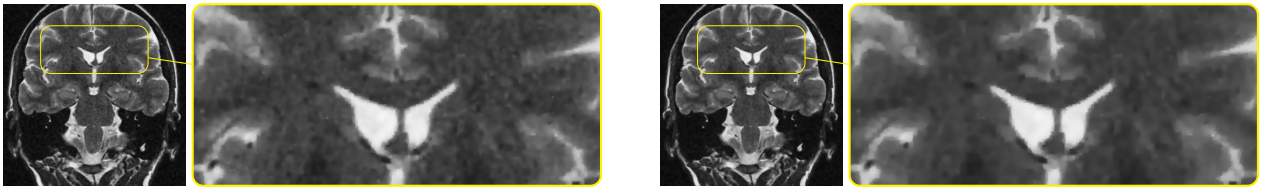

(i) M-Restored-PSNR

(j) M-Restored-SSIM

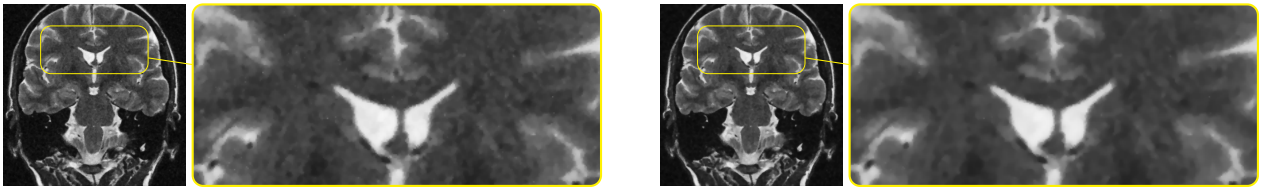

(k) P-Restored-PSNR

(l) P-Restored-SSIM

FIGURE 5.4: Visual comparison on actual MRI scan of Patient50 corrupted by zero-mean white Gaussian noise with $\sigma^2 = 0.015$ and restored from various methods.

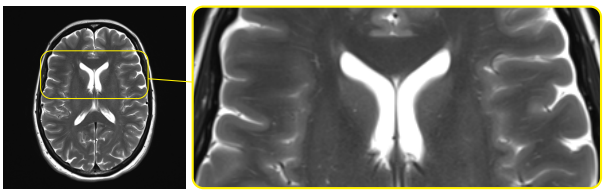

(a) Original

(b) Noisy

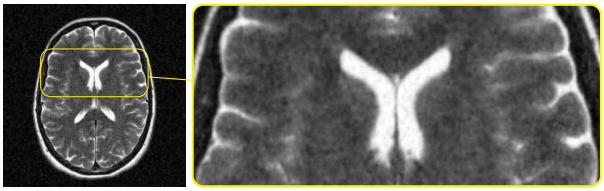

(c) PM-Restored-PSNR

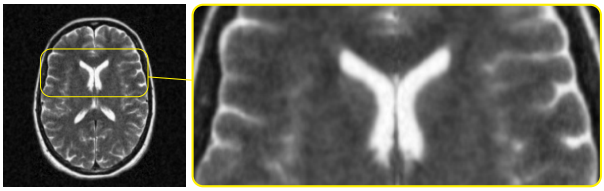

(d) PM-Restored-SSIM

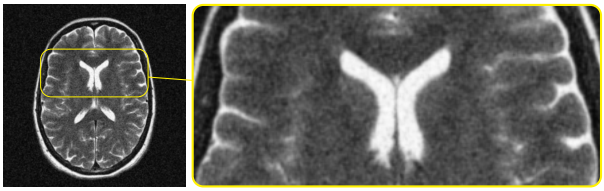

(e) C-Restored-PSNR

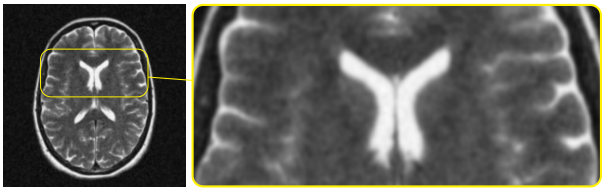

(f) C-Restored-SSIM

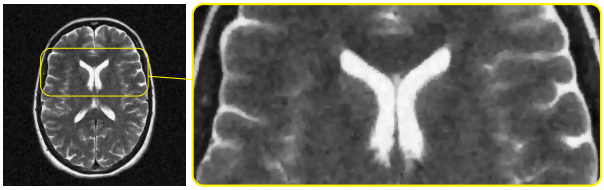

(g) WZ-Restored-PSNR

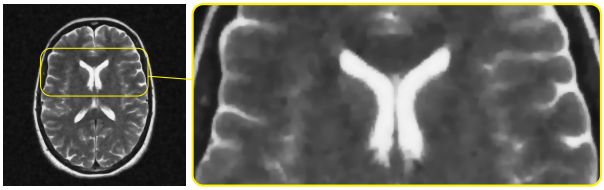

(h) WZ-Restored-SSIM

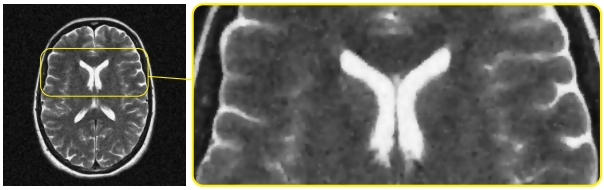

(i) M-Restored-PSNR

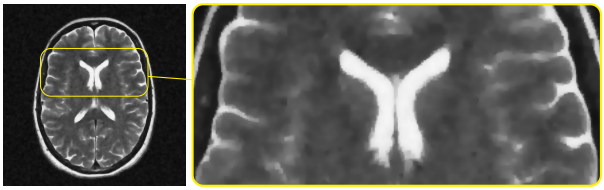

(j) M-Restored-SSIM

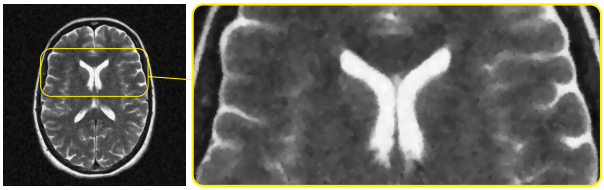

(k) P-Restored-PSNR

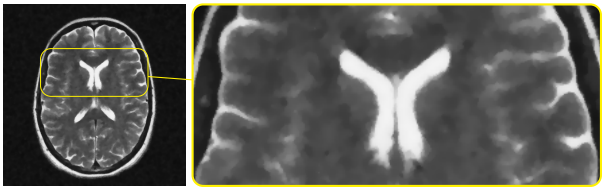

(l) P-Restored-SSIM

FIGURE 5.5: Visual comparison on actual MRI scan of Patient55 corrupted by zero-mean white Gaussian noise with $\sigma^2 = 0.015$ and restored from various methods.

5.4 Conclusion

We have established a consistent and stable numerical scheme for the denoising process and have used the cubic Hermite spline to approximate the best possible diffusion function using a direct search algorithm. Furthermore, we have proved that our method can provide better results than others in the $SSIM$-index.

Eventually, It is worth pointing out that the experimental results depend on various factors such as the choice of the numerical approximation method, the characteristics of the diffusion function, and the initialized parameters' values and their precision; Which means that one could achieve better results while choosing different numerical methods, another diffusion function, or several values of the initialized parameters. Thus, it would be challenging to devise an algorithm that estimates global optimum with the best adaptive diffusion function and numerical approximation method.

Chapter 6

Conclusion

Since 1980, the appearance of different forms of diffusion equations models in image processing and analysis has had a tremendous impact on the technological advancement of artificial vision systems that involves digital images. This thesis has provided a new model that belongs to the general class of anisotropic nonlinear diffusion equations.

First, we have surveyed the most remarkable research studies in the literature concerning the (non)linear and (an)isotropic diffusion filtering in image processing and analysis. Then, we have directly analyzed the Perona-Malik diffusion equation behavior in two-dimensional space by investigating the temporal variation of the gradient magnitude of the image at the edge points. Eventually, we have presented and interpreted a new anisotropic nonlinear diffusion model and have suggested a possible strategy to investigate the existence and uniqueness of solutions for the proposed model.

Next, we have introduced a quasilinear second-order elliptic problem and have examined it by showing at first the existence of a minimizer in an appropriate functional space that involves Orlicz spaces via a variational approach. Then, we have demonstrated the uniqueness of solutions by employing the monotonicity property of a nonlinear operator.

After that, we have presented an initial boundary value problem as an anisotropic nonlinear diffusion partial differential equation. In the beginning, we used an implicit iterative method (discretization in time-variable only) to approximate the nonlinear evolution problem by nonlinear elliptic problems. Then, we have employed the variational approach to show the existence and uniqueness of weak solutions for each elliptic problem. Lastly, we have used an energy estimate and a monotonicity property of a nonlinear operator to confirm the existence of unique weak solutions for the evolution problem.

Finally, we have considered the numerical approximation method, namely the explicit finite difference method, to implement different nonlinear diffusion models. We have proved that our scheme is a consistent and stable numerical model. Then, we have illustrated some experiments on different actual brain Magnetic Resonance Imaging (MRI) scans and have shown that the proposed model has impressive results compared to others in terms of the Structural SIMilarity Index ($SSIM$).

Nevertheless, we assume that there are many new results that we need to seek, especially those that are likely to consist of a straightforward extension of the proposed model. Moreover, we can list some of the future work as perspectives:

- At the theoretical level, we aim to examine the stability and regularity of the weak solution of the initial-boundary value problem (4.1).
- It is of great interest at the numerical level if we study and apply other numerical approximation methods on the proposed model (4.1), such as the additive operator splitting method and the fast explicit diffusion method developed by Weickert in [59, 58], Krylov subspace spectral [24], finite element method, or Mixed Finite Element Method [28, 27].

Appendix A

Mathematical tools

In this Appendix, we recall some mathematical tools used in this thesis, such as inequalities, functional spaces, convergence, and compactness theorems.

A.1 Matrices

- we write $\mathbf{A} = \left(a_{ij}\right)$ to mean an $n \times n$ matrix with $(i,j)^{th}$ entry a_{ij}.
- $\mathrm{tr}\,(\mathbf{A}) =$ trace of the matrix $\mathbf{A}$.
- $\det(\mathbf{A}) =$ determinant of the matrix $\mathbf{A}$.
- $\mathbf{A}^{\top} =$ transpose of the matrix $\mathbf{A}$.

A.2 Geometry

- $\mathbb{R}^2 = 2$-dimensional real Euclidean space, $\mathbb{R} = \mathbb{R}^1$.
- $e_1 = (1,0)^{\top}$ and $e_2 = (0,1)^{\top}$ are the standard coordinate vector.
- An element x in $\mathbb{R}^2$ is defined as $x = (x_1, x_2)^{\top}$.
- Ω is an open subset of $\mathbb{R}^2$, $\partial\Omega =$ boundary of Ω, $\overline{\Omega} = \Omega \cup \partial\Omega =$ closure of Ω.
- $|\Omega| =$ surface area or measure of Ω.

A.3 Derivatives

- Assume $u : \Omega \to \mathbb{R}$, $x \in \Omega$.
- $\frac{\partial u}{\partial x_i}(x) = \lim_{h \to 0} \frac{u(x + he_i) - u(x)}{h}$, provided this limit exists.
- we write u_{x_i} or ∂u_{x_i} to denote $\frac{\partial u}{\partial x_i}$.

- a vector of the form $\alpha = (\alpha_1, \alpha_2, \ldots, \alpha_n)^\top$, where each component α_i is a nonnegative integer, is called a multiindex of order

$$|\alpha| = \alpha_1 + \alpha_2 + \ldots + \alpha_n. \tag{A.1}$$

- Given a multiindex α, we define

$$\partial^\alpha u(x) = \frac{\partial^{|\alpha|} u(x)}{\partial x_1^{\alpha_1} \ldots \partial x_n^{\alpha_n}}. \tag{A.2}$$

- $\nabla u = (u_{x_1}, u_{x_2})^\top$ = gradient vector of u.
- $\mathbf{H}_u = \begin{pmatrix} u_{x_1x_1} & u_{x_1x_2} \\ u_{x_2x_1} & u_{x_2x_2} \end{pmatrix}$ = Hessian matrix.
- Assume $\mathbf{f} : \mathbb{R}^2 \to \mathbb{R}^2$ is a function such that each of its first-order partial derivatives exists on $\mathbb{R}^2$. Then, we define the Jacobian matrix of $\mathbf{f}$ as

$$\mathbf{J_f} = \begin{pmatrix} \frac{f_1(x)}{\partial x_1} & \frac{f_1(x)}{\partial x_2} \\ \frac{f_2(x)}{\partial x_1} & \frac{f_2(x)}{\partial x_2} \end{pmatrix}. \tag{A.3}$$

- $\nabla \cdot \mathbf{f} = \frac{\partial f_1(x)}{\partial x_1} + \frac{\partial f_2(x)}{\partial x_2}$ = divergence of $\mathbf{f}$.

A.4 Inequalities

- Cauchy's inequality:

$$ab \leq \frac{a^2}{2} + \frac{b^2}{2} \quad (a, b \in \mathbb{R}). \tag{A.4}$$

- For all $a \geq 0$ and $b \geq 1$, we have

$$ab \leq a \exp(a) + b \log(b). \tag{A.5}$$

Proof. If $b \leq \exp(a)$ then $ab \leq a \exp(a) \leq a \exp(a) + b \log(b)$.
If $\exp(a) < b$ then $a < \log(b)$, which means $ab < b \log(b) < a \exp(a) + b \log(b)$. □

- Cauchy-Schwarz inequality

$$|x \cdot y| \leq |x| \, |y| \quad \left(x, y \in \mathbb{R}^2\right). \tag{A.6}$$

- A function $f : \mathbb{R}^n \to \mathbb{R}$ is called convex provided

$$f(tx + (1-t)y) \leq tf(x) + (1-t)f(y) \quad (x, y \in \mathbb{R}^n,\ 0 \leq t \leq 1). \tag{A.7}$$

- Assume $f : \mathbb{R}^n \to \mathbb{R}$ is convex. Then

$$f(y) \geq f(x) + \nabla f(x)(y - x) \quad (x, y \in \mathbb{R}^n). \tag{A.8}$$

- *Jensen's Inequality*[29]: For a real-valued convex function φ, numbers $s_1,\ s_2, \ldots,\ s_n$ in its domain, and positive weights α_i, Jensen's inequality can be stated as:

$$\varphi\left(\frac{\sum_{i=1}^{n} \alpha_i s_i}{\sum_{i=1}^{n} \alpha_i}\right) \leq \frac{\sum_{i=1}^{n} \alpha_i \varphi(s_i)}{\sum_{i=1}^{n} \alpha_i}. \tag{A.9}$$

A.5 Function Spaces

- $C(\Omega) = \{u : \Omega \to \mathbb{R} \mid u \text{ continuous}\}$.
- $C(\overline{\Omega}) = \{u \in C(\Omega) \mid u \text{ is uniformly continuous on bounded subsets of } \Omega\}$.
- $C^k(\Omega) = \{u : \Omega \to \mathbb{R} \mid u \text{ is k-times continuously differentiable}\}$.
- $C^k(\overline{\Omega}) = \{u \in C^k(\Omega) \mid \partial^\alpha u \text{ is uniformly continuous on bounded subsets of } \Omega, \text{ for all } |\alpha| \leq k\}$.
- $C^\infty(\Omega) = \{u : \Omega \to \mathbb{R} \mid u \text{ infinitely differentiable}\} = \bigcap_{k=0}^{\infty} C^k(\Omega)$.
- $C_c^\infty(\Omega) = \{u \in C^\infty(\Omega) \mid \text{ with compact support}\}$.

A.5.1 Lebesgue Spaces

- $L^p = \left\{u : \Omega \to \mathbb{R} \mid u \text{ is Lebesgue measurable, } \|u\|_{L^p(\Omega)} < \infty\right\}$, where

$$\|u\|_{L^p(\Omega)} := \left(\int_\Omega |u|^p \, dx\right)^{\frac{1}{p}} \quad (1 \leq p < \infty). \tag{A.10}$$

- $L^\infty = \left\{u : \Omega \to \mathbb{R} \mid u \text{ is Lebesgue measurable, } \|u\|_{L^\infty(\Omega)} < \infty\right\}$, where

$$\|u\|_{L^\infty(\Omega)} := \operatorname{ess\,sup}_\Omega |u|. \tag{A.11}$$

- If Ω is also bounded. Then, for $1 \leq p \leq q \leq \infty$, the embedding $L^q(\Omega) \subset L^p(\Omega)$ is continuous.

A.5.2 Sobolev Spaces

- fix $1 \leq p \leq \infty$ and let k be a nonnegative integer. $W^{k,p}(\Omega)$ consists of all locally integrable functions $u : \Omega \to \mathbb{R}$ such that for each multiindex α with $|\alpha| \leq k$, $\partial^\alpha u$ exists in the weak sense and belongs to $L^p(\Omega)$.

- if $p = 2$, we write
$$H^k(\Omega) = W^{k,2}(\Omega) \quad (k = 0, 1, \ldots). \tag{A.12}$$

- if $u \in W^{k,p}(\Omega)$, we define its norm to be
$$\|u\|_{W^{k,p}(\Omega)} := \begin{cases} \left(\sum_{|\alpha| \leq k} \int_\Omega |\partial^\alpha u|^p \, dx \right)^{\frac{1}{p}} & (1 \leq p < \infty) \\ \sum_{|\alpha| \leq k} \operatorname{ess\,sup}_\Omega |\partial^\alpha u| & (p = \infty). \end{cases} \tag{A.13}$$

- We denote by $W_0^{k,p}(\Omega)$ the closure of $C_c^\infty(\Omega)$ in $W^{k,p}(\Omega)$.

- We denote by $H^{-1}(\Omega)$ the dual space of $H_0^1(\Omega) = W_0^{1,2}(\Omega)$.

- We have the following chain of imbeddings
$$H_0^1(\Omega) \hookrightarrow L^2(\Omega) \hookrightarrow H^{-1}(\Omega). \tag{A.14}$$

A.5.3 Orlicz Spaces

- Let φ be a real-valued function defined on $[0, \infty)$ satisfying
  - $\varphi(0) = 0$, $\varphi(s) > 0$ if $s > 0$, $\lim_{s \to \infty} \varphi(s) = \infty$,
  - φ is nondecreasing,
  - φ is right continuous.

  Then, the real-valued function ϕ, defined on $[0, \infty)$ by
$$\phi(s) = \int_0^s \varphi(r) \, dr, \tag{A.15}$$
  is called an N-function. It is proved that any N-function is continuous, strictly increasing, and convex [3].

- Let ϕ be an N-function and ϕ^* a function satisfying

$$\phi^*(t) = \max_{t \geq 0} (st - \phi(s)). \tag{A.16}$$

  Then ϕ^* is also an N-function, and it is called the *polar function*.

- An N-function ϕ is said to satisfy Δ_2-condition near infinity if there exists $s_0 > 0$ and a positive constant M such that for every $s > s_0$

$$\phi(2s) \leq M\phi(s). \tag{A.17}$$

- Let Ω be a bounded domain and ϕ be an N-function
  - The Orlicz space $L_\phi(\Omega)$ is the set of all (equivalence classes modulo equality a.e. in Ω of) measurable functions $u(x)$ defined on Ω and satisfying

$$\int_\Omega \phi(|u(x)|)\, dx < \infty. \tag{A.18}$$

  - The Orlicz class is a linear space if and only if ϕ satisfies Δ_2-condition near infinity.
  - The Orlicz space $L_\phi(\Omega)$ is a Banach space endowed with the norm

$$\|u\|_{L_\phi(\Omega)} = \inf\left\{k : \int_\Omega \phi\left(\frac{|u(x)|}{k}\right) dx \leq 1\right\}, \tag{A.19}$$

    (this norm is due to Luxemburg [36]).

A.5.4 Spaces Involving Time

Let X be a real Banach space, with norm $\|\quad\|$ and $T > 0$ be a fixed time.

- The space

$$L^p(0,T;X) \tag{A.20}$$

  consists of all strongly measurable functions $u : [0,T] \to X$ with

$$\|u\|_{L^p(0,T;X)} := \left(\int_0^\top \|u(t)\|^p\, dt\right)^{\frac{1}{p}} < \infty \tag{A.21}$$

  for $1 \leq p < \infty$ and

$$\|u\|_{L^\infty(0,T;X)} := \operatorname{ess}\sup_{0 \leq t \leq T} \|u(t)\| < \infty. \tag{A.22}$$

- The space

$$C([0,T];X) \tag{A.23}$$

consists of all continuous functions $u : [0,T] \to X$ with

$$\|u\|_{C(0,T;X)} := \max_{0\le t\le T} \|u(t)\| < \infty. \tag{A.24}$$

A.6 Convergence and Compactness

We denote by Ω an open bounded subset of $\mathbb{R}^2$. Assume $1 \le p < \infty$ and $q := \frac{p}{p-1}$.

- Let $\{u_m\}_{m=1}^{\infty}$, $u \in L^p(\Omega)$. We say u_m converges to u in $L^p(\Omega)$, written

$$u_m \to u \text{ in } L^p(\Omega), \tag{A.25}$$

provided

$$\lim_{m\to\infty} \|u_m - u\|_{L^p(\Omega)} = 0. \tag{A.26}$$

- A sequence $\{u_m\}_{m=1}^{\infty} \subset L^p(\Omega)$ converges *weakly* to $u \in L^p(\Omega)$, written

$$u_m \rightharpoonup u \text{ weakly in } L^p(\Omega), \tag{A.27}$$

provided

$$\int_\Omega u_m v dx \to \int_\Omega uv dx \quad \text{as } m \to \infty, \tag{A.28}$$

for each $v \in L^q(\Omega)$.

- Assume $u_m \rightharpoonup u$ weakly in $L^p(\Omega)$. Then

$$\{u_m\}_{m=1}^{\infty} \text{ is bounded in } L^p(\Omega),$$

and

$$\|u\|_{L^p(\Omega)} \le \liminf_{m\to\infty} \|u_m\|_{L^p(\Omega)}. \tag{A.29}$$

- *Weak compactness* in $L^p(\Omega)$: Assume $1 < p < \infty$ and the sequence $\{u_m\}_{m=1}^{\infty}$ satisfies

$$\sup_m \|u_m\|_{L^p(\Omega)} < \infty. \tag{A.30}$$

Then there exist a subsequence $\left\{u_{m_j}\right\}_{j=1}^{\infty}$ and $u \in L^p(\Omega)$ such that

$$u_{m_j} \rightharpoonup u \text{ weakly in } L^p(\Omega). \tag{A.31}$$

- In the case $p = \infty$, we say that $\left\{u_{m_j}\right\}_{j=1}^{\infty} \subset L^\infty(\Omega)$ converges weakly star to $u \in L^\infty(\Omega)$, written

$$u_{m_j} \rightharpoonup u \text{ weakly\_}^* \text{ in } L^p(\Omega), \tag{A.32}$$

provided (A.28) holds for all $v \in L^1(\Omega)$.

- *Uniform integrability* and *weak convergence* in $L^1(\Omega)$ [19]: Assume $\{u_m\}_{m=1}^{\infty}$ be a sequence of functions in $L^1(\Omega)$ satisfying

$$\sup_m \|u_m\|_{L^1(\Omega)} < \infty. \tag{A.33}$$

Suppose also

$$\lim_{l\to\infty} \sup_m \int_{\Omega\cap\{|u_m|\geq l\}} |u_m|\, dx = 0. \tag{A.34}$$

Then there exist a subsequence $\left\{u_{m_j}\right\}_{j=1}^{\infty}$ and $u \in L^1(\Omega)$ such that

$$u_{m_j} \rightharpoonup u \text{ weakly in } L^1(\Omega). \tag{A.35}$$

A.7 Convergence Theorems for integrals

- *Fatou's lemma*: Let $\Omega \subset \mathbb{R}^2$ be measurable and let $\{u_m\}_{m=1}^{\infty}$ be nonnegative and measurable functions. Then

$$\int_\Omega \liminf_{m\to\infty} u_m dx \leq \liminf_{m\to\infty} \int_\Omega u_m dx. \tag{A.36}$$

- *Lebesgue's Dominated Convergence*: Let $\Omega \subset \mathbb{R}^2$ be measurable, let $\{u_m\}_{m=1}^{\infty}$ be integrable functions and

$$u_m \to u \quad a.e.. \tag{A.37}$$

Suppose also

$$|u_m| \leq v \quad a.e., \tag{A.38}$$

for some integrable function v. Then

$$\int_{\mathbb{R}^n} u_m dx \to \int_{\mathbb{R}^n} u dx. \tag{A.39}$$

Bibliography

[1] R. Aboulaich, S. Boujena, and E. El Guarmah. “A Nonlinear Parabolic Model in Processing of Medical Image”. In: *Mathematical Modelling of Natural Phenomena* 3.6 (2008), pp. 131–145.

[2] R. Aboulaich, D. Meskine, and A. Souissi. “New diffusion models in image processing”. In: *Computers & Mathematics with Applications* 56.4 (2008), pp. 874–882.

[3] R. A. Adams and J. J. F. Fournier. “8 - Orlicz Spaces and Orlicz-Sobolev Spaces”. In: *Sobolev Spaces*. Vol. 140. Pure and Applied Mathematics. Elsevier, 2003, pp. 261–294.

[4] G. Aubert and P. Kornprobst. *Mathematical Problems in Image Processing: Partial Differential Equations and the Calculus of Variations*. New York, NY: Springer New York, 2006.

[5] G. Aubert and L. Vese. “A Variational Method in Image Recovery”. In: *SIAM Journal on Numerical Analysis* 34.5 (1997), pp. 1948–1979.

[6] T. Barbu. “Robust Anisotropic Diffusion Scheme for Image Noise Removal”. In: *Procedia Computer Science* 35 (2014), pp. 522–530.

[7] T. Barbu, V. Barbu, V. Biga, and D. Coca. “A PDE variational approach to image denoising and restoration”. In: *Nonlinear Analysis: Real World Applications* 10.3 (2009), pp. 1351–1361. ISSN: 1468-1218.

[8] T. Barbu and C. Moroşanu. “Image Restoration using a Nonlinear Second-order Parabolic PDE-based Scheme”. In: *Analele Universitatii "Ovidius" Constanta - Seria Matematica* 25.1 (2017), pp. 33–48.

[9] C. A. Z. Barcelos and Y. Chen. “Heat flows and related minimization problem in image restoration”. In: *Computers & Mathematics with Applications* 39.5 (2000), pp. 81–97.

[10] K. Bredies and D. Lorenz. “Partial Differential Equations in Image Processing”. In: *Mathematical Image Processing*. Cham: Springer International Publishing, 2018, pp. 171–250.

[11] J. Canny. “A Computational Approach to Edge Detection”. In: *IEEE Transactions on Pattern Analysis and Machine Intelligence* PAMI-8.6 (1986), pp. 679–698.

[12] F. Catté, P. L. Lions, J. M. Morel, and T. Coll. “Image Selective Smoothing and Edge Detection by Nonlinear Diffusion”. In: *SIAM Journal on Numerical Analysis* 29.1 (1992), pp. 182–193.

[13] P. Charbonnier, L. Blanc-Feraud, G. Aubert, and M. Barlaud. “Deterministic edge-preserving regularization in computed imaging”. In: *IEEE Transactions on Image Processing* 6.2 (1997), pp. 298–311.

[14] P. Chen. “Existence and uniqueness of weak solutions for a class of nonlinear parabolic equations”. In: *Electronic Research Announcements in Mathematical Sciences* 24 (2017), pp. 38–52.

[15] J. J. Clark. “Authenticating edges produced by zero-crossing algorithms”. In: *IEEE Transactions on Pattern Analysis and Machine Intelligence* 11.1 (1989), pp. 43–57.

[16] I. El Mourabit, M. El Rhabi, A. Hakim, A. Laghrib, and E. Moreau. “A new denoising model for multi-frame super-resolution image reconstruction”. In: *Signal Processing* 132 (2017), pp. 51–65.

[17] L. C. Evans. *Partial differential equations*. American Mathematical Society, 2010.

[18] L. C. Evans. *Weak convergence methods for nonlinear partial differential equations*. American Mathematical Society, 1990.

[19] L. C. Evans and R. F. Gariepy. *Measure Theory and Fine Properties of Functions, Revised Edition: Taylor & Francis Group*. Taylor & Francis, 2015.

[20] F. Gaillard. *Normal brain MRI*. Radiopaedia.org, rID: 42777. Accessed on 2020-04-19. 2016. URL: https://radiopaedia.org/cases/normal-brain-mri-5?lang=us.

[21] F. Gaillard. *Normal brain MRI (TLE protocol)*. Radiopaedia.org, rID: 40748. Accessed on 2020-04-19. 2015. URL: https://radiopaedia.org/cases/normal-brain-mri-tle-protocol?lang=us.

[22] F. Gaillard. *Normal MRI brain including MR venogram*. Radiopaedia.org, rID: 51158. Accessed on 2020-04-19. 2017. URL: https://radiopaedia.org/cases/normal-mri-brain-including-mr-venogram?lang=us.

[23] R. C. Gonzalez and R. E. Woods. *Digital Image Processing (3rd Edition)*. USA: Prentice-Hall, Inc., 2006.

[24] P. Guidotti, Y. Kim, and J. Lambers. “Image Restoration with a New Class of Forward-Backward-Forward Diffusion Equations of Perona–Malik Type with Applications to Satellite Image Enhancement”. In: *SIAM Journal on Imaging Sciences* 6.3 (2013), pp. 1416–1444.

[25] A. Hadri, H. Khalfi, A. Laghrib, and M. Nachaoui. “An improved spatially controlled reaction–diffusion equation with a non-linear second order operator for image super-resolution”. In: *Nonlinear Analysis: Real World Applications* 62 (2021).

[26] R. M. Haralick. “Digital Step Edges from Zero Crossing of Second Directional Derivatives”. In: *IEEE Transactions on Pattern Analysis and Machine Intelligence* PAMI-6.1 (1984), pp. 58–68.

[27] A. Hjouji, J. El-Mekkaoui, and M. Jourhmane. “Mixed Finite Element Method for Nonlinear Diffusion Equation in Image Processing”. In: *Pattern Recognition and Image Analysis* 29.2 (2019), pp. 296–308.

[28] A. Hjouji, M. Jourhmane, J. EL-Mekkaoui, and M. Es-sabry. "Mixed Finite Element Approximation for Bivariate Perona–Malik Model Arising in 2D and 3D Image Denoising". In: *3D Research* 9.3 (2018).

[29] J. L. W. V. Jensen. "Sur les fonctions convexes et les inégalités entre les valeurs moyennes". In: *Acta Mathematica* 30.none (1906), pp. 175 –193.

[30] M. Jourhmane. "Méthodes numériques de résolution d'un problème d'électro-encéphalographie". PhD thesis. University of Rennes 1, 1993, p. 142.

[31] B. Kawohl and N. Kutev. "Maximum and comparison principle for one-dimensional anisotropic diffusion". In: *Mathematische Annalen* 311 (1998), pp. 107–123.

[32] S. Kichenassamy. "The Perona–Malik Paradox". In: *SIAM Journal on Applied Mathematics* 57.5 (1997), pp. 1328–1342.

[33] J. J. Koenderink. "The structure of images". In: *Biological Cybernetics* 50.5 (1984), pp. 363–370.

[34] S. Li and P. Li. "Weak solutions for a class of generalised image restoration models". In: *International Journal of Dynamical Systems and Differential Equations* 8.3 (2018), pp. 190–203.

[35] X. Li and T. Chen. "Nonlinear diffusion with multiple edginess thresholds". In: *Pattern Recognit.* 27 (1994), pp. 1019–1037.

[36] W. A. J. Luxemburg. "Banach Function Spaces". PhD thesis. Electrical Engineering, Mathematics and Computer Science, 1955.

[37] B. J. Maiseli. "On the convexification of the Perona-Malik diffusion model". In: *Signal, Image Video Process* 14.6 (2020), pp. 1283–1291.

[38] B. J. Maiseli and H. Gao. "Robust edge detector based on anisotropic diffusion-driven process". In: *Information Processing Letters* 116.5 (2016), pp. 373–378.

[39] D. Marr and E. Hildreth. "Theory of edge detection". In: *Proceedings of the Royal Society of London. Series B. Biological Sciences* 207.1167 (1980), pp. 187–217.

[40] P. Perona and J. Malik. "Scale-space and edge detection using anisotropic diffusion". In: *IEEE Transactions on Pattern Analysis and Machine Intelligence* 12.7 (1990), pp. 629–639.

[41] P. Perona, T. Shiota, and J. Malik. "Anisotropic Diffusion". In: *Geometry-Driven Diffusion in Computer Vision*. Ed. by B. M. ter Haar Romeny. Dordrecht: Springer Netherlands, 1994, pp. 73–92.

[42] J. C. Pinoli. *Mathematical Foundations of Image Processing and Analysis, Volume 1*. USA: Wiley-ISTE, 2014.

[43] H. K. Rafsanjani, M. H. Sedaaghi, and S. Saryazdi. "Efficient diffusion coefficient for image denoising". In: *Computers & Mathematics with Applications* 72.4 (2016), pp. 893–903.

[44] L. I. Rudin, S. Osher, and E. Fatemi. “Nonlinear total variation based noise removal algorithms”. In: *Physica D: Nonlinear Phenomena* 60.1 (1992), pp. 259–268.

[45] O. Scherzer and J. Weickert. “Relations Between Regularization and Diffusion Filtering”. In: *Journal of Mathematical Imaging and Vision* 12.1 (2000), pp. 43–63.

[46] J. Stoer and R. Bulirsch. “Interpolation”. In: *Introduction to Numerical Analysis*. New York, NY: Springer New York, 2002, pp. 37–144.

[47] B. M. Ter Haar Romeny. “Differential structure of images”. In: *Front-End Vision and Multi-Scale Image Analysis: Multi-Scale Computer Vision Theory and Applications, written in Mathematics*. Dordrecht: Springer Netherlands, 2003, pp. 91–136.

[48] A. Tiarimti Alaoui and M. Jourhmane. “Edge-Preserving Smoothing of Perona-Malik Nonlinear Diffusion in Two-Dimensional Space”. Manuscript submitted for publication.

[49] A. Tiarimti Alaoui and M. Jourhmane. “Existence and Uniqueness of Weak Solutions for a New Class of Convex Optimization Problems Related to Image Analysis”. In: *Journal of Mathematics* 2021 (2021). Art. ID 6691795.

[50] A. Tiarimti Alaoui and M. Jourhmane. “Existence and Uniqueness of Weak Solutions for Novel Anisotropic Nonlinear Diffusion Equations Related to Image Analysis”. In: *Journal of Mathematics* 2021 (2021). Art. ID 5553126.

[51] L. Vese. “Problèmes variationnels et EDP pour l’analyse d’images et l’évolution de courbes”. PhD thesis. University of Nice Sophia Antipolis, 1996, p. 142.

[52] L. Wang and S. Zhou. “Existence and Uniqueness of Weak Solutions for a Nonlinear Parabolic Equation Related to Image Analysis”. In: *Journal of Partial Differential Equations* 19.2 (2006), pp. 97–112.

[53] Z. Wang and A. C. Bovik. “Mean squared error: Love it or leave it? A new look at Signal Fidelity Measures”. In: *IEEE Signal Processing Magazine* 26.1 (2009), pp. 98–117.

[54] J. Weickert. *Anisotropic diffusion in image processing*. Stuttgart: Teubner Verlag, 1998.

[55] J. Weickert. *Scale-Space Properties of Nonlinear Diffusion Filtering with a Diffusion Tensor*. Tech. rep. Laboratory of Technomathematics, University of Kaiserslautern, P.O, 1994.

[56] J. Weickert. “Theoretical Foundations of Anisotropic Diffusion in Image Processing”. In: *Theoretical Foundations of Computer Vision*. Ed. by W. Kropatsch, R. Klette, F. Solina, and R. Albrecht. Vienna: Springer Vienna, 1996, pp. 221–236.

[57] J. Weickert, C. Feddern, M. Welk, B. Burgeth, and T. Brox. “PDEs for Tensor Image Processing”. In: *Visualization and Processing of Tensor Fields*. Ed. by J. Weickert and H. Hagen. Berlin, Heidelberg: Springer Berlin Heidelberg, 2006, pp. 399–414.

[58] J. Weickert, S. Grewenig, C. Schroers, and A. Bruhn. “Cyclic Schemes for PDE-Based Image Analysis”. In: *International Journal of Computer Vision* 118.3 (2016), pp. 275–299.

[59] J. Weickert, B. M. Ter Haar Romeny, and M. A. Viergever. "Efficient and reliable schemes for nonlinear diffusion filtering". In: *IEEE Transactions on Image Processing* 7.3 (1998), pp. 398–410.

[60] R. T. Whitaker and S. M. Pizer. "A Multi-scale Approach to Nonuniform Diffusion". In: *CVGIP: Image Understanding* 57.1 (1993), pp. 99–110.

[61] A. Witkin. "Scale-space filtering". In: *IJCAI-83. Proceedings of the Eighth International Joint Conference on Artificial Intelligence (II)*. Vol. 2. 1983, pp. 1019–1022.

[62] B. Wu, E. A. Ogada, J. Sun, and Z. Guo. "A Total Variation Model Based on the Strictly Convex Modification for Image Denoising". In: *Abstract and Applied Analysis* 2014 (2014). Art. ID 948392.

[63] Y. L. You, W. Xu, A. Tannenbaum, and M. Kaveh. "Behavioral analysis of anisotropic diffusion in image processing". In: *IEEE Transactions on Image Processing* 5.11 (1996), pp. 1539–1553.

[64] F. Zhaoyong and Y. Zhaoyang. "On weak solutions for a class of nonlinear parabolic equations related to image analysis". In: *Nonlinear Analysis: Theory, Methods & Applications* 71.7 (2009), pp. 2506–2517.

[65] W. Zhou, A. C. Bovik, H. R. Sheikh, and E. P. Simoncelli. "Image quality assessment: from error visibility to structural similarity". In: *IEEE Transactions on Image Processing* 13.4 (2004), pp. 600–612.